THE RECIPROCAL RELATIONSHIP BETWEEN HYDRODYNAMICS AND BIVALVES

A Thesis
Presented to
The Academic Faculty

by

Sarah Kelly Delavan

In Partial Fulfillment
of the Requirements for the Degree
Doctor of Philosophy in the
School of Civil and Environmental Engineering

Georgia Institute of Technology
August 2010

THE RECIPROCAL RELATIONSHIP BETWEEN HYDRODYNAMICS AND BIVALVES

Approved by:

Dr. Donald R. Webster, Advisor
School of Civil and Environmental Engineering
Georgia Institute of Technology

Dr. Philip J. W. Roberts
School of Civil and Environmental Engineering
Georgia Institute of Technology

Dr. Terry W. Sturm
School of Civil and Environmental Engineering
Georgia Institute of Technology

Dr. Thorsten Stoesser
School of Civil and Environmental Engineering
Georgia Institute of Technology

Dr. Marc J. Weissburg
School of Biology
Georgia Institute of Technology

Date Approved: 17 May 2010

ACKNOWLEDGEMENTS

I would like to thank my advisor, Dr. Donald Webster, for 5 years of financial and academic support. Without the continued assistance of my advisor, this body of work would not be possible. I would also like to thank Dr. Marc Weissburg for use of the salt-water flume, use of several acoustic doppler velocimeters (ADV's), and other equipment. Students within the Weissburg Lab in the School of Biology, Miranda Watts and Morey Lafevre, helped with data collection, equipment use, and idea brainstorming. Miranda Watts was instrumental in experimental design and data interpretation. Thank you, Miranda and Morey.

This research was funded through several National Science Foundation fellowships and grants. The NSF:IGERT program, Signals in the Sea, provided fellowship support, equipment funding, and other monetary support. Also, an NSF grant to Dr. Marc Weissburg and Dr. Donald Webster provided a graduate assistantship and equipment funding.

Finally, I would like to thank my dissertation committee members: Dr. Terry Sturm, Dr. Thorsten Stoesser, Dr. Philip Roberts, and Dr. Marc Weissburg. Thank you for your continued support.

TABLE OF CONTENTS

LIST OF TABLES

LIST OF FIGURES

SUMMARY

The focus of this study was to determine the effect of clam presence and behavior on the crossflow of the ambient horizontal flow and the effect of ambient horizontal flow characteristics influence the clam feeding behavior. Hence, there is a reciprocal relationship between organisms and the physical environment, and this study ultimately addressed the role of hydrodynamics in the predator-prey relationship between bivalve clams, *Mercenaria mercenaria*, and their predators, blue crabs and whelks. The study concludes that clams alter the chemical odorant source characteristics and control the transmission of the chemical signal through altering the crossflow.

The first part of the study is a field experiment designed to quantify the effect of the presence and behavior of clams on the crossflow of the horizontal crossflow. The second part of this study is a two-part laboratory experiment designed to isolate the influence of environmental factors on clam behavior. One experiment quantifies the unsteadiness of the clam excurrent jet velocity time record according to environmental cues such as the horizontal crossflow velocity, the density of the clam patch, and the size of the clam. The second laboratory experiment quantifies the unsteadiness of the jet velocity values according to the presence of predator cues in the upstream flow.

Clams are found, using an ADV system in the field, to alter the vertical distribution of velocity according to the sediment in which they are buried. Also, turbulence characteristics, such as Turbulent Kinetic Energy and Reynolds shear stress, are altered in the presence of clams according to the ambient horizontal crossflow velocity and treatment site.

The laboratory flume PIV system captured vector plots for two-dimensional planes

that bisect the clam excurrent siphons and clam jet velocity time records were extracted. A fractal analysis and a lacunarity analysis of the jet velocity time records found that clams alter their jet excurrent velocity unsteadiness according to the horizontal crossflow velocity. This behavioral change may contribute to the differences in the turbulence characteristics in the field experiment. Another result from the laboratory experiments is that the effect of clam patch density on the feeding activity was dependent on the size of the organism. This size/density dependent relationship suggests that predation by blue crabs dominates the system since larger clams are no longer susceptible to blue crab predation, whereas clams of all sizes are susceptible to whelk predation. Finally, clams increase the randomness of their excurrent jet velocity values when predator cues are located in the upstream flume flow. This suggests that the presence of predators elicits clam behavior that promotes the mixing and dilution of their chemical metabolites.

CHAPTER I

INTRODUCTION

The goal of this study is to quantify the excurrent siphon flow and modifications to the crossflow by the bivalve clam, *Mercenaria mercenaria*. The predator-prey relationship between blue crabs, *Callinectes sapidus*, and knobbed whelks, *Busycon carica*, and their bivalve clam prey, *Mercenaria mercenaria*, is influenced by the filter feeding behavior of clams, [178]. In this system, clams release chemical metabolites to the estuarine water through their excurrent feeding siphon, the chemicals are transported downstream by the flow, and predators encounter the chemicals and travel upstream to locate the clams. This interaction is mediated by three distinct phases of the chemical interaction: generation of the chemical signal, transport of the chemical downstream, and the acquisition of the chemical information. Much of the current literature on this predator-prey relationship is focused on the acquisition of the chemical plume and the behavioral reaction by the predator (e.g., [117], [82], and [186]). This study attempts to understand the generation and transmission of the clam metabolyte chemical signal, specifically how the behavior of the prey modifies the local flow dynamics that transport those chemicals.

Clam behavior modifies the release of chemical metabolites to the flow and potentially alters the distribution of boundary layer momentum. Clams bury themselves in the substrate and extend their feeding siphons into the water column. Water enters the incurrent siphon, passes through the interior of the clam body, and out through the excurrent siphon. Clams have the ability to control the height and diameter of the excurrent siphon and the rate at which they pump water out of the excurrent. Also, *Mercenaria mercenaria* have been known to control the times and manner in

which they feed ([150] and [37]). In fact, they have been known to stop feeding when predators are present in the upstream flow [151]. Further, the excurrent flow geometry appears similar to a jet-in-crossflow, which has been shown to modify the vertical distribution of momentum of the boundary layer (e.g., [7]). Analogous to the engineering examples, there is evidence that the presence and behavior of bivalves and other organisms modifies the momentum distribution of the boundary layer flow ([33], [195], and [131]). By altering the crossflow, clams may control the transport of their chemical signal downstream, and subsequently influence predation rates.

Understanding of biological influence on hydrodynamics requires extensive and detailed understanding of specific organisms, the types of behaviors that they display, and the environmental cues that alter those behaviors. There may be clam behavior that promotes certain hydrodynamic conditions within the predator-prey system that decrease the ability of predators to locate their prey. These hydrodynamic conditions may be controlled by the source characteristics, the boundary layer momentum characteristics, or both. There may be hydrodynamic characteristics that decrease the predation rates on the bivalve clam with respect to their predators that may, in turn, dictate the clam behavioral influence on the boundary layer momentum (see Figure 1.1).

The specific objectives of this study are as follows: 1)Determine the effect of the presence and pumping behavior of clams on the distribution of boundary layer momentum under natural field conditions, 2) Decouple the presence and behavior of clams by quantifying the filter feeding source characteristics for varying external hydrodynamic conditions in the laboratory flume, and 3) Quantify the filter feeding source characteristics in the presence of a blue crab predator in the laboratory flume.

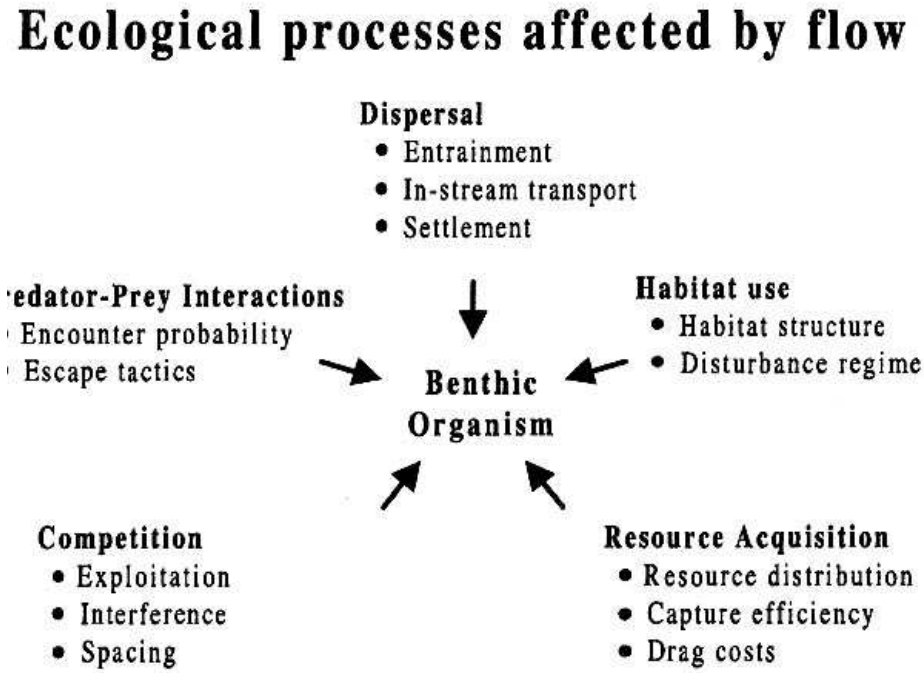

Figure 1.1: Pathways by which flow affects benthic organisms from Hart and Finelli (1999).

CHAPTER II

LITERATURE REVIEW

This chapter reviews studies related to the influence of the clam, *Mercenaria mercenaria*, on the crossflow, the mechanism of olfactory tracking, and the techniques used to address many of the study questions. The first section reviews studies on boundary layers in estuaries and the effects of biological organisms on the boundary layer. A section on jets-in-crossflow literature is included to inform of possible characteristics of the clam excurrent feeding jet. The next section outlines current knowledge about bivalves and specifically *Mercenaria mercenaria*, such as where they are found and how they filter feed. Clams release chemical metabolites through their excurrent siphons that create a chemical plume in the downstream turbulent flow. Therefore, a section reviews the nature of chemical plumes and how passive scalars are transported in turbulent benthic boundary layers. Finally, a section reviews organisms that use chemical plumes for tracking and clam predators to provide the context of chemically-mediated predator–prey interactions.

2.1 Field Boundary Layers

Acoustic Doppler velocimeters (ADV's) have typically been used in the recent past to quantify boundary layers in the field. These devices use acoustic waves to determine the three components of velocity averaged over a volume of the flowing liquid. Several studies have addressed the spatial accuracy of ADV's (e.g., [173] and [139]). Voulgaris and Trowbridge (1997) found that ADV's measure velocity and Reynolds stresses to within 1% of values recorded by laser Doppler velocimeters (LDV) and that the difference can be attributed to the size of the measurement volume. They also found that the deviation of the velocity value increased close to the sediment surface because

of intersection of the measurement volume with sediment grains. In fact, Precht et al. (2006), through their comparison of ADV and LDV data, found that ADV measurements are not reliable at distances from the bed within two and a half times the height of the measurement volume.

Other considerations that must be taken into account when using ADV's is that spikes must be removed from the raw data and that ADV's do not distinguish between turbulence and wave contributions to the velocity sample. Filters must be employed to remove anomalous spikes that occur due to aliasing of the acoustic signal [61]. Spikes in the data do not represent the true values of the velocity at those points in time and, if included, exaggerate the Reynolds stresses and turbulent kinetic energy. Goring and Nikora (2002) suggest several methods for removing spikes, such as an acceleration threshold or a phase-space threshold. Once the spikes have been removed, the wave energy must be distinguished from the turbulence energy. When using an ADV in a laboratory setting, where the researchers have greater control over the flow conditions, the values of velocity that are collected represent the turbulence energy of the flow. Field conditions are much harder to control and the data contain contributions to the flow from several energy sources. There are several studies that suggest ways to overcome this problem by removing the wave energy from the raw field data (e.g., [17] and [148]). Shaw and Trowbridge (2001) suggest using two measurement devices separated in space by a distance greater than the spatial scale of turbulence and less than the spatial scale of the wave energy. Bricker and Monismith (2007) develop a spectral method of removing wave energy from the time records that assumes equilibrium turbulence and no interaction between turbulence and waves.

The wave removal techniques and theory presented in Trowbridge (1998) and Shaw and Trowbridge (2001), and expanded by Feddersen and Williams (2007), can be used for wave removal and also to justify the assumption of horizontal homogeneity in calculations of Reynold's stresses. These articles assume that if two sensors (in our

case, ADVs) are separated by a distance that is between the spatial scale of wave energy and that of turbulence energy, the shear stresses at these two points are essentially equal, [164], [148], and [52]:

$$\overline{[u_i'(x_i + r_i)u_j'(x_i + r_i)]} = \overline{[u_i'(x_i)u_j'(x_i)]} \tag{2.1}$$

$$\overline{[u_i'(x_i)u_j'(x_i + r_i)]} = \overline{[u_i'(x_i + r_i)u_j'(x_i)]} \tag{2.2}$$

Smith et al. (2002) uses the horizontal homogeneity assumption to calculate Reynolds stresses without wave bias with simultaneous underwater PIV systems. The PIV image planes were separated by a distance of 1.5 m horizontally, [152]. Extensions beyond the assumption of homogeneity of Reynolds stress to include homogeneity of the mean velocity are common in field studies. Ferner et al. (2009) separated clam plot treatments by a distance of 5 m and calculated mean daily longitudinal velocity values at the same height above the substrate. They found no statistical difference in the mean velocity values for the two separated sites using the ADV's employed in the current study and at sites in close proximity to the current study [53]. Judge et al. (1992) and Powers and Kittinger (2002) both assumed equal flow rates with an approximate horizontal spatial distance of 1.2-1.5 m in their field channel experiments. There are several other examples of studies that assume mean velocity values are comparable over short distances in field settings, [84] and [174]. While this assumption has not necessarily been proven correct, it has been used extensively in field biological literature to demonstrate the relationship between biological organisms and hydrodynamics.

There are several examples of boundary layer profiles in the field that give insight into the types of information that is available to researchers (e.g., [79], [67], and [29]). Gross and Nowell (1985) used current meters at low frequency to capture velocity time records for the entire boundary layer. They were attempting to describe the

mean flow field using the shear velocity calculated from the velocity time records and the distance above the substrate. The velocity profiles gave estimates of the shear velocity to within 10% of the values calculated based on the inertial range of the velocity spectra. At the time (i.e., predating ADV technology), this was considered a good approximation of the mean flow. After the widespread use of ADV's, researchers were better able to determine shear velocities and approximations for the roughness length of the flow. Collins et al. (1998) assumed a logarithmic relationship between the velocity values and the height above the substrate. However, in the field, they found that the logarithmic profiles were confounded by rotary tidal currents, wind effects, wave action, and secondary flows.

A recent example of ADV use in the field developed a new system for controlling the height of the measurement volume by raising and lowering a platform in which the ADV was mounted [79]. Kawanisi and Yokosi (1994) measured boundary layer profiles over several tidal cycles in the Ota River estuary and found that stratification changes in the ebb and flood tides greatly influenced the boundary layer. Therefore, in tidal channels the boundary layer momentum is dependent on the temporal nature of the flux Richardson number [89]. The Hudson River estuary was also found to be consistent with the law-of-the-wall during flooding tides and inconsistent during ebb tides [165]. Trowbridge et al. (1999) determined that the stratification of the Hudson River estuary was insufficient to account for the differences over the tidal cycle. Therefore, field boundary layer characteristics are dependent on the temporal position of the tide and this must be taken into account when collecting field velocity time records. The control of field characteristics and contribution to the boundary layer hydrodynamics is often difficult and overwhelming. In a review of tidal flat hydrodynamics, Le Hir et al. (2000) looked at many of the physical forcing parameters that control flow. They concluded that organisms (both plants and animals) within the flow have an unknown contribution to bed roughness or changes to the momentum

distribution. In fact, they state that biological components may contribute to seasonal differences in the flow dynamics in natural settings.

A large portion of coastal estuaries are small, shallow, and tidally-driven, whereas much of previous research focus has been on larger estuaries. While clams are found in both types of estuaries along the eastern coast of North America, this study focuses on the small, tidal channels upstream of Wassaw Sound, Georgia, USA ([150], [54], and [151]). Several recent journal articles outline the ecological and hydrodynamic characteristics of the small estuary on Eprapah Creek on the Southeast Coast of Australia ([162], [161], [23], and [24]). Chanson et al. (2008) concluded that ADV data from small estuaries requires a specific, rather than general, post-processing technique to give usable velocity and turbulence information. Their study included hydrodynamic, physio-chemical, and ecological measurements collected simultaneously and extensively for the entire tidally-influenced reach of the small estuary [23]. They found that the largest velocities in the estuary occur directly before and after low tide and that the entire reach is controlled by the flood tide resulting in high resident times within the estuary [162]. Turbulence properties in Eprapah Creek were dependent flood and ebb tides, spring and neap tides, and location within the estuary [161]. The assumptions for large estuaries, with respect to turbulence characteristics, cannot be used for small estuaries due to large bathymetric to depth ratios [161]. Therefore, in small estuaries there is a wider range of hydrodynamic characteristics within a spatial extent when compared to large estuaries. In fact, in shallow estuaries the surface slope and shear stress dominates the flow equations [149], and the sediment does not dampen the turbulence [166].

2.1.1 Relationship Between Biota and Boundary Layers

The momentum distribution in a benthic boundary layer is affected by the flow characteristics such as velocity, elevation, depth of the flow, and a roughness size associated

with the sediment. Jackson et al. (2007) found that with larger roughness elements, the ability of crabs to locate prey decreased due to increased turbulence. Stream invertebrates and fish have also been shown to behaviorally alter the flow to lessen the forces that they experience [71]. It has also been shown that there are gradual changes in the types and species of benthic organisms depending on the flow characteristics along streams in Western Australia [68]. Growns and Davis (1994) found that as the hydrodynamic characteristics along a river channel altered, the distribution of organisms also gradually altered. However, when flow conditions were modified to increase turbulence and decrease flow rate in a study by Robson et al. (1999), there was no difference in biological abundances over the short term.

Biological entities can alter the roughness characteristics of the flow through changes to the sediment or other objects such as bed forms or biological structures. Structures in the flow include macrophytes such as sea grass beds or marine plants; infaunal structures such as mussel shells or tubes protruding from the sediments; algal mats that coat and cement the sediments; or organism bodies such as crabs, snails, or sponges. The presence and behavior of organisms in the flow can act to stabilize or destabilize the sediments and modify the momentum of the boundary layer [125]. For example, *Hydropsyche siltalai* significantly lower the ambient velocity of the flow downstream of larvae microhabitats [46]. Flow streamlines are modified by the size and shape of biological obstructions in the flow. The quantity and quality of food particles available to feeding marine organisms is modified by flow interactions with the organism body [1]. Abelson et al. (1993) hypothesized that body shape dictates the types of particles available for consumption. Their velocity profile is based on the one-seventh power law developed for turbulent pipe flow:

$$u(z) = U\left(\frac{z}{z_o}\right)^{\frac{1}{7}} \tag{2.3}$$

with U as the free stream velocity, $u(z)$ as the flow velocity at height z, and z_o is the boundary layer thickness. Concentration models indicate that small height-to-width

body sizes were presented more often with benthic sediments while large height-to-width body size had more access to suspended particles [1]. Large height-to-width organisms, such as sea grass beds (*Spartina alterniflora*) change sediment transport and flow characteristics. Chemical plumes downstream of sea grass mimics had more dilute concentrations than plumes without obstacles in the flow [56]. These habitats are home to many marine organisms that could use the sea grass beds to hide visually, mechanically, or chemically.

The hydrodynamics of the flow is also affected by the density of the sea grass within the patches. Higher density patches tended to cause streamlines to travel over and around the patches rather than through, as in the case of low density beds [16]. With ambient streamlines traveling over the patches, the sea grass bed may be considered one structure with small height to width ratio, whereas the low density patches are considered a group of individual cylinders in the flow. Bouma et al (2007) found that sediment transport varied considerably through beds of sea grass mimics in field, laboratory, and model studies. Therefore, the effect of biological obstacles in the flow is complicated by the size, shape, and abundance of the organisms. The system is more complicated than simply concluding that macrophytes stabilize or destabilize the sediments.

Biota has historically been categorized in the sediment/biological literature as either sediment stabilizers or destabilizes [190]. Stabilizers influence the bed by protecting the sediments from resuspension by physically covering the sediments, or providing cohesion between sediment grains. Destabilizers increase the roughness of the sediments by digging action or by increasing the shear stress on the bed by modifying streamlines. Somewhat counter intuitively, the same biological behavior can be considered both stabilizing and destabilizing [87]. For example, snails leave a trail as they move through the sediment. With smooth bed conditions, the trail increases the roughness of the bed; with rough bed conditions, the trail smooths the bed [87].

Cadisflies have been found to increase the bed stability by building feeding nets in the pore spaces between sediment grains increasing the critical shear stress necessary for sediment scour [19], and *Hydropsyche* increases the critical shear stress by silk threads between gravel [154].

Other benthic organisms modify the flow by modifying the sediment size. Deposit feeders alter the sediment grain size by ingesting small grains, leaving higher proportions of larger grains [104]. After ingestion, larger sized fecal pellets also increase the mean sediment size [88]. The natural life process of ingestion and digestion by deposit feeders significantly increases the roughness length of the flow.

Biota also significantly decrease the roughness length by creating a biological mat or crust over the top layer of sediments [195]. Wright et al. (1997) found a field site in the dry Tortugas that would be dominated by bed forms, but the roughness was controlled by shrimp burrows and worm mounds due to the presence of the crusted algal/sediment mat. They assumed that the bed shear stress consisted of the sum of form drag, τ_{fd}, and skin friction, τ':

$$\tau_o = \tau_{fd} + \tau' \tag{2.4}$$

Scour occurs when the bed shear stress, τ_o, is above a critical level, τ_{cr}.

Cementing of the sediment grains by biologically-secreted mucus could increase the critical shear stress necessary for sediment entrainment [125]. The velocity profile equation used by Wright et al. (1997) and many other studies to determine the roughness length and the friction velocity is

$$\frac{u(z)}{u_*} = \frac{1}{\kappa} \ln \frac{z}{z_o} \tag{2.5}$$

where κ is the von Karman constant, 0.41, z is the height above the sediment, $u(z)$ is the fluid velocity, u_* is the wall shear velocity, and the roughness length, z_o, is assumed to be the z intercept of the logarithmic velocity profile. The total roughness height,

k_b, is assumed to be $30z_o$ and consists of contributions from the grain roughness, bed form roughness, and biological roughness.

The above approach was also used to determine the biological effects on the boundary layer momentum in the lower Chesapeake Bay where organisms dominate the bed roughness features [196]. Equation 2.5 was used in many studies to determine how biology affects the logarithmic velocity layer; however, other features of turbulence and boundary layers also may be affected. Periphyton communities cover much of the benthic sediments in streams, and are best described as algal mats that grow on stream sediments. The effect of periphyton mats on velocity distribution, kurtosis coefficients, Reynolds stresses, relative turbulence intensity, coefficient of eddy diffusivity, velocity spectra, and Kolmogorov turbulence scales in a laboratory flume was determined [129]. The biota modified the turbulence quantities selectively, not only near the sediments but throughout the logarithmic layer [129]. The authors used Equation 2.5 to determine the roughness length, and the following equation for the Reynolds stresses

$$-\frac{\tau_t}{\rho} = \overline{u_i' u_j'} = \begin{vmatrix} \overline{u'u'} & \overline{u'v'} & \overline{u'w'} \\ \overline{v'u'} & \overline{v'v'} & \overline{v'w'} \\ \overline{w'u'} & \overline{w'v'} & \overline{w'w'} \end{vmatrix} \tag{2.6}$$

with ρ as the water density.

With Equations 2.5 and 2.6, Nikora et al. (1997) concluded that the periphyton mat modified the velocity distribution, Reynolds stress, coefficient of eddy diffusivity, and velocity cross spectra. Dense aggregations of mussels form a sediment covering that stabilizes sediments, as with periphyton mats, but adds roughness height due to the shell structure and feeding siphons. Van Duren et al. (2006) used Equation 2.5 to quantify the boundary layer and turbulence intensity over actively pumping mussel beds in the laboratory. They found that the shell structure added a form drag contribution to the bed shear stress and an internal boundary layer formed over the

mussel bed. Another study of laboratory mussel beds did not have evidence of an internal boundary layer [18], but they did not adequately resolve the velocity profile in the large velocity gradient region. Unlike Nikora et al. (1997), van Duran et al. (2006) determined that turbulence intensity was highly affected by the presence of biota, particularly when the mussels were actively pumping. This indicates that other bivalves, especially those that increase the form drag of the system, may also alter the boundary layer. A study by Nikora et al. (2002) found that the development of the internal boundary layer was dependent on the density of bivalves within the bed and that the beds were too small for the second log layer to develop extensively. The bivalve clam, *Mercenaria mercenaria*, create bumps and pockets in the sediment as they bury themselves and project their siphons into the water column, which may increase the form drag in the boundary layer. However, over coral reefs it has been determined that the local roughness has less of an effect on shear and mixing than larger scale roughness features of the water/sediment interface [144]. Therefore, the local size and shape of the roughness characteristics associated with the presence and shape of bivalve clams may have little effect on the macroscale shear and mixing over the region. Van Duren et al. (2006) determined that the biological effects were less pronounced at higher ambient flow rates, which may indicate that local scale characteristics are more important in low flow conditions. These results may be species specific due to an earlier study that found the opposite effect with the deposit feeder *Spiophanes krøyeri*; low flow rates resulted in the lowest effects on the boundary layer momentum by the deposit feeder [157].

A review of the biological/sediment literature concluded that the impact of organisms on the flow generally decreases with increasing sediment transport [87]. However, Jumars and Nowell (1984) based these assumptions on Equation 2.5. They termed their conclusion as an envelope of biological effects that modify the momentum of lower velocity flows with particular influence when the flow characteristics are close

to the critical shear stress [87]. There is one study that does not oversimplify the logarithmic boundary layer by using Equation 2.5. Crimaldi et al. (2007) found that the siphon presence and the jet flow of mimic bivalves in flume experiments modified the velocity profile and the turbulence intensity distribution. They did not attempt to find a roughness coefficient or velocity stress for the flow, but did include the Reynolds stress effects [33]. They used bivalve mimics in a laboratory flume with an otherwise smooth bed and concluded that the presence of siphons and excurrent jets had a large impact on the turbulence intensity throughout the logarithmic layer. A field study of bivalve mimics, although poorly executed, supported their flume results [84]. Despite the low number of studies conducted in this research area, previous literature leads to the conclusion that biota effects on hydrodynamics are spatially, temporally, species, and situation specific.

2.2 Jets in Crossflow

The excurrent siphon of the bivalve clams, *Mercenaria mercenaria*, appears much like a vertical jet-in-crossflow. Depending on the source characteristics: velocity, height, and diameter, the excurrent flow could be a laminar or turbulent jet. Also, the ambient conditions of the receiving flow dictate the cross flow effects. Early experimental and numerical studies determined the viscous stability of laminar vertical jets with and without thermal buoyancy [115]. They found that a symmetric mode is unconditionally stable, an asymmetric mode is unstable, and that positive thermal buoyancy destabilizes the jet [115]. If the sediment and the ambient fluid are at different temperatures, a pumping clam will change temperature to gradually match that of the water [38]. Hence, there is a thermal exchange between the clam body and filtered fluid resulting in the release of thermally-altered fluid to the ambient flow. In this case, the siphon excurrent fluid temperature will be altered compared to the receiving fluid temperature and buoyancy will have an effect.

Other researchers have studied laminar jets into immiscible fluid over a range of Reynolds numbers [145]. The fluid exiting the clam will have fewer particles and more chemical metabolites and will have a slightly different density than the ambient fluid. Although they have slightly different densities, they cannot be considered immiscible fluids. Chhabra et al. (2005) studied turbulent jets into a quiescent fluid of greater viscosity. They found that when the viscosities are equal, the turbulent stress dominates [25]. At an ambient to jet viscosity ratio of 20, the jet has the lowest velocity decay rate, the lowest mass flux, and the lowest value of velocity spread rate.

There are many experimental studies capturing the jet velocity [78], turbulence intensity and kinetic energy [15], and entrainment velocity [48] of turbulent axi-symmetric jets. These studies are concerned with near field characteristics of the turbulent jet flow. Velocity profiles in the jet should approach a self-similar shape if the jet velocity is steady. High Reynolds number self-preserving jets have been studied and determined to be self-similar at 70 diameters downstream of the jet orifice [198] and have decreasing amounts of unmixed ambient fluid reaching the centerline with increasing Reynolds numbers [34]. Steady jet flow is required for self-similarity, therefore these analyses may not apply to clam excurrent flow, depending on the siphoning characteristics.

Tidal conditions in the clam habitat provide quiescent to highly turbulent ambient flow, hence clam siphons appear be more closely related to jets-in-crossflow than axi-symmetric jets. It has been determined that the turbulence level in the wake of a jet in crossflow is higher and in a more equilibrium state than in the flow upstream of the jet [94]. However, it is the non-equilibrium turbulence upstream of the jet that controls much of the transport of concentration, mass, and momentum of the system [94]. Kim and Benson (1992) concluded that turbulence intensity of the fluid may not provide enough information about the dynamics of the system because the location of highest intensity does not contribute to the entrainment.

There are several flow structures present in the near field of the interface of a jet into the ambient crossflow such as wake vortices, shear-layer vortices, horseshoe vortices, and counter-rotating vortex pairs [60] that can be viewed in Figure 2.1. These structures have been attributed to many sources and have been the center of much study and debate [122]. Morton and Ibbetson (1996) outline the findings of the classical literature and address the resulting inconsistencies in the explanations for the source of the circulation. They concluded that all of the structures listed above are present in all jet-in-crossflow cases, but the stability and strength of the structures depend on the flow characteristics such as jet Reynolds number and jet-velocity-to-ambient-velocity ratio. The most controlling of the characteristics is the ratio of the jet velocity and crossflow velocity, v/U. For example, the wake vortices are alternating vertical vortices downstream of the jet originating from the separation of the upstream boundary layer and are entrained into the jet. They are much less dominant and regular at low v/U values [60], which are comparable to the range of clam excurrent velocities. In the case where v/U is close to unity, wake vortices are less dominant than jet-shear layer vortices [113]. Andreopoulos (1985) found that the large scale vortex rings are shed from the jet entrance at intervals that depend on the Reynolds number of the jet, Re_j, and the velocity ratio, v/U. Another study also found that the frequency of the vortex shedding depends on the velocity ratio between the jet and the crossflow, and that this frequency is the same as that of the upstream recirculation frequency [98]. In fact, the frequencies calculated in this study confirm that the wake vortices of jets are not the same phenomenon as the Karman vortex street shed from cylinders in a flow [98].

Jet trajectory is also controlled by the velocity ratio between the jet and the ambient crossflow. Near-field trajectories follow a power law relationship that depends on the angle in which the jet enters the crossflow, the height of the jet orifice, and the velocity ratio, v/U [197] (see Figure 2.2). An extensive study by Andreopoulos and

Rodi (1984) suggests that as v/U decreases, the bending of the jet in the near field increases and the crossflow streamlines deflect vertically over the jet streamlines. For large v/U, the jet is more erect and the crossflow streamlines deflect around the jet, see Figure 2.1. The authors claim that at low v/U values, the crossflow strength tends to suppress the leading side of the jet orifice forcing much of the jet flow to increase in velocity and exit out downstream half of the orifice. There are several numerical studies of jets in crossflow that compare simulation results to the experiments of Andreopoulos and Rodi (1984) and others (e.g., [40], [155], [128], and [127]). The numerical results of Sykes et al. (1986) suggest that the vortex pair that dominates the downstream jet cross-section can be attributed to the streamwise vorticity of the vertical jet for large values of the velocity ratio. A turbulent jet in laminar crossflow, with a v/U of 2, resulted in counter rotating vortex pair dominating the cross-section [73]. Sykes et al. (1986) was less conclusive about the source of the vortex pair under low v/U conditions than high velocity ratios. Demuren (1992, 1993) found that at low v/U values, it is necessary to model the flow within the jet pipe since the strength of the crossflow was such that it forced the flow out through the downstream half of the jet orifice at a higher velocity, see Figure 2.1.

It should be noted that Andreopoulos and Rodi (1984) compared their turbulent jet characteristics to dye visualizations of laminar jets in laminar crossflow. Therefore, the numerical studies that compare their results to Andreopoulos and Rodi (1984), also compare their results to laminar jet dye visualization (e.g., [180], [39], [40], [155], [128], and [127]). In fact, Demuren (1992) used a laminar flow to test the numerical grid and found that multigrid convergence rates are quite good in comparison to single grids. Morton and Ibbetsen (1996) used both laminar and turbulent crossflow and jets and found that a vortex pair was present over a large range of v/U and Reynolds numbers. In fact, Meyer et al. (2007) found that there were less distinct vortical structures as turbulence increases and that most dye visualization studies

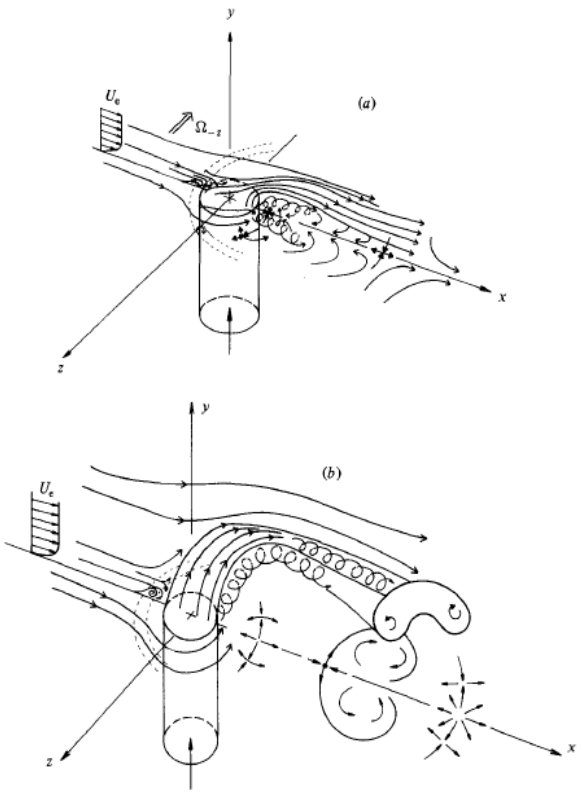

Figure 2.1: A 3D view of a jet in crossflow from Andreopoulos and Rodi (1984).

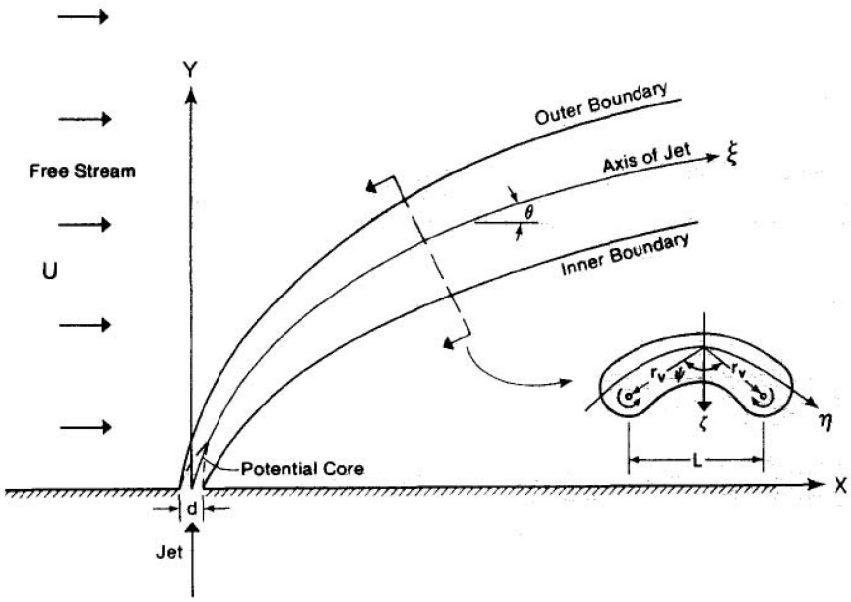

Figure 2.2: A 2D view of a jet in crossflow from Rajaratnam and Gangadharaiah (1983).

that show the vortical structures use laminar flow for both crossflow and jet. There are also several studies that use laminar theoretical assumptions applied to turbulent jets ([94] and [73]). The jet Reynolds number, Re_j, that indicates a turbulent or laminar jet is under some debate in the literature. Boguslawski and Popiel (1979) set a limit that round jets can be considered turbulent above a jet Reynolds number of 10^3. However, Richards et al. (1993) considered their jets as laminar and used jet Reynolds numbers of 1957 and Wygnanski and Fiedler (1969), with a jet Reynolds number of at least 10^5, measured turbulence intensity of approximately 0.1% and claimed that the jet was essentially laminar. Table 2.1 outlines the characteristics of several jets-in-crossflow studies. The indications of laminar or turbulent in Table 2.1 are those claimed by the authors of the respective papers.

The velocity ratio controls the shape of the jet cross-section and subsequently the entrainment of ambient flow into the jet. The result of greater entrainment in the excurrent jet of the clam is lower concentration of clam metabolites in the downstream plume. With a v/U value much less than one, the jet is severely bent over and remains in the crossflow boundary layer [122]. Morton and Ibbetson (1996) found that entrainment is highly dependent on the velocity ratio and has a maximum where the modified velocity ratio, $\frac{v}{U}(\frac{d}{l})^{0.5}$, has a value of 4.3, where d is the diameter of the jet and l is the length of the jet orifice. Values of the modified velocity ratio above and below this value have lower entrainment values [122]. Adler and Baron (1979) developed an equation for the entrainment and cross-sectional area of a jet-in-crossflow system and were able to compare their mathematical model to previous experimental data. They accurately predict the mixing and velocity fields of the downstream jet [4]. The momentum of the entrained fluid is responsible for the bending of the jet seen in Figure 2.2 [27] and the entrained fluid enters on the downstream side of the jet [122]. There is also evidence to suggest that the angle the jet orifice to the ambient flow direction has influence on the entrainment rate [180] Wegner et al. (2004) found

numerically that there were higher rates of entrainment with higher rates of jet unsteadiness controlled by the angle in which the jet enters the flow. More entrainment of the receiving fluid leads to lowered concentrations of a passive scalar in the jet fluid. Therefore, depending on the ambient conditions there may be various velocity values and siphon angles that would promote mixing of clam metabolites.

Since there may be multiple clams buried in the same area, there may be multiple-jets-in-crossflow. The many jets may interact to affect entrainment or the presence of structures in the flow [170]. In fact, for air jets into vertical crossflow of water, the spacing of the multiple jets affected the stability of the flow [170].

2.2.1 Unsteady Jets

There is evidence that an unsteady jet results in higher entrainment rates. Chang and Vakili (1995) found that periodic disturbances to the steadiness of the jet flow increases the entrainment rate by creating vortex rings in the jet flow. In fact, lower frequency of disturbances, especially at lower velocity ratios, lead to higher trajectories of the vortex rings [22]. With higher vortex trajectories, more ambient fluid is entrained into the jet cross-section by the vortex. Therefore, unsteady jets that have lower frequencies of disturbance have higher rates of mixing and lower scalar concentrations. Hermanson et al. (1998) also found that pulsed jets had more persistent vortex rings than steady jets and entrained more ambient fluid. They found that at low frequency pulsing rates, the vortex rings were more widely spaced and therefore did not interact with one another [72]. As the frequency increased the jet behaved more like a steady jet. Johari et al. (1999) looked at both the frequency of the pulsed jet and the duty cycle (the fraction of the pulse period that the jet is turned on) to find a combination that optimizes the entrainment. They found that vortex rings that did not interact with one another resulted in the largest persistence and

Table 2.1: Comparison of jet literature. Method is either numerical or experimental measurements, Fluid is the type of fluid used in the jet or the receiving fluid, Regime is the flow regime for the jet or the crossflow: laminar, turbulent or no flow, Re is the Reynolds number of the jet or the cross-flow, v is the vertical jet velocity in ms^{-1}, d is the jet diameter or dimensions in mm, U is the bulk crossflow velocity, and v/U is the jet to crossflow velocity ratio.

Steady Jets											
		Jet					Crossflow				
Paper	Method	Fluid	Regime	Re	$v\ ms^{-1}$	$d\ mm$	Fluid	Regime	Re	$U\ ms^{-1}$	v/U
[198]	exp.	air	turb.	1×10^5		26.4	air	no flow			
[115]	exp,num.	water	lam.				water	no flow			
[197]	theo.		turb.								4,6,8
[4]	theo.		turb.					turb.			
[15]	exp.	air	turb.			38.5	air	no flow			
[143]	exp.	water	turb.	3.2×10^4,5.3×10^4,8.3×10^4	2.5,4.12,6.46	12.7	water			0.92	2.73,4.52,7.05
[7]	exp.	air	turb.	2.05×10^4,4.1×10^4,8.2×10^4		50	air	turb.		13.9	0.5,1,2
[6]	exp.	air	turb.	5×10^3,2×10^4,8.3×10^4,4.1×10^4		50	air	turb.		13.9	0.25-4
[155]	num.		turb.		2,4,8	unity					2,4,8
[128]	num.							weak			
[27]	num.	air	turb.	1.14×10^4	9	20	air			0.9	
[98]	exp.	air		6×10^3-1×10^5	10 - 120	10	air		5×10^4-5×10^6	1-60	1-14
[34]	exp.	air	turb.	1.5×10^3-2×10^4			air	no flow			
[127]	num.							weak			
[39]	num.		turb.						1.1×10^5		1.8
[94]	num.				27.6	25.0				12	
[40]	num.	air	turb.				air				0.5,2.0
[73]	theo.		turb.					weak			
[145]	num.	water	lam.	1957,1585,...,908	0.120,0.0717,0.2337	3.19,5.8,4.7	water	no flow			
[60]	exp.	air	turb.	7.6×10^3-1.14×10^5	3-45		air		3.8×10^3-1.14×10^4	1.5-4.5	2-10
[78]	exp.	air	turb.	1×10^5			air	no flow			
[22]	exp.	water	turb.	1.87×10^3	0.1488	12.7	water	lam.			1.5-6.7
[122]	exp.	water	lam,turb.		0.1-1	2-19	water	lam,turb.	100-1200	10-120	1-100
[170]	exp.	air		3.7×10^3-3×10^4		0.5,0.7,1	water	turb.	1.3×10^4-4×10^4		
[48]	exp.	water	turb.				water	no flow			
[180]	num.		turb.	2.05×10^4	6.95	50				13.9	0.5
[25]	exp.	water	turb.	2000			sugar-water	no flow			
[113]	exp.	air	turb.	2400	1.3,4.95	24	air	turb.		1.5	1.3,3.3
Unsteady Jets											
		Jet					Crossflow				
Paper	Method	Fluid	Regime	Re	$v\ ms^{-1}$	$d\ mm$	Fluid	Regime	Re	$U\ ms^{-1}$	v/U
[72]	exp.	water	turb.	1.48×10^4	0.988	13	water	lam.		0.152	
[83]	exp.	water	turb.	2250,4500	0.75,1.50	3	water	tam.		0.15	
[13]	exp.	air	turb.	1300	10,20	1×100	air	no flow			
[20]	exp.	water	lam,turb.	1×10^3-1×10^4			water	no flow			
[81]	exp.	water				5	water	lam.		0.05,0.1	0.04-0.7
[147]	num.		lam.	600				lam.			1-6

penetration into the flow field [83]. Therefore, reducing the duty cycle at fixed frequency or decreasing the frequency at a fixed duty cycle increases the dilution of the pulsed jet. Pulsed jets always had higher penetration and more rapidly downstream dilution than non-pulsed jets [83]. The velocity ratio does have an effect on the types of vortices that form with the pulsed jets [147]. Above a velocity ratio of two, vortex rings are formed and below the velocity ratio of two, hairpin vortices form when with direct numerical simulation by Sau and Mahesh (2008) and the hairpin vortices are compared to horseshoe vortices [81]. For low Reynolds numbers shedding of hairpin vortices is periodic and the frequency depends on the Reynolds number [147]. Jabbal and Zhong (2008) used a synthetic jet powered by a diaphram, therefore having both source and sink characteristics, to identify vortical structures that would delay separation on a 2D cylinder. They begin with a laminar jet in a laminar boundary layer and assume that the vortical structures created will also be present with synthetic jets and turbulent flow. They find a velocity ratio limit of 0.4 for the formation of hairpin vortices rather than the 2.0 that Sau and Mahesh (2008) determined.

There are several studies with synthetic or zero-net-mass-flux jets into quiescent flow that may also give insight into unsteady jets in general. The spreading rate of the zero-net-mass-flux jet is larger than a steady jet for the entire measurement domain of Cater and Soria (2002). Their results are similar to those outlined above by Johari et al. (1999) who studied pulsed jets into a crossflow. Cater and Soria (2002) determined that at low Reynolds numbers and high pulse frequencies the vortices in the dye stream completely interact and have little ambient fluid entrainment. However, when laminar vortex rings are present and not interacting with one another, entrainment rates are much higher due to persistence of the vortex rings [20]. Bera et al. (2001) looked at both zero-net-mass-flux jets and those with constant outward mass flux but similar pulsing behavior. They found that both types of pulsed jets had

higher entrainment than steady jets and both fostered the formation of laminar vortex structures. However, they found that the constant outward mass flux jet vortices formed farther downstream than the vortices for the zero-net-mass-flux jets.

2.3 Bivalve Clams, Mercenaria mercenaria

There are many reviews and studies that discuss the importance of understanding olfactory tracking and how it affects community structure and ecological trophic levels. However, many studies have considered the source chemical release characteristics as a constant in the process rather than a variable. There are few studies that characterize the behavior of the source and how it changes with shifting environmental characteristics. An early review of the factors that affect bivalve feeding and growth looked at quantity of food, salinity, pH, temperature, and light intensity, but they did not determine how fluid dynamics affects bivalves [194]. Also, a review of olfactory predation presents several studies that address the ability of prey to alter their release characteristics in response to several of the factors presented above[184]. The review states that there is little understanding of source alterations due to flow characteristics. The current study concentrates on the olfactory predation system of blue crabs and knobbed whelks and their infaunal clam prey, *Mercenaria mercenaria*.

Clams are bivalve organisms that bury themselves in the sediment and extend their tubular siphons to the sediment surface. Clams feed by drawing water in through an incurrent siphon, filtering out the food particles, and releasing the filtered water back to the water column through their excurrent siphon. As the water passes through the body of the clam, waste metabolites are picked up and carried out through the jet-like excurrent siphon. The metabolites released are transported downstream with the ambient flow and create the chemical plume that is tracked by predators. The following subsections discuss the environments where clams settle and are found; general information on the behavior of bivalves; how pumping, filtering, and growth

rates are modified; and the results of clam mimic studies.

2.3.1 Locations and Larval Settlement

The environments in which clams live are dependent upon several factors occurring throughout the clam life cycle. Clam larvae are carried by the flow and must settle to the sediment before becoming adult clams. Hence, larval settlement is highly dependent on hydrodynamics of the flow. In fact, hydrodynamics may be the single most important factor contributing to benthic ecology [70]. Fluid motion determines the settlement location of bivalve larvae and therefore affects the density of adult clam aggregations. The study by Hart et al. (1996) suggests that larvae are not merely passive particles but actively seek settlement in locations of specific hydrodynamic conditions because the location of settlement may determine the likelihood of reaching adulthood. The search for specific hydrodynamic conditions suggests that fluid mechanics affects the entire lifecycle of clams. If predators are less successful in specific flow conditions, clam larvae that settle in regions characterized by these conditions may have higher likelihood of survival and therefore greater fitness. Locations that have higher clam densities or larger numbers of adult clams may be hydrodynamically desirable settlement regions. Larval settlement in the regions that already have adult clams present could have several effects on clam populations. Juvenile clams may be somewhat protected if settlement occurs in patches of adult clams. High density patches may appear as one large, hard to eat prey. Also, higher density could mean that loss of only a few clams out of the group minimally influences the overall population. Alternatively, juveniles may be at greater risk when settling in established clam beds. Higher clam densities may release a larger flux of odorant and, therefore, be more attractive to potential predators. There may be an advantage to large nearest neighbor distances to decrease the odorant release flux. Although, there is evidence

that the presence of pumping clam siphons increases the variability of larval settlement and on a large scale could enhance settlement in already established clam plots [47].

Once the larvae settle, the clam environment must provide food, shelter, and other necessary aspects of life. A survey completed in the Chincoteague Bay area of Maryland determined abundances of *Mercenaria mercenaria* according to bottom type and current [188]. The researchers found that there were higher abundances of clams in shell hash sediments compared to mud and sand and higher abundances in regions where the currents were relatively high for the surrounding region. These findings suggest several possible explanations for the high clam densities. It is possible that larger numbers of larvae are settling in regions of high flow rates and abundant angular sediments. It could also suggest that more clams are reaching maturity and surviving in these regions. Both high currents and large, jagged sediments contribute to higher roughness Reynolds numbers and therefore more turbulent flow regimes. Further, these two factors may contribute to creating hydrodynamic conditions that hinder the predation success of dominant tracking predators.

2.3.2 General Bivalve Behavior

Hart and Finelli (1999) suggest that fluid motion is the dominant forcing that controls stream communities. Therefore, ecological researchers should concentrate on the cause and effect relationship between hydrodynamics and benthic organisms, see Figure 1.1.

Adult clams display several documented behaviors during their lifecycle that correlate with factors in the environment. The bivalve *Mya arenaria*, a soft-shell clam, has been found to orient their body such that the siphons are side-by-side in a plane perpendicular to the dominant current direction [171]. The researchers suggest that this orientation reduces the refiltration of fluid that has already passed through the

excurrent siphon. In fact, Monismith et al. (1990) found that significant refiltration occurred when the incurrent siphon of a clam mimic is downstream of the excurrent siphon. Clams that are subject to tidal flow with two dominant and opposite current directions, would decrease refiltration by orienting their siphons perpendicular to the current. Clam orientation does not seem to affect stomach content [158] which suggests that refiltration avoidance only partially explains the behavior.

Benthic infauna are not resource limited [172]. Virnstein (1977) studied the effects of predators on infauna determining that density and diversity of infaunal species increased when predators were not present. Predators control the local abundances of bivalves rather than food or space limitations. Hence, clam behavior that avoids predation would increase fitness more than behavior that controls conspecific interactions. Studies of clam behavior in reaction to predator cues imply that clams are able to change their feeding behavior to avoid being detected by specific predators ([150] and [151]). Changes in feeding behavior also change the chemical plume source characteristics. Prey that perceive predator cues stop feeding, which stops the chemical release through the excurrent siphons and may decrease predation events. Because clams change their behavior according to chemical cues, they also may be changing their behavior due to the hydrodynamic cues. Thorin et al. (1998) attempted to determine the types and frequency of siphon behaviors and found that *Mya arenaria* have siphons extended 85% of the time and that they do not extend their siphons above the sediment. These general clam behaviors appear to be part of the everyday activities of the organism and they additionally affect the source characteristics of the chemical plume.

2.3.3 Pumping, Filtering, and Growth

Clams feed on phytoplankton and other small organic particles in the water column by using their internal pump to pull water in through the incurrent siphon, filtering the

food particles out of the water, and releasing the filtered water back to the ambient fluid. The distinction between pumping, filtering, and clearance rates is often unclear in the literature and are often treated as synonyms. Pumping rates refer to the volume of water being pumped through the body of the clam over a specified time period. Whereas filtering rate is the amount of food particles removed from the pumped water. Clearance rates refer to the amount of food particle loss in the ambient fluid through the action of pumping bivalves. Although similar, these three parameters describe different aspects of clam feeding. Clam growth rates are dependent upon all three of the above aspects of feeding. The volume pumped, the amount filtered, and the amount of food available in the water column can all affect the growth and fitness of bivalves.

2.3.3.1 Pumping Rates, Direct and Indirect Methods

There have been two schools of thought when determining the pumping rates of clams and other bivalves, the direct method and the indirect method. The direct method either captures the liquid as it exits the clam siphon or otherwise determines the actual amount of liquid leaving the clam. The indirect method assumes that clams completely remove all food particles from the water as it passes through the body and the researchers measure the amount of particles present in the ambient fluid over time. The indirect method essentially equates the clearance rates and pumping rates assuming that the filtering rates are 100%. A recent example of the indirect method, using thermal correlation between the sediment, the fluid, and the body of the clam, attempted to determine bivalve pumping rates [38]. Defossez et al. (1997) determined that when the sediment and ambient fluid temperatures were sufficiently disparate, changes in the internal temperature of the clam were correlated with pumping activity. While the clam was actively pumping its internal temperature became more similar to the ambient fluid temperature; during times of inactivity, the internal temperature

more closely matched that of the sediment. While it is a novel study, it is highly intrusive and equates thermal gradients with pumping rates.

Until recently directly determining bivalve pumping rates has been quite difficult and the indirect methods proved to be the best proxy. Before the use of non-intrusive laser and sonar systems, and even before hot-wire anemometry was in widespread use, the direct methods were highly intrusive and not very environmentally relevant. For example, one study inserted a plastic tube into a mussel excurrent, ground down part of the shell, inserted another tube into the forced opening, and the entire mussel was embedded in plaster of paris [156]. With this apparatus, they captured the excurrent flow and compared it to the given incurrent flow. Their most significant finding was that mussels had resting periods during the pumping behavior every 3-4 minutes [156]. However, with the intrusive nature of the measurement the clams may not be behaving in a normal manner. A slightly less intrusive method slips a rubber cone over the body of the clam capturing only the excurrent siphon flow and leaving the incurrent siphon outside of the cone [44]. This method was used to determine that mussel pumping rates are not constant and have resting periods where the bivalve retracts and the redeploys the excurrent siphon [36]. Davids (1964) also found that as the concentration of particles in the ambient fluid increases, the pumping rate decreases. This could mean that because of the high concentration, the clam requires less flow to retain the same amount of food particles. The pumping rates could also decrease if the clam filter is being overwhelmed with food particles and pseudofeces must be expelled from the system. A very complicated example of the direct method introduces dye to the incurrent siphon at a rate that nearly overwhelms the incurrent siphon while the flow rate of the incurrent dye is monitored [30], it took several experimental attempts before clams would pump with the introduced dye. This study found that larger clams have larger average pumping rates, but they did not record the temporal variability in the pumping rate. De Bruin and Davids (1970) found

that bivalves vary their pumping rates over the long term between 250-300 ml/hr and they found that the thumb of a rubber glove was the best method for capturing the excurrent liquid. The direct methods described above have attempted to get actual pumping rates of bivalves without assuming that clearance rates are indicative of pumping rates. However, the direct methods described are highly intrusive not only in the flow, but to the organism itself. Hence, the results of these methods are not indicative of unimpeded clam behavior.

There are a few direct method measurements of bivalve pumping through the use of hot-wire anemometry and thermister probes. *Mercenaria mercenaria* excurrent velocities were collected using a hot-wire anemometer near the outlet of the siphon. Average velocities of 10 to 14 cms^{-1} were found and did not vary according to size of the clam [141]. A study of brachiopods (sessile, two-valved, marine animals) measured fluid velocity through the shells via the use of a temperature thermister [99]. The velocities found for brachiopods are not directly applicable to our system since the ambient water flows between the shells and not through siphons, but the measurement technique could be useful. Temperature thermisters and hot-wire anemometry are only intrusive to the flow and do not disturb the animal. Also, given that bivalve flow rates vary in both the short [156] and long [37] term, having a long time record of the pumping rates (rather than an average or point measure) is necessary. A non-intrusive measurement technique that quantifies clam excurrent pumping rates over large temporal scales at high frequency is needed for complete understanding of the pumping rates of bivalves.

2.3.3.2 Filtration and Clearance Rates

Hydrodynamics appears to affect both clearance rates and filtration rates. A review by Jørgensen (1996) details the lack of agreement among studies of bivalve filter feeding stating that the rate of filtering is not affected by the fluid dynamics as some

studies have concluded [85]. The review states that the effects attributed to hydrodynamics are actually the result of other experimental conditions. For example, there are a few studies that determined that higher concentrations of microorganisms (e.g., [102], [135], and [41]) or higher suspended silt concentration (e.g., [103]) in the ambient fluid correspond to lower filtration rates. These studies used indirect methods to determine pumping rates, assuming that 100% of the particles that entered the incurrent siphon were filtered out before leaving the excurrent siphon. The indirect methods are non-intrusive, but they employ a questionable assumption. Several studies attempted to determine how the ambient current affects the filtering behavior of bivalves with differing results. Some studies found that as ambient flow velocity increased, filtering also increased ([175] and [41]). Others found that filtering decreased with increasing ambient velocity [192] or that filtration first decreased and then increased with increasing velocity [28]. Temperature increases have been found to both decrease [175] and have no effect [41] on filtration rates. The discrepancy between the results of these studies is explained by Jørgensen (1996) as differences in the experimental conditions and that the behavior of the bivalves is based on environmental conditions.

Clearance rates also depend on additional environmental factors, such as the amount of turbulent mixing in the water column and the rates of fluid transfer at the benthos. A concentration boundary layer, i.e. a layer of fluid depleted of particles, is formed over beds of mussels when the water column is not fully mixed [2]. Frank et al. (2008) used Particle Image Velocimetry (PIV) and geometry of the excurrent siphon to compare the excurrent volumetric flow rate to the clearance rate of particles in the fluid. They found mean jet velocities of $2.4 \pm 0.14\ cm/s$ and maximum jet velocities of $4.8\ cm/s$, [58].

2.3.3.3 Growth and Velocity

Growth of mussels varies with season, location in bed, tidal zone, and geographic location [85]. All of these factors could be due to spatial or temporal characteristics of the flow hydrodynamics. The flow physics could control growth responses through changes in clam pumping ability, changes in pumping characteristics, the formation of concentration boundary layers, or other predator affects. Predators have certain hydrodynamic conditions in which they have heightened tracking success ([82] and [54]) and clams are able to modify their behavior in response to predators [150]. If clams are able to modify their behavior according to one environmental factor, the presence of predators, it follows that other environmental factors may also trigger behavioral changes. The infaunal worm, *Sipunculus sp.* changes from deposit feeding to suspension feeding with increased current velocity [157]. Therefore, clams could also modify their behavior in response to hydrodynamic conditions to modify their apparency to predators and increase fitness. Costs could be associated with different behaviors, some being more costly than others. Clams that behave one way may be expending more energy than those in different environmental conditions that do not trigger those behaviors. Therefore, it is important to know how hydrodynamics change the behavior of bivalves and what costs are associated with them.

There have been several studies that look at the effect of flow rate or current on the growth of bivalves, with mixed conclusions. Several studies found that bivalve growth rates increased as current velocities increased ([175] and [66]). Other studies found reduced growth rates with increasing ambient velocity ([3] and [191]). There is also a study that suggests that there is no effect of current speed on bivalve growth in the field [86]. The lack of consistency between these studies suggests that growth responses could be species specific. In fact, Ackerman and Nishizaki (2004) found that even though mussel growth rates decreased at higher ambient velocities, the degree of reduction was species specific. Both of the studies that suggest that growth rates

are positively correlated with ambient velocity (i.e., [175], [66]) and the field study that found no correlation (i.e., [86]) addressed the clam *Mercenaria mercenaria*. This suggests that *Mercenaria mercenaria* has a positive growth response to high currents, at least in laboratory studies. Other factors, besides growth, that could be affected by high cost behavior is the amount or quality of progeny produced by the bivalve. Troost et al. (2009) looked at growth rates of several native bivalves and compared that to those of an introduced oyster using a Particle Image Velocimetry (PIV) system. They collected PIV flow fields of the incurrent flow and modelled the exhalent flow to determine reasons for the disparate growth rates in different bivalve species [163].

2.3.4 Model Bivalves

Indirect methods overestimate the clearance rates by benthic organisms by assuming complete filtration of the incurrent flow and that the system is fully mixed over the water column [2]. Several flume experiments have been completed using clam mimics to determine actual clearance rates. The first used one clam mimic to determine the refiltration rates according to orientation of the siphon pair to the prevailing current direction [116]. They found that refiltration rates were larger when the excurrent siphon was upstream of the incurrent siphon [116]. The second study looked at the effect of a bed of model bivalves on the creation of a concentration boundary layer. They found that clams in dense beds could reduce refiltration by increasing siphon height and decreasing excurrent velocity with increasing ambient flow rate [131]. Refiltration is indicative of low mixing in the water column, which increases the likelihood of forming a concentration boundary layer. Increased mixing of the clam effluent with the surrounding fluid leads to less refiltration. With a decrease in refiltration by increasing siphon height and decreasing excurrent velocity with increasing ambient velocity, the chemical plume characteristics are altered. The release of

the chemical source has an impact on the downstream concentrations available to potential predators. The concentration boundary layer results in the laboratory flumes with clam mimics were confirmed by similar results over zebra mussel beds in Lake Erie [2]. Therefore, clearance rates are not necessarily equal to the pumping rates. The factors that affect the refiltration are clam density, the ratio of excurrent and ambient velocity, the height of the clam siphon, and the roughness Reynolds number, Re_* [133]. These factors are the source characteristics that modify the downstream chemical plume. A concentration boundary layer forms when there is not sufficient energy in the system to fully mix the water column. The momentum distribution of the boundary layer is affected by the presence of siphon mimics and the jet-like excurrent flow in laboratory tests [33] and field tests [84]. Therefore, the bivalves change the momentum distribution and mixing in the boundary layer.

2.4 Odorant Plume Structure

Chemical odorant plumes occur where there is a release of chemicals to flow, such as pheromone releases to attract mates, metabolite release from prey items, chemical leakage from unexploded weapons, sewage release in outfalls, releases of cooling water from power plants, etc. There have been many studies conducted to understand the nature of biologically-relevant chemical plumes and this section concentrates on the findings of those studies and how they contribute to the understanding of chemical plumes as a whole. The earliest attempts to characterize biologically-relevant chemical plumes studied odorant release to the air in arrangements modelled after the pheromones released by female moths to attract potential mates [124]. Murlis and Jones (1981) found that the odorant plume is not smoothly distributed and is made up of many odorant filaments rather than a constant concentration. Male moths locating females in such a plume are presented with many spikes or bursts of concentration and their sensory system must be tuned to this type of stimulus. Moth behaviors

highlighted above have been connected to the chemical plume characteristics [123]. Statistical predictions of plume concentrations may be useful in defining the nature of the chemical plume [123].

Later studies moved to aquatic environments with a focus on olfactory predation rather than pheromone tracking. The fundamental difference between moth tracking and the aquatic systems is that in moth studies the chemical source is promoting the tracking males. In the predator-prey systems the chemical source would have larger fitness values with deterrence of successful tracking. This may lead to different tracking strategies of the predators and different release strategies by the prey. Odorant plumes in the marine environment have odorant bursts with higher concentrations and greater onset slopes near the centerline and source of the odorant plume [118]. However, they also found that high concentration peaks and high onset slopes could be found very far from the source. This agrees with the results of Murlis and Jones (1981) for pheromone plumes in air.

The next steps in understanding the nature of chemical plumes was to quantify the plumes under different hydrodynamic conditions. Chemical plumes were sampled under two ambient velocities, at several different heights above the substrate and the results indicate that more discrete odorant pulses at all heights were present for higher velocities [121]. A field study confirmed the intermittency of the concentration and also found that the height of the concentration bursts decreases with distance from the source [202]. The time-averaged concentration gradients are stable and give an indication of the source location. However, the time scales necessary for time-averaging are much longer than the predators are using to make tracking decisions [57]. The tracking organisms of this system are not using the time-averaged concentrations for navigation in the chemical plumes. There must be other types of source directional information that the chemical plumes provide to the predators. Webster et al. (2001) determined that if the sensors of the predator are spatially separated by a distance

Table 2.2: Tracking mechanisms and example organisms from Vickers (2000).

Mechanism	Description	Organisms
chemotaxis	chemically modulated orientation	bacteria
rheotaxis	up-current mechanical orientation	crustaceans
anemotaxis	up-wind mechanical orientation	moths

of at least an integral length scale, the instantaneous concentration gives indication of the relative location of the plume centerline. Predators using this type of sensor comparison would use instantaneous concentration samples to locate prey, rather than a time-averaged concentration.

Fluid velocity is not the only factor that modifies the concentrations of the plume. Sediment characteristics and obstacles present in the flow contribute to turbulence. A flume study of chemical plumes downstream from a marsh grass mimic found that the mimics altered the odorant filament characteristics ([55] and [101]). Increasing the size of the bed roughness elements decreases the variance of the fluctuations [142]. Source characteristics also affect the plume such as release location, release velocity, and release diameter [177]. Since the release characteristics affect the plume, prey items may be able to control their chemical releases to control the information in the downstream plume. Clams may be able to reduce predation by changing their behavior, such as the velocity of their excurrent flow, the height and diameter of their siphons, and the flow conditions in which they choose to feed.

2.5 Tracking Organisms

Studies over the past few decades describe the importance of understanding the flow physics that mediate animal navigation during olfactory tracking [178]. The mechanisms involved in chemical plume tracking are chemotaxis, rheotaxis, and anemotaxis [168], see Table 2.2.

Organisms of all size scales from bacteria to macroorganisms use these mechanisms to extract information about their environment and move toward high resource areas,

[117]. A basic understanding of chemo- and rheo-tactic behavior through study of the tracking organisms and robotic mimics, give researchers a better understanding of animal perception and behavior [9]. There are many similarities between the tracking behaviors of organisms that are characteristic of olfactory tracking in general. However, the differences may highlight strategies particular to the hydrodynamic conditions that each species encounters.

2.5.1 Examples of Tracking Organisms

The dependence of olfactory navigation on flow physics is demonstrated by comparing the predation strategies and sensory mechanisms of several animal species [182]. Organisms track in air and water and span a large range of size scales, and they consequently use many receptor types and behaviors to manipulate ecological interactions [200].

2.5.1.1 Moths

The most documented ecological tracking system is the male moth tracking the pheromone plumes released from female moths. Females release their pheromones to the atmosphere and the chemicals advect down wind. When odorant filaments are encountered by male moth chemosensors, one of several tracking behaviors is initiated [169]. There are many research studies that breakdown the particular behaviors associated with moth tracking and the mechanisms that trigger them. For example, Baker and Kuenen (1982) used wind tunnels to determine that when air flow stops, male moths zigzagged along the stationary plume and that when the chemical source was removed they flew in wider paths [11]. They concluded that wider paths were an attempt to reconnect with the lost odorant plume. Another study determined that moths have an ideal frequency of chemical encounter; in fact, with higher levels of turbulence, moths took straighter and more direct paths to the odorant source [105].

Moth tracking behaviors have been correlated with firing rates of male antennal neurons [10]. The examples above are only a few of the many studies quantifying the behavior of moths and the cues embedded in pheromone chemical plumes. Moths are able to extract the necessary information with brief exposure to the pheromones. Therefore, accurate quantification of the chemical plume is the key to understanding moth tracking dynamics [169].

2.5.1.2 Crayfish

Crayfish rely on their sense of olfaction for orientation in their environment with a heavy dependence on chemo- and mechanosensors located on multiple appendages [63]. Crayfish were found to have better success in locating a food source with decreased search time in artificial streams with increased turbulence intensity [119]. Several studies of crayfish olfaction have concentrated on how the characteristics of the chemical source, under differing turbulence regimes, altered tracking success. Chemical source characteristics, such as location, height, and proximity, modified the downstream chemical plume [91]. Keller et al. (2001) also found that the chemical source arrangement modified crayfish search behavior with higher tracking efficiency when sources were separated. Crayfish were also found to have decreased success in locating the source of a pulsed plume compared to a continuously released plume [96]. These two studies suggest that the characteristics of the chemical source greatly influence tracking success and efficiency. Therefore, the information available to the predator is dictated by a combination of the way the chemicals are released and the characteristics of the ambient flow.

2.5.1.3 Stomatapods

Stomatapods are predatory crustaceans that sample odors by flicking their antennules to locate food, mates, and shelter [110]. Several tracking studies have used an

interdisciplinary approach to quantify the concentrations and velocities at the antennae. Researchers used Laser Induced Fluorescence (LIF) in a study to quantify the concentrations at the antennae of actively tracking stomatapods [110]. Their study found that in laboratory cases of wave-affected flow stomatapods were presented with sharper, longer, and more numerous odorant bursts than in unidirectional flow, which results in more efficient tracking [110]. Wave motion and unidirectional flow, therefore, are associated with specific tracking behaviors. This suggests that the information embedded in the odorant plumes, which dictate the behavior, is also specific to those flows. These researchers also completed a study using Particle Image Velocimetry, PIV, to quantify the flow surrounding the antennules during the forward and backward flicking motion [109]. They found that the velocity passing the antennules was much faster during the outward flick than the return stroke resulting in directionally specific boundary layer and concentration profiles. They hypothesized that sampling occurs during the outward flicking motion. To better understand the velocities and concentrations sampled by stomatapods, model antennae were constructed [108]. The researchers compared results from antennae models with field studies and previous lab experiments. Due to the flicking, the volume of water sampled at the ends of the antennae is larger than at the base, and sample volumes at both locations are higher than stationary antennae would sample [108].

2.5.1.4 Lobsters

Lobsters are another example of an intensively studied organism that uses antennule flicking. An early study established lobsters as tracking organisms by inducing different behavioral responses to turbulent chemical plumes in a flume as opposed to a controlled stimulus pattern [120]. They recorded three orientation responses that correlated with plume encounter, distance orientation, and local food search. Virtual antennae sensors were designed and tested by Crimaldi et al. (2002) to model the

interception of chemical signals by lobsters. Flicking of the antennas increases the frequency of signal encounter and creates a two-dimensional sample of the scalar concentration distribution [32]. Antennae flicking increases the volume of water sampled, the area of plume sampled, and the frequency of bursts sampled. Sensor flicking modifies potential odorant encounter, hence it is a mechanism that is similar to the use of multiple sensors by crayfish and crabs and the zigzagging pattern of male moths. Studies of neuron response of lobster antennae have been reviewed , and the authors conclude that although lobster systems are less complex than mammal sensory systems the insights gained from using them as test organisms are applicable across a wide range of species ([42] and [75]).

2.5.1.5 Snails and Whelks

Snails and whelks are slowly moving predators that could increase their sampling volumes by sampling over larger temporal periods [138]. A field study proposed that the composition of amino acids released from prey items were controlling the predatory response by mud snails [201]. They determined that the flux of amino acids, rather than the specific amino acids present, was responsible for the tracking behavior of mud snails. Therefore, the release flux had more effect on tracking than other plume characteristics, such as chemical composition or instantaneous concentration. This implies that larger individual prey, larger aggregations of prey, or injured prey may be more attractive to mud snails due to elevated release flux of attractive chemicals. This idea is supported by the fact that slowly moving whelks have equal or higher tracking success in more turbulent flow in both field studies and laboratory flume studies ([138] and [54]).

2.5.2 Blue Crabs

This study is focused on the predator–prey interaction between the blue crab, *Callinectes sapidus*, and clam, *Mercenaria mercenaria*. Blue crabs are a fast moving,

macroorganisms that use olfactory navigation to find clam (and other) prey. Tracking is a habitat specific behavior [117], and blue crabs have varying success according to the characteristics of the habitat [82].

2.5.2.1 Success and Preference of Blue Crabs

The success and efficiency of blue crabs tracking to clam prey is dependent on both the flow physics and the presence of chemical cues [187]. Laboratory studies determined that blue crabs had low success and low efficiency during tracking events under fully rough bed-turbulent flow regimes compared to smooth bed-turbulent flow regimes ([186], [187], and [82]). These studies determined that blue crabs tended to move slower, have higher degrees of turning, and less contact with both the plume and the source under more intense turbulent flow conditions. The researchers suggest that under hydrodynamic conditions that are not conducive to predatory tracking success, prey items may be in a hydrodynamic refuge. However, a hydrodynamic refuge from one predator may not be a refuge from another predator species. Recall that several of the predators presented above; crayfish, snails, and whelks; had equal or greater search success in more intense turbulent flows.

A field study, although rudimentary, confirmed that clams had higher rates of mortality due to predation by blue crabs under what they termed as "reduced flow rates" compared to "enhanced flow rates" [138]. Their results suggest that the laboratory data of Weissburg and Zimmer-Faust (1993, 1994) are relevant to ecology in the field. However, another field study that quantified crab tracking success found that crabs had very little success under zero to low flow conditions, but success remained high under all other flow speeds [56], despite the fact that they used flow categories that matched those of Weissburg and Zimmer-Faust (1993, 1994). They found that crab success does not diminish and that the crabs walked in straighter paths toward the source with increasing flow velocity. These results directly contradict the laboratory

results of Weissburg and Zimmer-Faust (1993, 1994).

The laboratory studies of Weissburg and Zimmer-Faust (1993, 1994) and the field results of Powers and Kittinger (2002) used pumping live clams as their tracking stimulant. The odorant sources used by Finelli et al. (2000) were cracked clams, cracked clam amino acid mimics, cracked oysters, and cracked oyster amino acid mimics; they did not find a significant difference in tracking success among these odorant treatments. One explanation for the discrepancy may be that tracking success is highly dependent upon the specific source chemicals. Cracked clams and intact clams release different chemicals to the surrounding fluid [201], and cracked clams scent may be more attractive to blue crabs. A second explanation is that source flux controls predation rates. Source characteristics such as pulsing have been determined to affect predatory success of blue crabs [92]. Source chemical flux is much higher for injured prey items, which could give fundamentally different chemical plume characteristics and increase the information in the plume. However, blue crabs prefer clams of a small size range, despite the fact that they can consume prey over a wide range [114]. This suggests that crabs prefer to find small clams that release small amounts of chemicals compared to large clams that have higher flux rates. If blue crabs are looking for small, easily eaten prey, then larger chemical flux would not be a stimulus for tracking that would be advantageous for blue crabs to track. A third explanation is that laboratory results fail to explain field phenomenon [138]. A final explanation is that there is a trade-off between the hydrodynamic effects and the source characteristics effects. With a large chemical release, blue crabs may not have diminished success in high turbulence environments. Alternatively despite low turbulence, low chemical release rate may also hinder predation success. This suggestion is supported by the results of Jackson et al. (2007) in which crab tracking was less affected when the source concentration was very high and highly affected with a low concentration source.

2.5.2.2 Chemical Sensors

Crustaceans, such as blue crabs and crayfish, have multiple sensors located on their appendages. The advantages of multiple sensors are an increase in the range, area, and volume of sampled water; an additive effect of the neuronal responses across the sensors; an ability to maintain foraging in the face of sensor damage or loss; and the tailoring of sensors to specific chemicals or flow conditions [43]. The location of sensors that have specific roles in the tracking process may be tailored to the information available in those positions.

Blue crabs have sensors on both their legs (thoracic) and antennules (cephalic) that are responsible for sampling different aspects of the chemical plume. Leg sensors are suggested to be responsible for transverse steering and near source localization, while antennules sensors control upstream movement within the narrowing plume [90]. Blue crabs use their antennules sensors to move upstream within the plume. Once close to the source, they use their leg sensors that are close to the sediment to do a localized search for the prey item. The multiple sensors allow chemical sampling in a large range of locations and separation distances. In fact, laboratory studies of chemical plume characteristics suggest that there may be an ideal separation distance between sensors [176]. If crabs separate their sensing appendages at a distance larger than an integral length scale, as suggested by Webster et al. (2001), they would be able to compare the samples from each appendage and determine where the plume axis is located in relation to their body location [176]. This comparison allows tracking crabs to maintain their position within the plume.

Blue crabs are known to modify their body angle to increase the separation distance between sensors despite a corresponding increase in the drag force [185]. This suggests that blue crabs are turning their bodies to maximize their comparative abilities between sensors. It also suggests that the drag forces, although not minimized,

are not powerful enough to hinder upstream motion. When flow rates are high, however, drag and lift forces on the crab body may be powerful enough to hinder crab tracking ability. This may help to explain the laboratory results of [186] and [187] that crab success decreases in higher turbulence intensity regimes. Crab tracking may be hindered by drag and lift forces in high flow rates rather than the chemical concentration signal in the plume. A recent study was able to decouple turbulence from flume velocity and found that crab tracking was still less successful in higher turbulence regimes with similar flow velocities to low turbulence regimes [82]. This suggests that the presence of high drag and lift forces is not the dominant reason for lowered crab success in high turbulence intensity flow.

2.5.3 Predator Mimics

The research described above suggests that each tracking organism has sensors and behaviors tailored to the specific source and hydrodynamic characteristics that they encounter. In the design of chemical tracking machines it would be limiting to model the behavior of only one species of animal [63]. Tracking machines should be able to locate chemical sources in a wide range of flow conditions and spatial and temporal scales. There may be advantages to combining the tracking behavior of multiple organisms. It may also be important to incorporate the specific physical characteristics of the tracking organisms, such as flicking appendages or spatially-separated multiple sensors [43]. The following sections describe simulations of robot algorithms and trials of actual robots that mimic animal tracking behavior.

2.5.3.1 Simulations and Algorithms

There have been several biologically-inspired algorithms proposed for tracking to a chemical source through a moving fluid. Many early algorithms were based on moth tracking of pheromone plumes due to the abundance of research on moths. One study compared simple algorithms of increasing complexity to the success rates in

moth tracking events under the same source and flow conditions [12]. This study found that the simulations were, at best, less than half as successful as moths at finding the source. However, even the simplest algorithms appeared to mimic actual moth tracking and were successful at least some of the time [12]. Another example of a study based on simple algorithms is composed of simulations tracking in a simple chemical gradient [45]. The algorithms of this study were inspired by tracking microorganisms, such as amoeboid cells, and macroorganisms, such as echinoderms. These organisms have very simple behaviors that allow them to move up the chemical gradient. Dusenbery (2001) found that the model of tropotaxis gave the best results in moving toward the source. However, this simulation modelled a smooth gradient of concentration, rather than a turbulent flow regime. As a result, this study has limited applicability for biomimectic robots. Crab and crayfish tracking behavior can be taken into account by adding multiple chemosensors and mechanosensors to the algorithms. Simulations that use both chemosensors and mechanosensors have found that tracking performance is significantly dependent upon the weightings of the different types of sensors [183]. Therefore, both chemical and mechanical information is important for tracking and should be incorporated into the simulation algorithms. Having only one type of sensory mechanism limits the tracking ability of either an organism or robot due to the unpredictability of the fluid motion [62]. Under the best of circumstances, not all of the sensory modalities will provide information consistently, and therefore it is advantageous to have multiple sensory strategies built into the tracking simulations.

2.5.3.2 Robots

Robot tracking trials have not performed as well as simulations suggest and, therefore, are much less successful than animal tracking [62]. This is attributed to the unpredictability of the natural environment and our current inability to completely

understand the nature of the information contained in chemical plumes. Two simple algorithms were tested by a biomimetic robot lobster that used only the difference in concentration between two sensors [64]. These algorithms did not have flow sensors and the trials revealed that the tracking events of the robot did not resemble lobster tracking and had little success locating the chemical source [64]. The trials confirm that mechanosensors are an integral part of the tracking process.

Olfactory navigation is highly dependent on both the chemical and hydrodynamic information embedded in the chemical plume. More sophisticated robot tests include the use of mechanosensors to determine fluid velocity [50] and [51] and sensors for vehicle position, depth, altitude, attitude, and speed [100]. In fact, these studies found that a binary chemosensor was sufficient rather than a more sophisticated and sensitive sensor. The first of these three studies used underwater autonomous vehicles (AUVs) to map possible source locations using real-time data gathered by the vehicle [50]. Given possible vehicle failure, or loss of plume signal, the AUV can determine the statistical likelihood of the source location using the already gathered plume information. This system, although based on tracking animals, is much more sophisticated than earlier biomimectic robots. The researchers found that robots with many types of sensors and the ability to store statistical information are much more successful at source location than their less sophisticated predecessors [51] and [100]. This confirms that the interaction between animal tracking and plume characteristics is a complicated process.

2.6 Contributions of Current Research

It is hypothesized that clam fitness increases when clam metabolites are mixed to the degree that deters predation by blue crabs, and that the predator–prey interaction dictates clam behavior. Therefore, bivalves may be promoting the mixing of their metabolites in the chemical plume by altering the chemical source characteristics

and/or the boundary layer characteristics. The momentum distribution of a boundary layer flow may be controlled, at least in part, by actively pumping bivalves or even the presence of non-pumping bivalves. The effects may be specific to the type of sediment and the proximity of other bivalves (oyster reefs) or vegetation. It is further expected that the clam effects have relatively more influence during times of low ambient turbulence.

Hence, this study quantifies the effect of the presence and behavior of clams on the boundary layer flow over natural sediments in the field. To decouple the behavioral and physical aspects of clam influence, this study determines the effect of environmental conditions on the pumping behavior. Hence, this study quantifies the clam excurrent according to the flow regime and/or the presence of predators.

CHAPTER III

METHODS

3.1 Field Boundary Layer Measurements

3.1.1 Animal Collection and Storage

Hard clams (*Mercenaria mercenaria*) were collected in Wassaw Sound near Savannah, Georgia, USA (Figure 3.1). Collection occurred during low tide in the intertidal region of Cabbage Island where Ferner et al. (2009) has characterized the soil here with 85% sand, 3% silt, and 10% clay. Clams were collected in close proximity to beds of *Spartina sp.* and within 7.5 - 10 *cm* of the sediment surface, see Figure 3.1. Collected specimens were transported to a flow-through-tank facility at Georgia Tech's Priest Landing Marine Facility within 4 hours of collection. Clams were housed in a tank filled with sea water pumped directly from Wassaw Sound and fed on microorganisms in the sea water. Within 3 to 4 days of collection, clams were returned to Wassaw Sound and replaced with newly collected specimens.

At least one hour prior to velocity data collection, clams were placed in the sediments directly below and upstream of the instrument measurement volume (see Figure 3.2). Specimens were placed halfway buried in the sediments with the siphon end upward and were allowed to completely bury themselves. Each treatment had between 16 and 20 clams buried with equal spacing in an area of 0.38 m^2 below one of the two measurement devices used in each data collection event (see Figure 3.2).

3.1.2 Measurement Locations

Five field sites were employed for collection of vertical measurement sequences with and without the presence of *Mercenaria mercenaria*. The field sites were representative of the types of habitats in which clams can be found in Wassaw Sound and

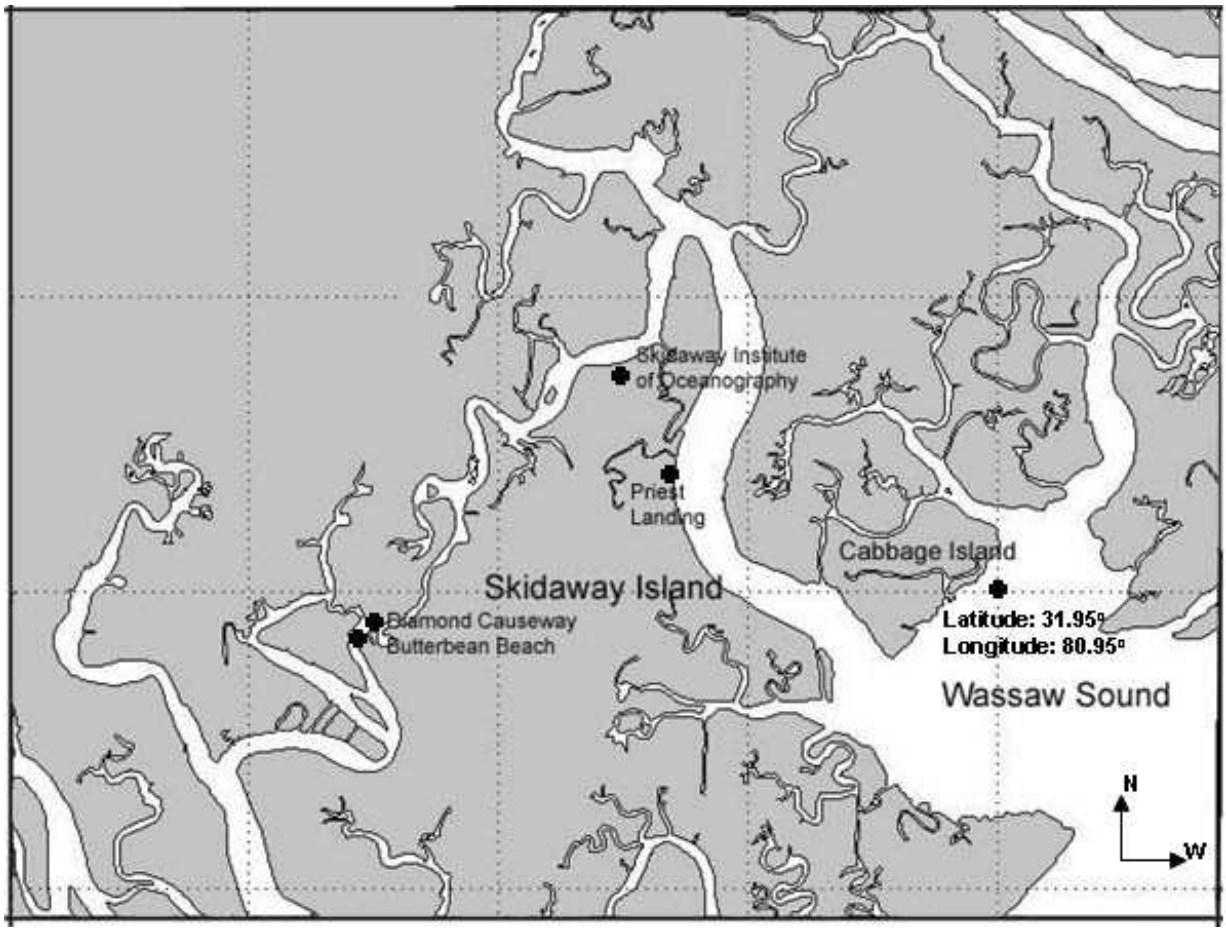

Figure 3.1: Map of Wassaw Sound and surrounding tidal creeks and islands

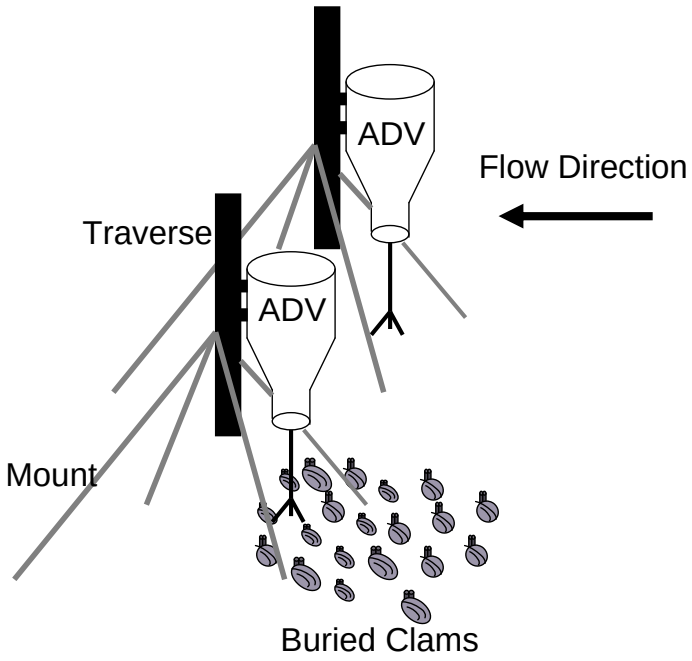

Figure 3.2: Schematic of ADV deployment. The measurement locations for the two probes were separated by 1.0 m, and 16 to 20 clams were buried below and upstream of one of the probes.

adjacent tidal rivers. The treatment sites are located in Wassaw Sound at the entrance of the Wilmington River (four sites shown in Figure 3.3 and Figure 3.4) or at the border of the Skidaway River Narrows and Moon River (Figure 3.5). See Figure 3.1 for the relative location of the Priest Landing and Butterbean Beach sites. For all sites, the flow is primarily in one dominant direction (along the channel).

The sediment in Wassaw Sound consists of a mud and sand mixture that is referred to here as "mud" (Figures 3.6 and 3.7) and is characterized by Ferner et al. (2009) at their House Creek site to contain 50 % sand, 18% silt, and 31.1 % clay. At average low tides, the mud flats in this area are exposed and two measurement devices were deployed, in close proximity using the horizontal homogeneity assumption, [164], for each data collection. One ADV of the pair had clams buried within the underlying sediments. Data collection began after the probe tips were submerged by the incoming tide.

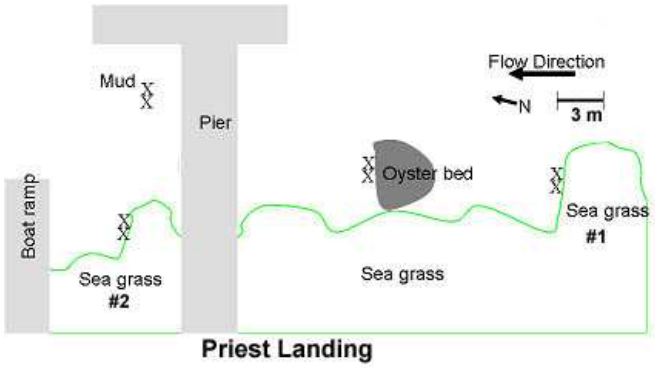

Figure 3.3: Plan view diagram of treatment sites at Priest Landing. The crosses represent the locations where ADVs were placed for data collection. This diagram does not include the sand treatment site.

Figure 3.4: Photograph of the boat launch and pier at Priest Landing.

Figure 3.5: Photograph of the sand treatment site at Butterbean Beach in the Skidaway River Narrows. The Diamond Causeway appears in the upper-left portion of the photograph.

Figure 3.6: Photograph of a human leg sinking in the sediment at Priest Landing. The sediment is a mixture of sand and mud and is referred to as mud in this thesis.

Figure 3.7: Photograph of the mud treatment site at Priest Landing during a higher than average low tide (the treatment site is covered by seawater). The sediment at this site is mud without shell hash. Oysters and sea grass are not present at this site.

Clams also are found in sediments that contain more sand than mud. This treatment is referred to as "sand" and is one of the dominant substrate types on Cabbage Island, Figure 3.1, where clam specimens were collected. The sand site was adjacent to the Diamond Causeway Drawbridge off of the Isle of Hope in the Skidaway Narrows on the County Park Beach (also known as Butterbean Beach) that is inland from Wassaw Sound (Figures 3.1 and 3.5).

The two additional sites incorporated naturally occurring obstacles in the flow in Wassaw Sound. Clams are often found in the sediment surrounding oyster beds (Figure 3.8). The oyster bed used for data collection was approximately 3 m in diameter (Figures 3.3 and 3.9). The sediment adjacent to the oyster beds in this area was composed of mud.

Clams also can be found in Wassaw Sound adjacent to *Spartina sp.* (sea grass) beds (Figure 3.10). Two sea grass treatment sites were selected for this study, shown in Figure 3.3. The measurement devices were deployed directly downstream of the sea grass beds and the sediment was characterized as mud (Figures 3.11 and 3.12), see Table 3.1.

Figure 3.8: Photograph of oysters growing on a cinder block at Priest Landing.

Figure 3.9: Photograph of the oyster bed treatment site at Priest Landing.

Figure 3.10: Photograph of sea grass, *Spartina sp.*, at Priest Landing.

Figure 3.11: Photograph of the sea grass #1 treatment site at Priest Landing at low tide.

Figure 3.12: Photograph of the sea grass #2 treatment site at Priest Landing at low tide.

3.1.3 Measurement Equipment

The measurement equipment consisted of two Acoustic Doppler Velocimeters (ADV's) and two field mount traversing mechanisms. The ADV's used in this study are SonTek/YSI Acoustic Doppler Velocimeter Autonomous (Hydra) systems. One probe was a 16-MHz ADV, and the other was a 10-MHz ADV. These probes previously were used in Ferner et al. (2009) to compare measurements that were separated by a distance of 5 m. The 16-MHz probe had a sampling volume of 0.09 cm^3 with a sampling distance of 5 cm from the acoustic transmitter, a resolution of 0.01 cms^{-1}, and an accuracy of 1% of measured velocity, which corresponds to ± 0.25 cms^{-1} for the three-component velocity data. The 10-MHz probe had a sampling volume of 0.25 cm^3 and a sampling distance of 10 cm from the acoustic transmitter, with all other factors being the same as the 16-MHz probe. The velocity and time were recorded according to the sampling rate specified by the user, yielding a velocity time record for the measurement volume. For the ADV's used in this study, the measurement volume could not be any closer to the sediment than $z = 1.013$ cm according to the criteria reported by Precht et al. (2006). Field mount traversing devices were used to control the height of the ADV's (Figure 3.2) with a screw crank that adjusted the height of the measurement volume by 2 mm for each revolution of the crank. The distance from the probe to the measurement volume was verified in a laboratory flume before field deployment. The ADV probe was manually placed in the initial position at low tide using standard measurement equipment to within a half a millimeter. The traverse was manually operated from an inflatable boat located downstream of the ADV's.

3.1.4 Data Collection

Data were collected between July 31, 2008 and September 2, 2008. Table 3.1 summarizes the data collected. Two measurement devices collected velocity time records

nearly simultaneously and the centers of the measurement volumes were separated by a traverse distance of 1.0 m, which is within the assumed range of validity of the horizontal homogeneity assumption (for description of this assumption see Section 2.1). One measurement device had clams buried in the sediment below and directly upstream of the measurement volume. The other measurement device collected velocity measurement sequences without the presence of clams in the sediment. The ADV probes were deployed at the measurement site at low tide and clams were placed in the sediment and allowed to bury.

The ADV probes measured all three components of velocity. The ADV probes were aligned such that the x-axis (u velocity component) aligned with in the principal direction of flow, downstream along the channel. The transverse direction (y-axis and v velocity component) had a positive direction toward the left bank of the tidal river as you faced inland. The z-axis (w velocity component) was aligned as positive upward from the measurement volume center. The water depth was at least 10 cm when data collection began, and often, due to surface wave action, the beginning water depth was larger. When the data collection began the depth was at least 10 cm and the measurement volume was approximately 1 to 1.5 m from the shoreline. At the end of the data collection, the water depth was approximately 2 to 2.5 m deep and 15 to 30 m from the shoreline.

The ADV probes collected velocity data at the height of the measurement volume for periods of 300 s with a sampling frequency of 10, 16, or 25 Hz depending on the collection event (specified in Table 3.1). Ferner et al. (2009) used a burst time of 120 s with collection frequencies of 10 and 16 Hz for similar sites in Wassaw Sound and repeated the measurements over 8 weeks with 6 measurement collections. They determined that this was a representative collection time over the tidal cycle for the time records to have stationary statistics. Smee et al. (2008) used 240 s burst collection periods for another similar field site within Wassaw Sound. Stationary statistics for

time records are determined by first collecting a time record of much greater length, determining the statistical measures for the time record, and decreasing the collection time while the statistical values remain unchanged. After the 300 s collection period of this study, there was a 60 s adjustment period in which the handle of the traversing mount was turned by the operator and the measurement volume was moved vertically to a new measurement location. Since there were two ADV's deployed during each data collection, time record bursts from individual ADV's were paired with their sister bursts from the same data collection event and were matched for time collected and height of the measurement volume. The collection periods for the two probes were offset by either 150 s or 60 s depending on the deployment (specified in Table 3.1). Data were collected at the following measurement volume heights z = 1.3, 1.7, 2.2, 2.8, 3.5, 4.3, 5.2, 6.2, 7.3, 10, and 14 cm or z = 1.3, 1.7, 2.2, 2.8, 3.5, 4.3, 5.3, 7.0, and 10 cm with $z = 0$ at the sediment surface. Complete vertical sequences took up to 66 minutes to collect and were consistently collected during flood tide. Over that time period the tidal change was quite significant, which indicates that the vertical measurement sequences do not correspond to a snapshot of a boundary layer profile. Rather the vertical measurement sequence corresponds to the characteristics of the velocity over the full 66 minute period.

3.1.5 Data Analysis

A time record processing procedure was used to remove low correlation value bursts, sample spikes in the record, and energy due to wave motion [14]. Individual bursts were discarded if the correlation coefficient reported by the software had an average value below 70 for the entire burst. The threshold value of 70 was specified by the probe manufacturer. A spike filtering process was used to remove and replace bad data points through the phase-space threshold method described by Goring and Nikora (2002). This method uses the assumption that in phase space good data

Table 3.1: Summary of the ADV field data collection during Summer 2008 in Wassaw Sound and the tidal rivers of Skidaway Island and Isle of Hope, Georgia.

site	ADV	sample frequency (Hz)	#clams	#bursts collected	date	sample start time	ADV pair offset (min)	sample end time	low tide	high tide
mud	10MHz	10	-	21	8/6/08	8:45 am	3	12:08 pm	6:53 am	1:39 pm
mud	16MHz	16	20	21	8/6/08	8:42 am	-	12:05 pm	6:53 am	1:39 pm
sand	10MHz	25	20	9	9/2/08	6:37 pm	1	8:06 pm	5:20 pm	11:36 pm
sand	16MHz	25	-	9	9/2/08	6:36 pm	-	8:05 pm	5:20 pm	11:36 pm
oyster	10MHz	10	-	9	8/8/08	9:27 am	3	11:08 am	8:17 am	3:16 pm
oyster	16MHz	16	18	9	8/8/08	9:24 am	-	11:05 am	8:17 am	3:16 pm
seagrass #1	10MHz	10	16	11	8/11/08	1:15 pm	3	3:14 pm	10:55 am	5:48 pm
seagrass #1	16MHz	16	-	11	8/11/08	1:12 pm	-	3:11 pm	10:55 am	5:48 pm
seagrass #2	10MHz	10	-	14	8/26/08	1:04 pm	1	4:34 pm	11:15 am	5:48 pm
seagrass #2	16MHz	16	20	14	8/26/08	1:03 pm	-	4:33 pm	11:15 am	5:48 pm

cluster together and that points that lie outside of this cluster are spikes that should be removed. The replaced values are used only for the wave energy removal process described below and are not included in the turbulent flow statistics calculations.

Next, the principle direction of flow was calculated at the highest point in the measurement sequence (consistent with the procedure of Nikora et al. 2002), and data at each measurement location in the sequence were rotated to align with this direction. Rotation of the velocity time records maximizes the u velocity and aligns the two measurement devices [130]. Further, the rotation, based on the highest point in the measurement sequence, allowed for all points in the sequence to have the same coordinate axis for direct comparison of turbulence characteristics at each height above the substrate.

Finally, the time record processing procedure removed the wave energy from the velocity time record using spectral decomposition [17]. Bricker and Monismith (2007) assume that the wave energy and turbulence energy do not overlap in scale. The wave energy can be removed from the power spectral density by assuming that the peak in the power spectral density curve represents wave energy. By removing this peak, they assume that the remaining energy can be attributed to turbulence. Without removal, wave energy can mask the turbulent kinetic energy of a system and give false values for turbulence quantities. This is a particular problem in relating turbulence characteristics calculated in the field to those calculated in laboratory flumes without wave energy inputs.

Turbulence characteristics for each height in the measurement sequence were calculated for the processed velocity time records, specifically the average velocity , turbulent kinetic energy ($TKE = \frac{1}{2}(\overline{u'u'} + \overline{v'v'} + \overline{w'w'})$), and Reynolds stress ($\overline{u'w'}$).

3.2 Bivalve Excurrent Velocity Measurements

3.2.1 Animal Collection and Storage

Clams were collected at the Skidaway Institute of Oceanography near Savannah, Georgia during summer months. Collection occurred during low tide in the intertidal region of Cabbage Island in close proximity to beds of *Spartina sp.* and within 7.5-10 cm of the sediment surface. They were transported to the Georgia Institute of Technology Environmental Fluid Mechanics Laboratory within 24 hours of collection. During the winter months, clams that were imported from Florida were purchased from the Dekalb Farmers Market in Decatur, Georgia. Clams were housed in an aquarium filled with artificial sea water with salinity between 28 and 35 *ppt*. Sand covered the bottom of the aquarium to allow clams to acclimate to laboratory conditions and bury themselves. The aquarium temperature was maintained at room temperature (roughly 22 degree Centigrade) and the pH was approximately 8.0. Clams were fed every other day during data collection periods with commercially available slurry of live phytoplankton (DT's Live Marine Phytoplankton) purchased from local aquarium/pet stores. After several weeks the clams were replaced by fresh organisms.

3.2.2 Flow Facility

The flow facility was an artificial seawater flume located in the Environmental Fluid Mechanics Laboratory at the Georgia Institute of Technology (Figure 3.13). This biological-grade flume was 0.76 m wide and 13.5 m long with a level bed. The bed was covered with a thin layer of sand with a median diameter of $d_{50} = 1.1\ mm$. The side walls of the flume were constructed of acrylic for optical transparency. A centrifugal pump recirculated artificial seawater through the flume. The flow depth was controlled by the height of a downstream sharp edged weir, and the flow rate was

calculated via the Kindsvater-Carter equation for rectangular weirs, [95], as

$$Q = \frac{2}{3}\sqrt{2g}C_{de}L_e H_e^{\frac{3}{2}} \tag{3.1}$$

where

$$L_e = L + k_L \tag{3.2}$$

$$H_e = H + k_H \tag{3.3}$$

$$C_{de} = 0.602 + 0.075\frac{H}{P} \tag{3.4}$$

and $k_H = 0.001\ m$, $k_L = 0$ (for the weir width equal to the width of the channel), H = height of fluid above weir, P = height of weir, L = width of the weir.

The test section was located 6.2 m downstream of the flume entrance. A 7.8 cm by 45.7 cm by 118.7 cm false bottom section filled with sand was located in the center of the test section, and the sand depth for the remainder of the flume is 2.9 cm. The false bottom section allowed for clams to bury themselves within the sediment and feed naturally.

The bulk flow rates employed for the experiments are $U = 0.55$, 1.2, 1.98, and 2.86, cms^{-1}, as measured by determining the depth of the fluid and calculating the velocity using the Kindsvater-Carter sharp weir equation, [95]. The roughness Reynolds numbers were less than 10 for each case.

3.2.3 Particle Image Velocimetry

3.2.3.1 PIV Equipment

Particle Image Velocimetry, PIV, was used to quantify the clam excurrent velocity. PIV is a non-intrusive means of determining planar velocity fields in moving fluids. This method uses a laser sheet to illuminate seeding particles in a plane while a camera captures images of the particles (Figure 3.13). Sequential PIV images are used to determine the particle displacement and velocity in the illuminated plane.

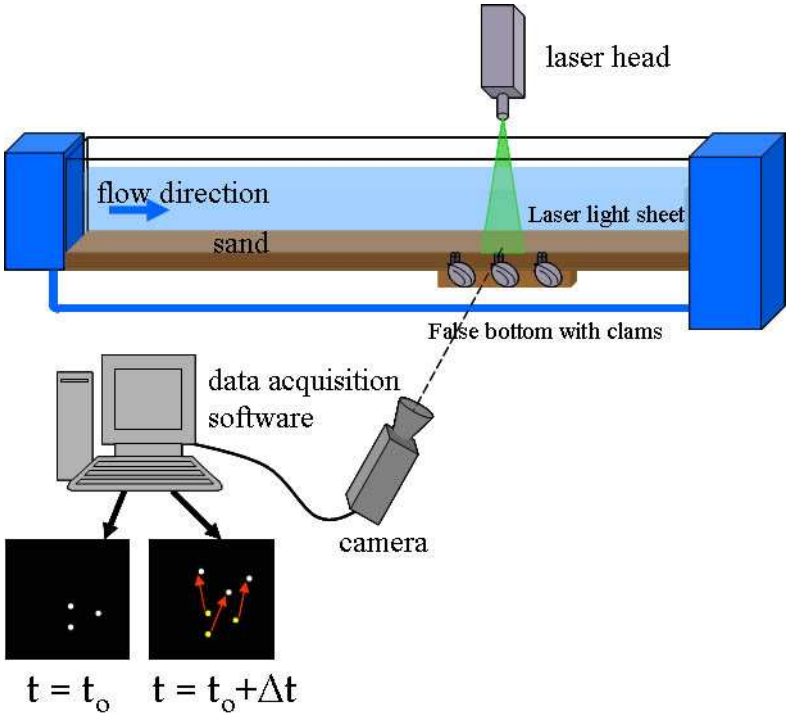

Figure 3.13: Schematic of the laboratory sea water flume and set up for the Particle Image Velocimetry (PIV) system. Clams were buried in sand sediment in a false bottom section that was 7.8 *cm* deep, whereas the sediment in the majority of the flume bed was 2.9 *cm* deep. The Nd:YAG laser was located above the flume and was pointed downward. The PIV camera was located beside the flume and viewed the measurement section through the acrylic side wall.

Previously, the PIV technique has been used to determine the flow fields around organisms and their appendages (e.g., [109], [21], and [136]).

The laser was a double head Solo III manufactured by New Wave Research with a wavelength of 532 nm, 50 mJ of energy per laser pulse, and an exiting beam diameter of 4 mm. The beam passes through a system of lenses that form a planar laser sheet (specifically, a symmetrical convex lens of 0.5 m focal length and a planar-concave cylindrical lens with a 19 mm focal length). The laser was mounted above the flume and the laser sheet passes through the fluid surface of the flume above the excurrent siphons of the feeding bivalves (Figure 3.13). The water surface was smooth and temporally constant, which led to minimal variation of light transmittance.

Particles of titanium dioxide (< 5 μm diameter) were suspended in the fluid, move with the flow, and were illuminated in the laser sheet. Several types of seeding particles were tested to determine which would be most useful in these experiments. Clams are filter feeders and remove particles from the flow of certain size ranges and organic content, [163]. We tested the following types of seeding particles: corn starch, kaolin, titanium dioxide, and several types of glass balls. Titanium dioxide resulted in a good balance between the number of particles passing through the clam and suitable illumination by the laser sheet. Titanium dioxide was also used by Frank et al. (2008) in their clam jet PIV experiments and do not appear to influence the clam behaviorally.

Images of the illuminated particles were captured on a monochrome Kodak Megaplus camera model ES 1.0 with a dual channel eight-bit digital output and a Charged Coupled Device (CCD) sensor array. The camera used a Nikon MicroNikkor lens with a 60 mm focal length and outputted images of 1024 by 1024 pixels with image sizes specific to each image capture series. Both the laser and camera were triggered by a precision pulse generator (Berkeley Nucleonics model 500D). Image pairs were captured at a frequency of 10 Hz and a delay of 10 ms between images of the pair was employed.

The images were captured by a Coreco SE Series frame grabber board with a 10,000 kbytes host frame buffer and a 2 system memory frame buffer configured to work with Windows 2000. An image required roughly 1 Mbyte of system space and the images are stored on a hard drive array using Video Savant software (IO Industries). A typical image sequence file used roughly 4.6 Gbytes of memory depending on the number of images collected. Also an error propagation analysis was completed and the uncertainty in the velocity measurements is 0.98 mms^{-1}, which is roughly 2% of the measured velocity values. Seeing that the fluctuations are on the same order as the mean velocity values, the uncertainty in the velocity values is quite small.

3.2.3.2 PIV Analysis

The PIV algorithm determined the fluid velocity at discrete points in the images and was written by Dasi (2004) based on several earlier PIV algorithms, [31], [189], and [69]. Details of the algorithm are provided by Dasi (2004) and are summarized here. First, a background image file was created for the even and odd images of the pairs. The background image was subtracted from the individual images in order to increase the contrast of the particles. The images were then spatially divided into 32 $\times$ 32 interrogation bins and a cross-correlation analysis was performed between the first and second image in the pair. A Gaussian peak fit analysis was performed on the cross-correlation data to determine the displacement vector between images. In a second pass, the interrogation bins in the first and second image were shifted by half of the displacement estimate backwards and forwards, respectively, to "center" the interrogation bin region in the individual image. The correlation analysis was repeated and a new estimate of the displacement vector was calculated. The centering process was repeated until the interrogation bin position correction was less than 0.005 pixels. The displacement vectors were then divided by the delay period between laser

pulses (10 ms) to yield the velocity vector. The velocity fields created by the cross-correlation analysis contain a few bad vectors associated with the edges of the image or noise. The bad vectors were removed via a temporal filtering procedure. The filter assumes a Gaussian distribution for the magnitudes of the velocity vectors and removes samples that do not correspond to within 3 to 4 times the standard deviation for that interrogation bin.

3.2.4 Data Collection Procedure

Clams of the desired size range are placed on the sediment of the flume false bottom with desired nearest neighbor distances and allowed to bury themselves under low flow conditions. For an individual clam (see numbered clams in Table 3.2), data were collected for 450 s for a randomly chosen bulk velocity value. The bulk velocity in the flume was changed to another of the four targeted velocity values after the first data collection is complete. This was repeated until the organism has experienced all targeted bulk velocity values. During collection, events such as siphon movement, organism interference, etc., were recorded so that those events can be removed from the time record analysis.

3.2.4.1 Laboratory Flume Experiment with Size and Nearest Neighbor Distance

The experimental parameters and the individual clams that were used are displayed in Table 3.2. PIV images were collected for a plane that bisects the clam excurrent siphon for clams of two size ranges, 4.86 $\pm$ 0.22 and 7.32 $\pm$ 0.32 cm, clam plots with two nearest neighbor distances, 3 and 9 cm , and four bulk velocity values, 0.55, 1.2, 1.98, 2.89 cms^{-1}. This first set of experiments attempts to quantify clam pumping behavioral responses that correspond to these factors. Clams may alter their pumping behavior according to their proximity to other clams because of the potential for refiltration of fluid or the additive predation potential with the downstream chemical plume. Also, juvenile or small clams have higher predation pressure from blue

Table 3.2: Summary of treatments employed for the first set of experiments designed to examine the influence of nearest neighbor distance (NND), horizontal crossflow velocity, and clam size.

		NND = 3 cm				NND = 9 cm			
focal	length	Crossflow velocity (cms^{-1})				Crossflow velocity (cms^{-1})			
clam	(cm)	0.55	1.2	1.98	2.86	0.55	1.2	1.98	2.86
1	4.68	×	×	×	×	×	×	×	×
2	5.16	×	×	×	×	×	×	×	×
3	4.92	×	×	×	×	×	×	×	×
4	4.6	×	×	×	×	×	×	×	×
5	4.92	×	×	×	×	×	×	×	×
6	7.3	×	×	×	×	×	×	×	×
7	7.54	×	×	×	×	×	×	×	×
8	6.91	×	×	×	×	×	×	×	×
9	8.57	×	×	×	×	×	×	×	×

crabs, which may influence their feeding behavior. Finally, since predator success is dependent on hydrodynamic conditions, prey behavior also may be dependent on hydrodynamic conditions.

After time records were recorded for the clams of this experiment, the nearest neighbor distances are altered and the clams were allowed to rebury themselves. The velocity measurements were repeated for varying bulk velocity treatments.

3.2.4.2 Laboratory Flume Experiment with Predator Effects

The second set of lab experiments collected PIV images for clam excurrent siphon velocities for clams with the size range of 4.63±0.15 cm, clam plots with a nearest neighbor distance of 3 cm, four ambient velocity values, 0.55, 1.2, 1.98, and 2.89 cms^{-1}, with predators (blue crabs) caged in the upstream flow or cages without predators in the upstream flow. The predators were caged upstream of the clam plot and had been recently fed a diet of frozen shrimp. It has been shown that predator cues in the upstream flow alter feeding behavior by inducing clams to reduce feeding or stop feeding altogether, [151], and that clams have diminished reaction to predators with higher rates of ambient turbulence, [150]. Predator cues in the flow may induce

Table 3.3: Summary of treatments employed for the second set of experiments designed to examine the influence of upstream predator and horizontal crossflow velocity.

clam	length (cm)	predator	Crossflow velocity (cms^{-1}) 0.55	1.2	1.98	2.86
1	4.76	no	×	×	×	×
2	4.76	no	×	×	×	×
3	4.60	no	×	×	×	×
4	4.45	yes	×	×	×	×
5	4.45	yes	×	×	×	×
6	4.76	yes	×	×	×	×

behavioral responses in the feeding clams according to the hydrodynamic conditions. Blue crabs have varying predation success in certain hydrodynamic conditions and clams may alter their feeding behavior depending on the physical characteristics when they detect the presence of predators. Therefore, PIV images were collected for clams for the four horizontal velocity values with and without predators in the flow and the experimental parameters are reported in Table 3.3.

3.2.4.3 Laboratory Flume Control PIV Data

Three types of control data sets were collected in the laboratory flume for comparison with the above data sets, (Table 3.4). First, a control data set was collected above the clam plot without clams present to understand the effects of bumps and pockets in the sediments. Second, PIV images were captured above an empty clam shell to simulated the effects of a non-pumping clam on the PIV images for all four of the horizontal velocity values above. Third, two data sets were collected for a man-made vertical jet (diameter of 0.95 cm) with two jet exit flow rates, 0.467 cm^3s^{-1} and 0.0 cm^3s^{-1} and bulk velocities equal to those above. The jet Reynolds number values for the two flow rates are within the range of those collected for the clam jets.

Table 3.4: Summary of control treatments employed.

	Jet flow rate (cm^3s^{-1})	diameter (cm)	Crossflow velocity (cms^{-1})			
			0.55	1.2	1.98	2.86
No clam, no jet			×	×	×	×
Clam shell only (6.99 cm)			×	×	×	×
Clam mimic	0.467	0.95	×	×	×	×
Clam mimic	0	0.95	×	×	×	×

3.2.5 Velocity Time Record Extraction

The sequence of velocity vectors for one interrogation bin were extracted to create a velocity time record for a point in the flow field. A point was chosen to correspond to the excurrent jet region of the flow in order to extract a velocity time record for the siphon vertical velocity. The point chosen varied according to the siphon location, siphon height, ambient velocity, and sufficient numbers of seeding particles, hence the extraction process required considerable manual observation of the images by the researcher. Clams move their siphons while feeding by changing the height, width, and direction; they even close their siphons and open them again on a frequent basis [156]. Also, for larger ambient flow velocities, visually locating the siphon jet within the flow field becomes increasingly difficult for the researcher. Therefore, the location of the extraction point depended on the individual organism and time record. There was little evidence that a systematic (i.e., programmable) method of determining an extraction point in the flow would give consistent results for this highly variable biological system.

Since clam pumping behavior was variable, part of the time record did not contain excurrent velocity information and was removed from the time record analysis. During resting periods, when the clam closed the excurrent siphon, the velocity time record did not provide velocities associated with the excurrent. The measured vertical velocity during the resting periods was due to the ambient flow. Further, recorded

values were removed from the velocity time record when the researcher could not identify the location of the excurrent jet. This occurred more often during larger ambient flow treatments. Other times, the presence of feces or pseudo-feces interferes with the seeding particle recognition by the PIV code. With all of these situations and behaviors removed from the time record, the remaining data were a reliable capture of clam excurrent velocity behavior. The amount of data that must be removed is highly dependent on the ability of the researcher to locate the clam jet in the images and varies greatly with the crossflow velocity.

3.2.6 Time Record Analysis

3.2.6.1 Spectral Analysis

Spectral analysis was employed to evaluate whether the time records of excurrent velocity possess periodicity. Fourier transform methods, or spectral analysis, are a statistical approach used to quantify the periodic aspects of a time record and is especially applicable to turbulence measurements. The Fourier transform equations allow one function to have two representations, one in the time domain and one in the frequency domain. The relationship between the two representations is the Fourier transform pair,

$$H(f) = \int_{-\infty}^{\infty} h(t) e^{-2\pi i f t} dt \qquad (3.5)$$
$$h(t) = \int_{-\infty}^{\infty} H(f) e^{2\pi i f t} df$$

where $h(t)$ is a function in the time domain and $H(f)$ is the same function in the frequency domain with t measured in seconds and f measured in Hz or cycles per second. The frequency domain can also be measured in angular frequency rather than Hz with the following formulae.

$$\omega \equiv 2\pi f \qquad (3.6)$$

Thus, Equation 3.5 becomes

$$H(\omega) = \int_{-\infty}^{\infty} h(t) e^{i\omega t} dt \tag{3.7}$$
$$h(t) = \frac{1}{2\pi} \int_{-\infty}^{\infty} H(\omega) e^{-i\omega t} d\omega$$

Often the time domain function is sampled at discrete points and is not a continuous function. With N consecutive sampled values separated by Δ interval in seconds the values of frequency will also be discrete rather than continuous.

$$f_n \equiv \frac{n}{N\Delta}, \qquad n = -\frac{N}{2}, ..., \frac{N}{2} \tag{3.8}$$

The maximum and minimum values of n in Equation 3.8 correspond to the Nyquist frequency values. Waves must be sampled twice during a cycle, which limits the frequencies that can be captured during discrete sampling. The Nyquist frequency is the limit frequency that the Fourier transform will resolve. If the time function is bandwidth limited to frequencies smaller than the Nyquist frequency, then the continuous function is completely described by the samples [140]. If the function is not bandwidth limited within the Nyquist range, the power of the function outside the range will be aliased, or falsely attributed, to frequencies within the Nyquist range [140]. The discrete Fourier transform pair becomes

$$H(f_n) = \sum_{k=0}^{N-1} h_k e^{2\pi i f_n t_k} \Delta = \Delta \sum_{k=0}^{N-1} h_k e^{2\pi k n/N} \tag{3.9}$$
$$h_k = \frac{1}{N} \sum_{n=0}^{N-1} H_n e^{-2\pi i k n/N}$$

The spectrum of the time record is defined as the Fourier transform of the autocovariance with the time lag as the independent variable. The first step is to define the time average of the velocity time record as

$$\langle U(t) \rangle \equiv \frac{1}{T} \int_0^T U(t) dt \tag{3.10}$$

with T being the time interval. The fluctuation is defined as

$$u(t) = U(t) - \langle U(t) \rangle \tag{3.11}$$

and the time average of $u(t)$ is zero. The autocovariance is

$$R(s) \equiv \langle u(t)u(t+s)\rangle \tag{3.12}$$

where s is the time lag. The autocovariance is independent of t because the time record is stationary. The autocovariance has a Fourier Transform pair as

$$\begin{aligned} R(s) &= \int_{-\infty}^{\infty} E(\omega)e^{i\omega s}d\omega \\ E(\omega) &= \frac{1}{2\pi}\int_{-\infty}^{\infty} R(s)e^{-i\omega s}ds \end{aligned} \tag{3.13}$$

where $E(\omega)$ is the spectrum of the stationary time record.

The Fourier transform algorithm is computationally expensive and is cumbersome to use. The Fast Fourier Transform (FFT) algorithm was developed to compute a discrete Fourier transform with fewer computations than the original algorithm. The FFT algorithm outlined in Press et al. (1986) was used in the current research. Plotting the spectrum versus frequency reveals the relative amount of the time record variance that can be explained by a periodicity at a particular frequency.

3.2.6.2 Fractal Analysis

Fractal analysis was employed to evaluate the random nature of the time record of excurrent velocity. While studying the hydrology of the Nile River Basin, H. E. Hurst noticed that when the river discharge was high, there was a tendency for the next years' river discharge to also be high. He concluded that long records of natural phenomenon tend not to be random [77]. The values of rainfall, temperature, and discharge, were more correlated with each other than independence predicts. Hurst was able to suggest an equation that relates the range of values and a time lag to an exponent with a mean value of 0.73 [76].

$$\frac{R}{\sigma} = \left(\frac{N}{2}\right)^{H} \tag{3.14}$$

where R is a range, σ is the standard deviation from the range, and N is the number of samples in the time record. The exponent, H, is specific to the natural phenomenon

and time record in question. The first to use the H component and equation for time record analysis was Mandelbrot (1968) when he proposed the concept of fractal Brownian motion [106]. Equation 3.14 subsequently has been applied to time records as diverse as three-phased fluidized beds, economics, and stock market predictions [49].

Fractal analysis is a statistical tool that uses the concept of self-similarity at multiple scales, and the fractal dimension relates a spatial scale to the self-similar behavior [153]. The analysis is called Hurst's rescaled range analysis, giving values of the Hurst exponent, H. The H exponent is related to the fractal dimension through the following formula:

$$d_{fl} = 2 - H \tag{3.15}$$

with d_{fl} defined as the fractal dimension. The Hurst's rescaled range analysis yields a fractal dimension of the time record between a one dimensional line and a two dimensional plane. Random walk or Fractional Brownian motion has time record values with "jumps" or "step sizes" with magnitudes corresponding to Gaussian white noise and the Hurst's rescaled range analysis is a measure of the randomness of the differences in the values of the time record. Let $B(t)$ be an equally spaced time record (in this case, a clam jet velocity time record). The time record of step sizes $X(t)$ is defined by $X(0) = 0$ and $X(t) = [B(t) - B(t - \Delta t)]$. $c(t, u)$ is the cumulative departure of $X(t + y)$ from the mean $\langle X(t)\rangle_s$, for the subrecord where $u = 1, 2, ..., s$ and s is the time lag, and y is a time value from 1 to u,

$$c(t, u) = \sum_{y=1}^{u} [X(t + y) - \langle X(t)\rangle_s] \tag{3.16}$$

the sample range of $X(t)$ for lag s is:

$$R(t, s) = \max_{0<u\leq s} c(t, u) - \min_{0<u\leq s} c(t, u) \tag{3.17}$$

and the sample variance of $X(t)$ is:

$$S^2(t,s) = \frac{1}{s}\sum_{u=1}^{s}\{X(t+u) - \langle X(t)\rangle_s\}^2 \tag{3.18}$$

giving the rescaled range Equation [49]:

$$\frac{R(t,s)}{S(t,s)} \propto s^H \tag{3.19}$$

In practice, H is calculated via Equation 3.19 and the fractal dimension of the time series is then determined using Equation 3.15. The Hurst value is determined by the slope of a least squares regression of a plot of $\frac{R(t,s)}{S(t,s)}$ versus the time lag, s. Mandelbrot (1968) termed this type of plot a pox diagram, and an example is given in Figure 3.14.

Values of the fractal dimension between $1 \leq d_{fl} < 1.5$ indicate that the time series has long term persistence or correlation. A fractal dimension between $1.5 < d_{fl} \leq 2$ has anti-persistent or anti-correlative properties. In the case of $d_{fl} = 1.5$, the time series has completely random step sizes as with random walk or fractional Brownian motion [134]. As the value of the fractal dimension approaches 1.5 from above or below, the time record becomes more random. There are other methods proposed to determine the Hurst exponent, such as using a detrending moving average [8], but the method described above fits the needs of this research. Estimates of the fractal dimension are averaged over the ensemble of time records to yield an ensemble averaged value of d_{fl} for each treatment case.

Pox diagrams are also useful in confirming the results of the spectral analysis (Figure 3.14). There are two phenomena that may occur in a pox diagram when there is a dominant frequency in the time record [49]. At large time lag values, corresponding to low frequencies, there will be a discontinuity in the slope of the pox diagram when there is a dominant low frequency present in the time record. When there is a dominant high frequency in the time record, the values on the pox diagram will be more closely spaced at time lag values that are the reciprocal of those

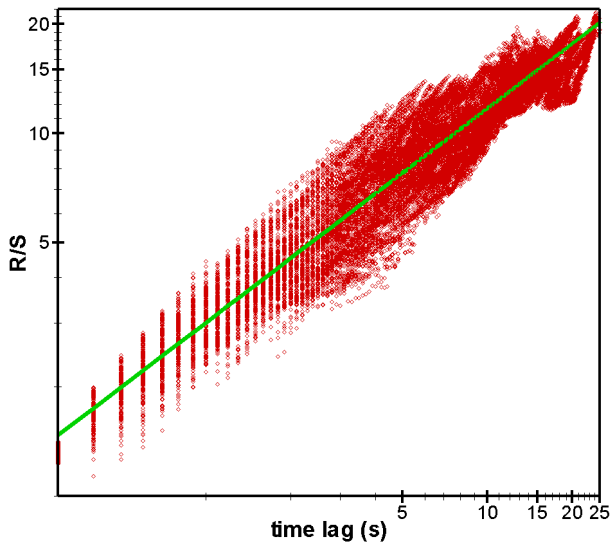

Figure 3.14: Example pox diagram. The H value for this case is 0.575 yielding a d_{fl} of 1.425.

frequencies. These characteristics may be used to reiterate the presence or lack of periodicities in the velocity time records of the clam excurrent.

3.2.6.3 Lacunarity Analysis

Lacunarity analysis is employed to quantify the "look" of the distribution or quantify the size and location of the "space" between values of the velocity. While the fractal dimension is considered a measure of how much space is filled or the amount of "mass" within a geometric space, lacunarity is a measure of how the space is filled with that mass. Lacunarity is a means of quantifying the "texture" of distributions that appear very different, yet have the same fractal dimension, [5]. Figure 3.15 shows an example of two "carpets" with the same fractal dimension but the image on the left is more "lacunar" since it has larger size gaps [107].

Lacunarity analysis has been extended beyond the description of the distribution of fractals to spatial distributions of real data sets and multifractals, [137]. Historically, lacunarity analysis has been used to describe the heterogeneity of binary data sets, which is a function of the fraction of sites that are occupied, the size of the box

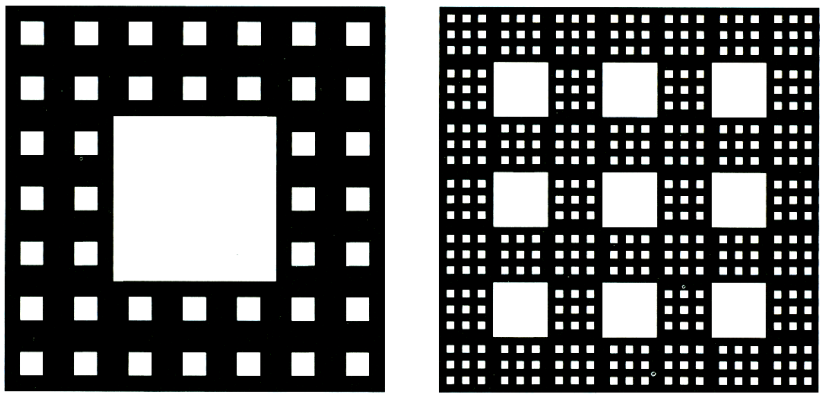

Figure 3.15: Sierpinski carpets from Mandelbrot (1977) have the same fractal dimension value and differing textures. The carpet on the left is more "lacunar" since it has larger size gaps

space of interest, and the geometry of the data set [137]. Plotnick et al. (1996) extended the binary analysis of the gliding box method proposed by Allain and Cloitre (1991) by applying it to quantitative data by summing the distribution within the box of interest.

Tolle et al. (2003) proposed a new method of calculating the lacunarity of a data set due to the limitations of the gliding box method that more directly measures the spatial gaps. However, an extension of the gliding box method is sufficient for the type of data sets in this study [159]. The Allain and Cloitre (1991) method chooses a unit box of size r and adds the values in the box, p (i.e. the integral of the velocities in our case). Since the analysis was first used for binary data, where there are no negative values, the velocity record must be shifted to contain only positive values. In practice this is accomplished by subtracting the lowest velocity value from each value in the discreet time record. The negative consequence of not shifting the record is that the average mass (or first moment) may approach zero for some values of the gliding box, which leads to an erroneously large lacunarity estimate. After shifting the record, the gliding box is centered on each point in the data set and the values within the box are summed, resulting in a distribution of box masses, $B(p, r)$. The distribution is converted into a probability distribution function by dividing by the total number of boxes, $B(r)$:

$$Q(p, r) = \frac{B(p, r)}{B(r)} \tag{3.20}$$

The first and second moments of the probability distribution are calculated:

$$Z^{(1)}(r) = \sum_{p} pQ(p, r) \tag{3.21}$$

$$Z^{(2)}(r) = \sum_{p} p^2 Q(p, r) \tag{3.22}$$

The gliding box lacunarity is defined as:

$$\Lambda_{GB}(r) = \frac{Z^{(2)}(r)}{Z^{(1)}(r)^2} \tag{3.23}$$

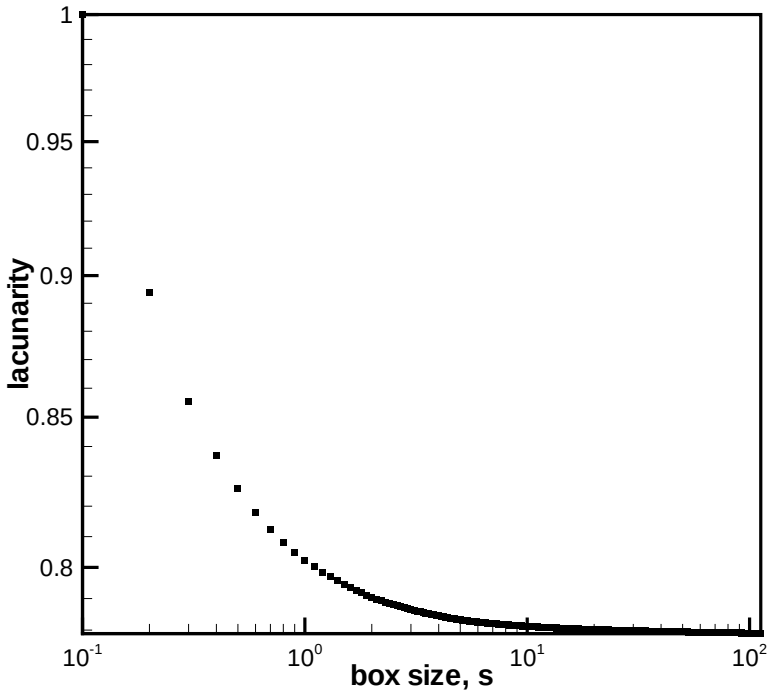

Figure 3.16: Lacunarity as a function of box size (i.e., time segment) for Gaussian white noise.

Tolle et al. (2008) reduced the lacunarity expressions further to reduce the computational expense. The moments are then calculated:

$$Z^{(1)}(r) = \frac{1}{B(r)} \sum_{i=1}^{B(r)} p(i,r) \tag{3.24}$$

$$Z^{(2)}(r) = \frac{1}{B(r)} \sum_{i=1}^{B(r)} p(i,r)^2 \tag{3.25}$$

Lacunarity is then calculated using Equation 3.23.

Lacunarity is plotted versus the log of the size of the box, r, see Figure 3.16 which is the lacunarity plot for a white noise time record. Pure fractals have a linear lacunarity plot (example shown in Figure 5.12), and non-fractals have distinct breaks in the lacunarity plot at spatial scales of significance (example shown in Figure 5.13), or are concave up as for random values of gap sizes in the distribution (example shown in Figure 5.11).

CHAPTER IV

FIELD EXPERIMENTS ON IMPACT OF CLAMS ON CROSSFLOW

This chapter presents the velocity measurements collected in the field for the simultaneous clam versus no clam bed treatments. Results are presented for each of the five sites: mud substrate, sand substrate, downstream of oyster bed, and downstream of sea grass bed #1 and #2. These sites are representative of the conditions in Wassaw Sound and the shallow tidal estuary. As described in the Methods Chapter, all bursts and measurement sequences were processed for low correlation, spike removal, and wave energy extraction. The resulting data consist of one or two measurement sequences for each site, where the measurement sequence consists of simultaneously collected time records of velocity at sequential elevations above the bed. The diagram in Figure 3.3 depicts the location of the mud, sea grass, and oyster bed sites and the sand site is indicated in Figure 3.1. With the incoming tide, the sea grass bed site #1 is the farthest upstream of all of the treatments at Priest Landing. The oyster bed site is roughly 30 m downstream of the sea grass bed site #1. Farther downstream and farther into the main body of water is the mud treatment site. Finally, the second sea grass site is more shoreward and slightly downstream of the mud site. The sand site is located much farther inland.

4.1 Results for the Mud Site

Mud is the predominant substrate in the region around Priest Landing, where most of our measurements were taken. In fact, measurement sites presented in following

sections with upstream obstacles (i.e., oyster bed or sea grass bed) possess mud substrate also. Therefore, other than the sand treatment site, the results for the mud site can be considered benchmark results or results that do not include structures in the flow.

The ADV's captured two sequential sequences for the mud site during an incoming tide. Without clams present the velocity measurement sequences should be typical of those captured over mud substrates in similarly shallow, relatively small estuaries. They should be comparable to laboratory velocity profiles over fine grained sediments; although, the tide is coming in as the measurements are collected and the measurement sequences do not represent a snap-shot of the boundary layer profile. Also, since it has been shown that the largest velocities in small estuaries occur just before and after low tide (Trevethan et al. 2008), the average velocities recorded later in the collections should be smaller values than those recorded in the beginning of the collection as is shown in Figure 4.1. While the data have been rotated to maximize the velocity vectors in the dominant flow direction, the rotation for the entire measurement sequence is based on that calculated for the collection point that is highest in the water column. Therefore, the longitudinal velocity component may not be maximized throughout the measurement sequence and it is important to take into account the transverse velocity component.

Higher in the water column the velocity values with and without clams tend to follow one another closely with a slight decrease in the mean velocity values when clams are present (Figure 4.1). Close to the substrate the velocity measurement sequences tend to be quite disparate when compared to the differences higher in the water column, Figure 4.1, particularly for the longitudinal velocity values. Figure 4.2 is a plot that is designed to show disparities between the velocity values collected with the ADV's, and this type of plot is used throughout this chapter. The velocity values collected simultaneously at the same elevation are plotted against one another and the

colors represent the height of the measurement volume above the substrate. When the ADV's collect similar velocity values, the symbols fall directly on the solid black line, and the distance of the symbol from the solid line indicates the difference in the velocity values collected with and without clams buried in the sediment. A pairwise comparison with a students T-test shows that the majority of the values collected for the cases with and without clams buried in the sediment are significantly different, most likely due to the large number of samples. The very few cases in which the values are not significantly different, the symbol falls on the 1-to-1 line in the plot. When plotted against each other, the average velocities for the mud case with and without clams tend to deviate more from each other closer to the sediment, Figure 4.2. In Figure 4.2(a), the U velocity appears to be larger without clams near to the bed. This implies that the behavior and presence of clams may decrease the ambient velocity of the boundary layer close to the sediments and has less influence higher in the water column. In fact, Figure 4.2(b) shows that both the V and W average velocity components also appear to be smaller in magnitude when clams are present closer to the sediment. The vertical velocity is in the downward direction and Figure 4.2(c) shows that clams are adding vertical momentum to the crossflow, particularly near the sediment. Clams appear to reduce the magnitude of the downward vertical velocity, possibly through the vertically upward excurrent feeding jets.

For comparison, histograms of the probability density functions for the mud case with and without clams for u' and w' velocity values at a height of 2.2 cm above the sediment have been included in Figures 4.3 and 4.4. These histograms appear to be symmetric and approximately Gaussian in shape.

From Figures 4.1 and 4.2, the clams do not seem to impact the average velocity values higher in the water column as much as near the sediment. This supports the assumption of two-dimensional flow at the top of the measurement sequence and justifies the decision to rotate the velocity values over the entire measurement

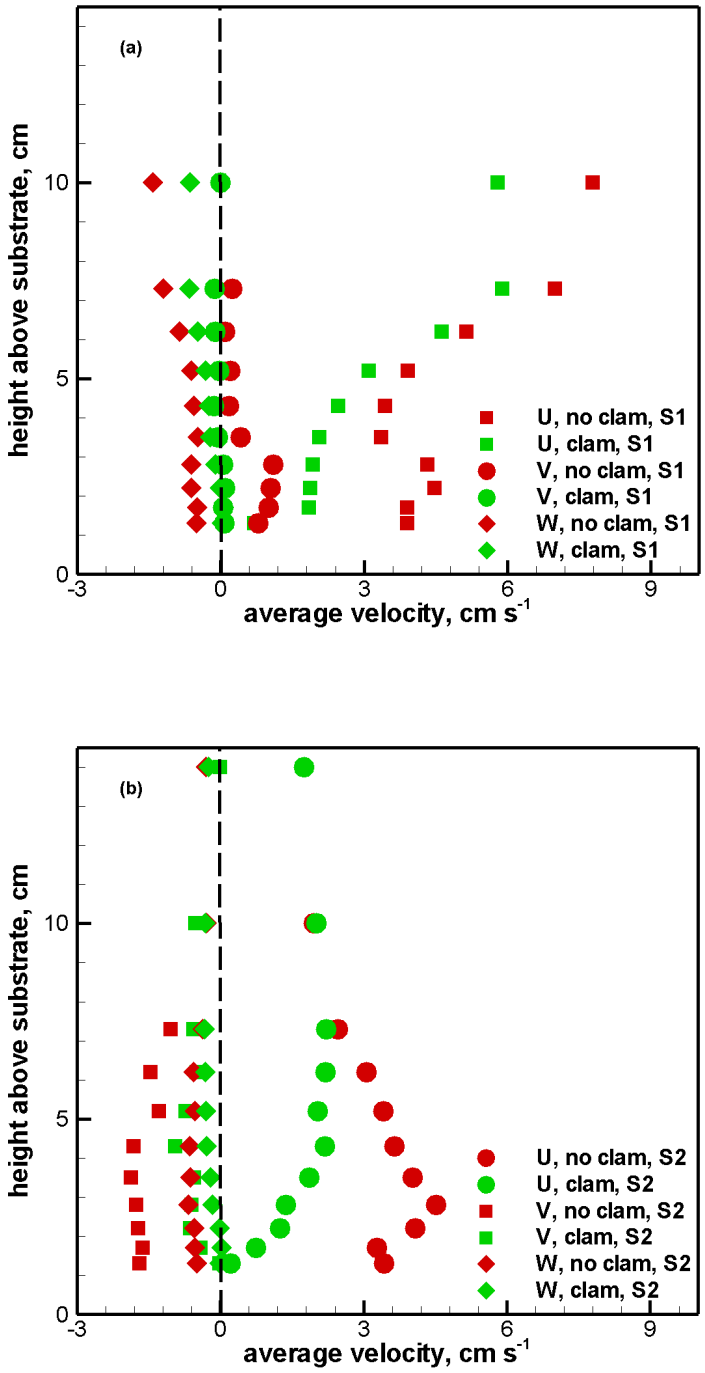

Figure 4.1: For the mud site, vertical measurement sequences of the average horizontal velocity components, (a) the first measurement sequence, S1 and (b) the second measurement sequence, S2. Samples with and without clams buried in the sediment were collected simultaneously at matching elevations. "S1" indicates measurement sequence #1, and "S2" indicates measurement sequence #2.

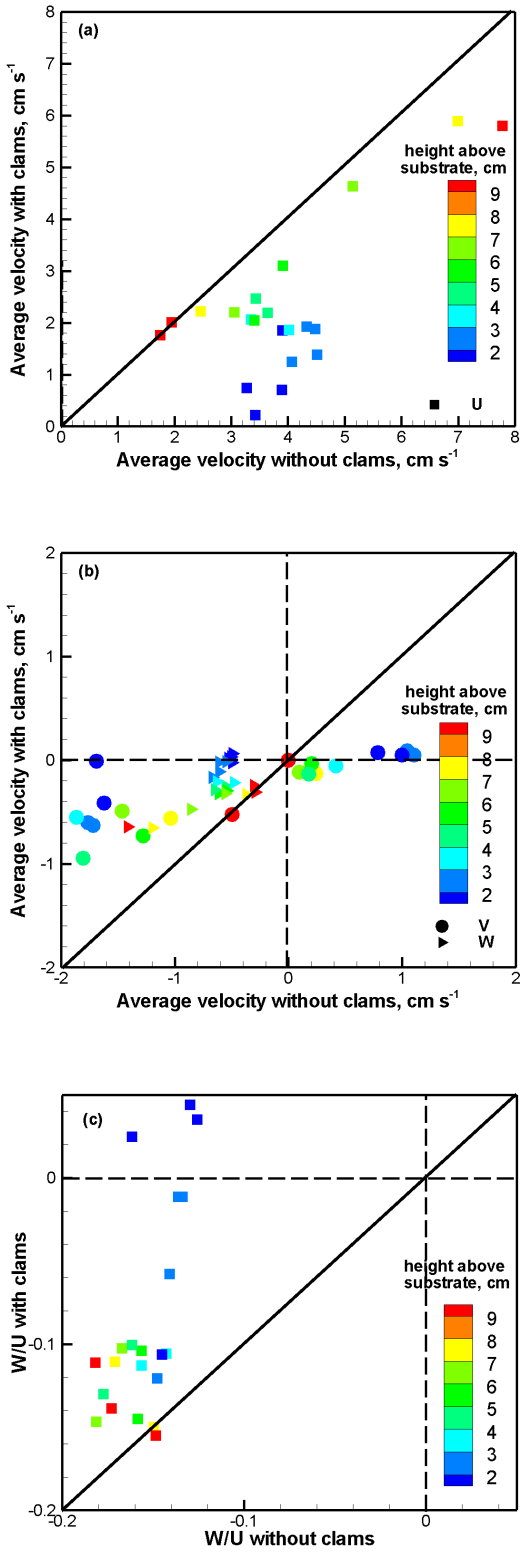

Figure 4.2: For the mud site, comparison of the average velocity components, (a) U, (b) V and W, and (c) $\frac{W}{U}$, with and without clams buried in the sediment. Samples were collected simultaneously at matching elevations. Data for two measurement sequences are included, and color indicates distance above the bed.

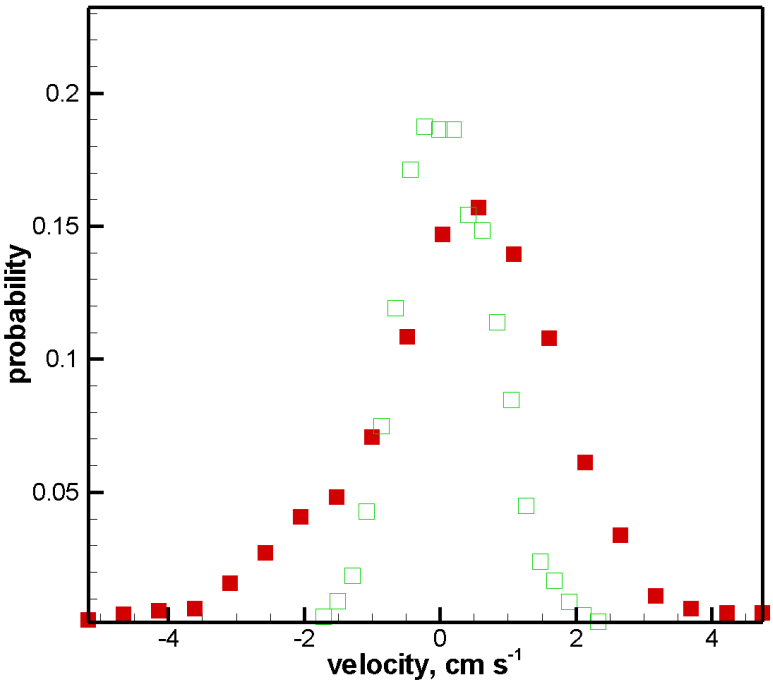

Figure 4.3: For the mud site, comparison of the probability density function of the u' velocity fluctuations at a height of 2.2 *cm* above the sediment. Samples were collected simultaneously. Red, solid symbols represents the data collection without clams buried in the sediment; Green, open symbols represents data collection with clams buried in the sediment

sequence based on the rotation in the top position.

Turbulence quantities, such as Turbulent Kinetic Energy, TKE, and Reynolds shear stresses can be considered within the horizontal homogeneity assumption and can be directly compared between the measurement devices [164]. An error analysis for the TKE and shear stress values give an error uncertainty of 1% of the calculated TKE and shear stress values. The TKE plot of the first mud measurement sequence is shown in Figure 4.5(a). Close to the sediment ($z \leq 4.3\ cm$) there is a peak value of TKE with clams that is not present when clams are not buried in the sediment and the clam case TKE values tend to be larger, for the first mud measurement series. Higher in the water column for S1, the TKE values tend to follow one another closely (Figure

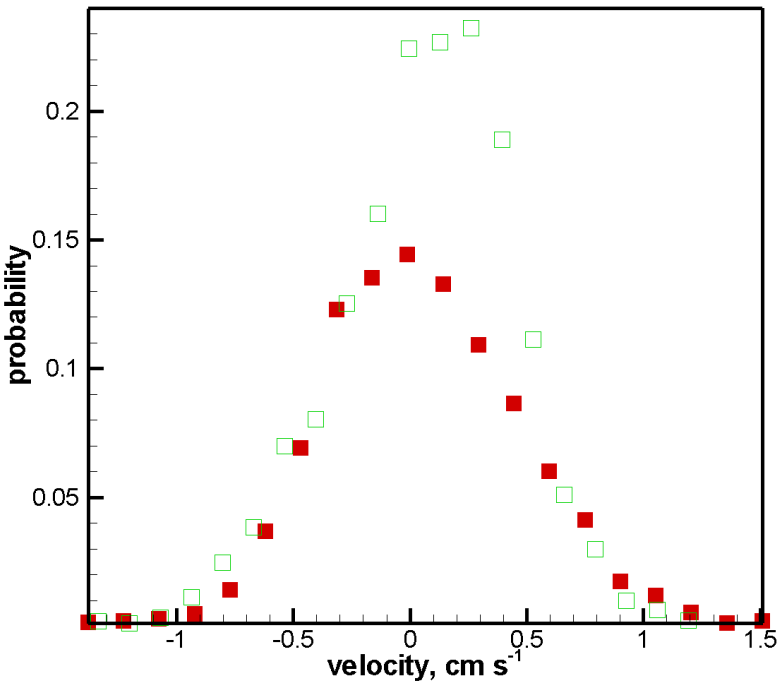

Figure 4.4: For the mud site, comparison of the probability density function of the w' velocity fluctuations at a height of 2.2 cm above the sediment. Samples were collected simultaneously. Red, solid symbols represents the data collection without clams buried in the sediment; Green, open symbols represents data collection with clams buried in the sediment

4.5(a)). Figure 4.5(b) shows the TKE values for the second mud measurement series. In this case, the clams slightly increase the TKE values close to the sediment. Also, higher in the water column the TKE plots for both the ADV's (with and without clams in the sediment) follow one another closely. Clam influence on the TKE is not necessarily universal and could be influenced by the ambient crossflow velocity or time within the tidal cycle.

The most significant Reynolds shear stress for a boundary layer-like flow is the $\overline{u'w'}$ component. For both cases of the mud treatment site, the Reynolds shear stress values are negative (Figure 4.6), which is the case with typical boundary layer flows. The negative Reynolds stress values are confirmation of the shape of the horizontal velocity measurements of Figure 4.1 for the U velocity values.

In the higher average velocity flow case (S1), the clams significantly reduce the Reynolds shear stress magnitudes close to the sediment, Figure 4.6(a). The second mud site measurement series, with smaller ambient velocities, has a larger magnitude peak Reynolds stress value and this peak is located higher in the water column when clams are buried within the sediments, Figure 4.6(b). With a lower average ambient velocity, the Reynolds shear stress peak appears to be naturally at a lower point, z = 2.2 cm, and the presence of the clams tends to increase the height of the peak to z = 3.5 cm. Higher in the water column, clams do not seem to influence the TKE values for the mud site for either crossflow velocity, Figure 4.6.

4.2 Results for the Sand Site

The sand treatment site was located at Butterbean Beach, located considerably inland of the other sites in this study, see Figure 3.1. This sand beach is likely man-made or man-maintained, but is fairly representative of sand sediments where the clams of this study were first gathered, Cabbage Island (see Figure 3.1). This site is located at the border/upstream channel connection of the Skidaway River and Moon River, both

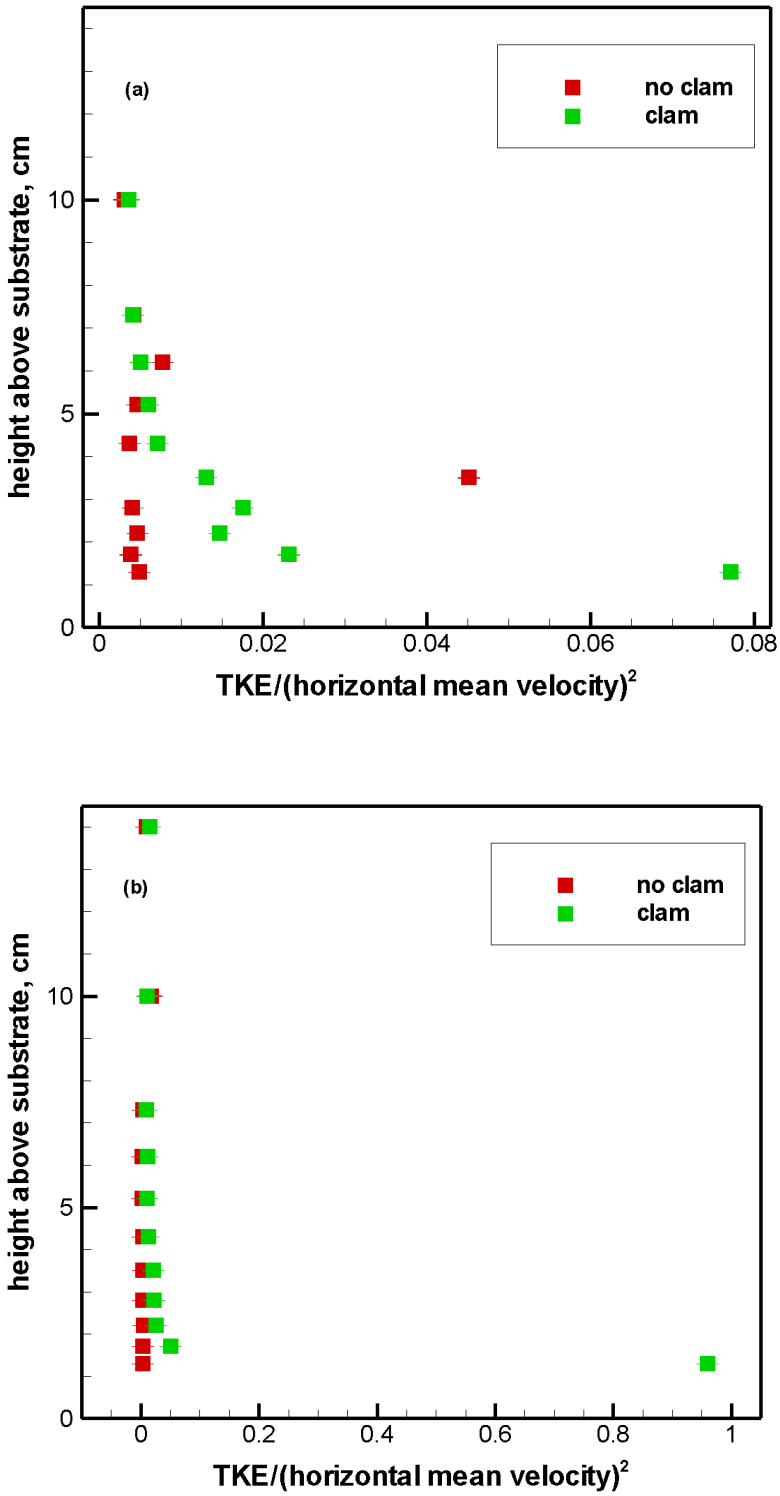

Figure 4.5: For the mud site, vertical measurement sequences of Turbulent Kinetic Energy (TKE) values, with and without clams buried in the sediment. (a) measurement sequence #1, and (b) measurement sequence #2. Error bars represent measurement uncertainty.

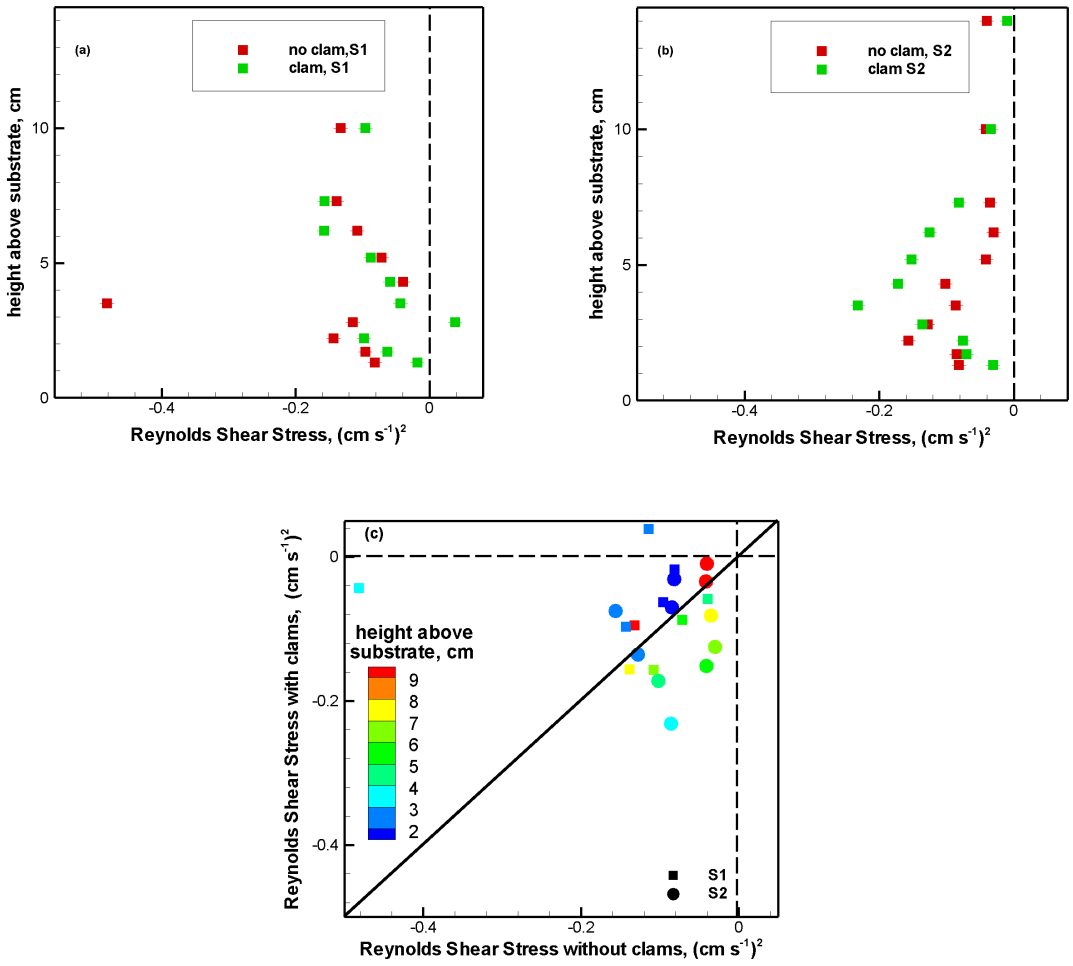

Figure 4.6: For the mud site, vertical measurement sequences of Reynolds shear stress ($\overline{u'w'}$) values, with and without clams buried in the sediment. (a) measurement sequence #1, (b) measurement sequence #2, and (c) comparison of values for the simultaneous measurements with and without clams for both measurement sequences. Error bars represent measurement uncertainty.

of which empty into the Atlantic Ocean through Wassaw Sound and Green Island Sound, respectively. Therefore, the sand site is located at a point where the tidal flow could come from either direction and determining downstream and upstream channel direction is difficult due to the variability and strength of the tides. The average velocity values are depicted in Figures 4.7 and 4.8. The V and W velocity values are very close to zero for this measurement sequence and both are smaller than the values in the longitudinal direction. Near the substrate, for both measurement devices, there is reverse flow (Figure 4.7) which could be explained by the tidal influence of both the Skidaway and Moon Rivers. The measurement sequences with and without clams appear to follow each other quite closely for all three coordinate directions with the clam measurement series having slightly larger magnitude values. Clams seem to minimally increase the magnitude of the U and V velocity over the entire measurement sequence, no matter whether the dominant flow direction is in the positive or negative x direction. Since there is reverse flow near the sediment, there are negative values of the velocity components according to the coordinate axis based on the dominant flow direction at the top of the measurement series. The clams seem to increase the magnitude of the velocity values giving larger velocity values with positive flow and smaller velocity values in the case of reverse flow. These results do not take into account the interplay between the tidally driven rivers. Therefore, these results should be considered a "special case" scenario and may not represent the effects of the sand sediments, alone.

Close to the sediment, clams appear to increase the velocity magnitudes of V and W in Figure 4.8(b). The presence of clams has less of an effect higher in the water column for both the V and W components. Clams within sand sediments have the opposite effect on the velocity vectors than that of the mud sediments, above. Figure 4.2 shows that near the sediment clams decrease all three velocity components in the mud site, whereas over the sand sediment, Figure 4.8, the presence of clams

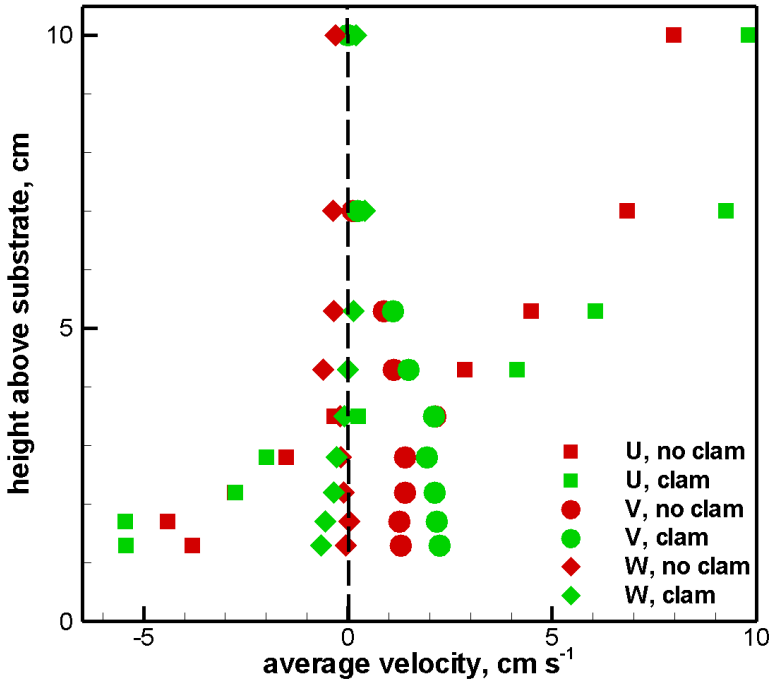

Figure 4.7: For the sand site, vertical measurement sequences of the average horizontal velocity components, U and V. Samples with and without clams buried in the sediment were collected simultaneously at matching elevations.

increases velocity magnitudes. Also, Figure 4.8(c) shows that clams are increasing the vertical momentum at nearly all the positions in the water column, particularly near the sediment.

Figure 4.9(a) shows the non-dimensionalized TKE values for both the clam and no clam cases for the sand site. Clams appear to reduce the TKE values and the peak TKE values, particularly close to the sediment. This result is comparable to the influence of jets on the TKE of the system in the jets-in-crossflow literature [7] and for clam mimic cases, [33].

The Reynolds shear stress for the sand site is plotted in Figure 4.9(b) and indicates that the $\overline{u'w'}$ shear stresses are quite small for both cases, with and without clams. Here, the shear stress values have both positive and negative values, which is consistent with Reynolds shear stress values of reverse flow. With reverse flow near the bed, in the sand case, the shear stress should be the opposite sign as that of the mud case, with positive velocity values. With clams in the sand sediment, the Reynolds shear stress values are generally increased in value and in some cases changing from negative values to positive values. In this case, the measurement sequence over the sediments with clams appears more like those of jets in crossflow cases with a modified boundary layer profile. The Reynolds shear stress values over the mud substrate (Figure 4.6), on the other hand, were consistently negative (the measurement sequence has a shape typical of that of a boundary layer over smooth sediment). This confirms that the velocity measurement sequences over these two sites are shaped considerably differently, as can be seen in the velocity measurement sequences of Figures 4.1 and 4.7.

4.3 Results for the Downstream of Oyster Bed Site

The mud, oyster, and sea grass treatment sites are located within 30 m of each another near the pier at Priest Landing, Figure 3.3. The substrate in this region is mud. The

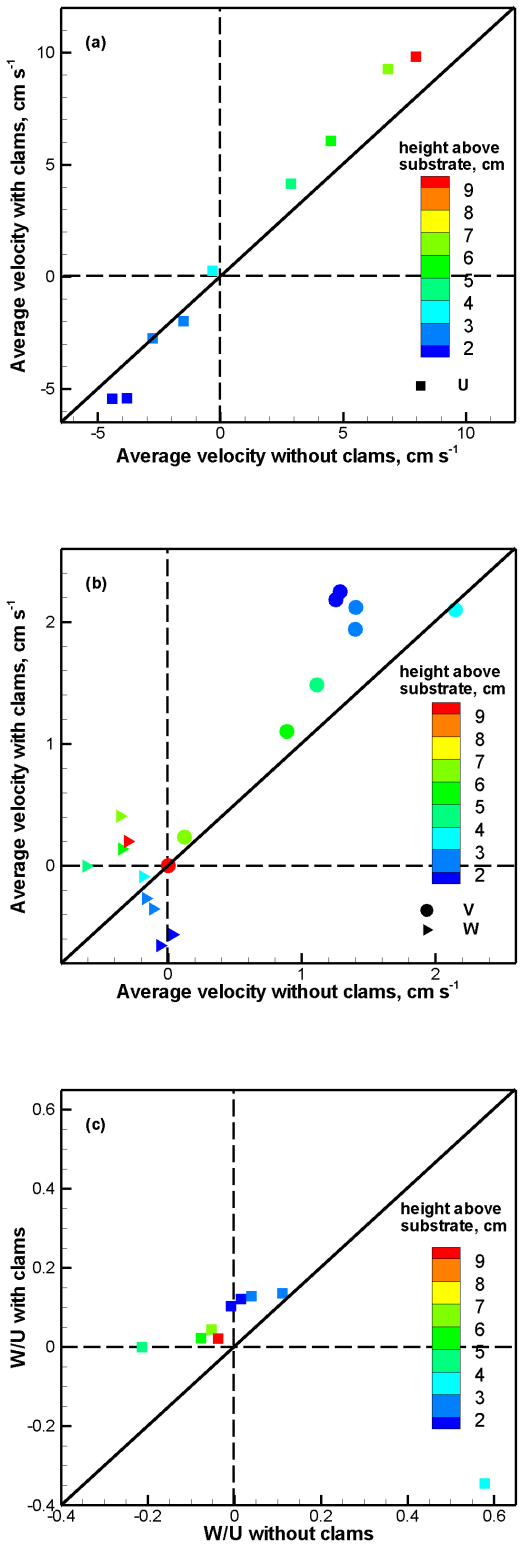

Figure 4.8: For the sand site, comparison of the average velocity components (a) U, (b) V and W, and (c) $\frac{W}{U}$, with and without clams in the sediment. Samples were collected simultaneously at matching elevations. Color indicates distance above the bed.

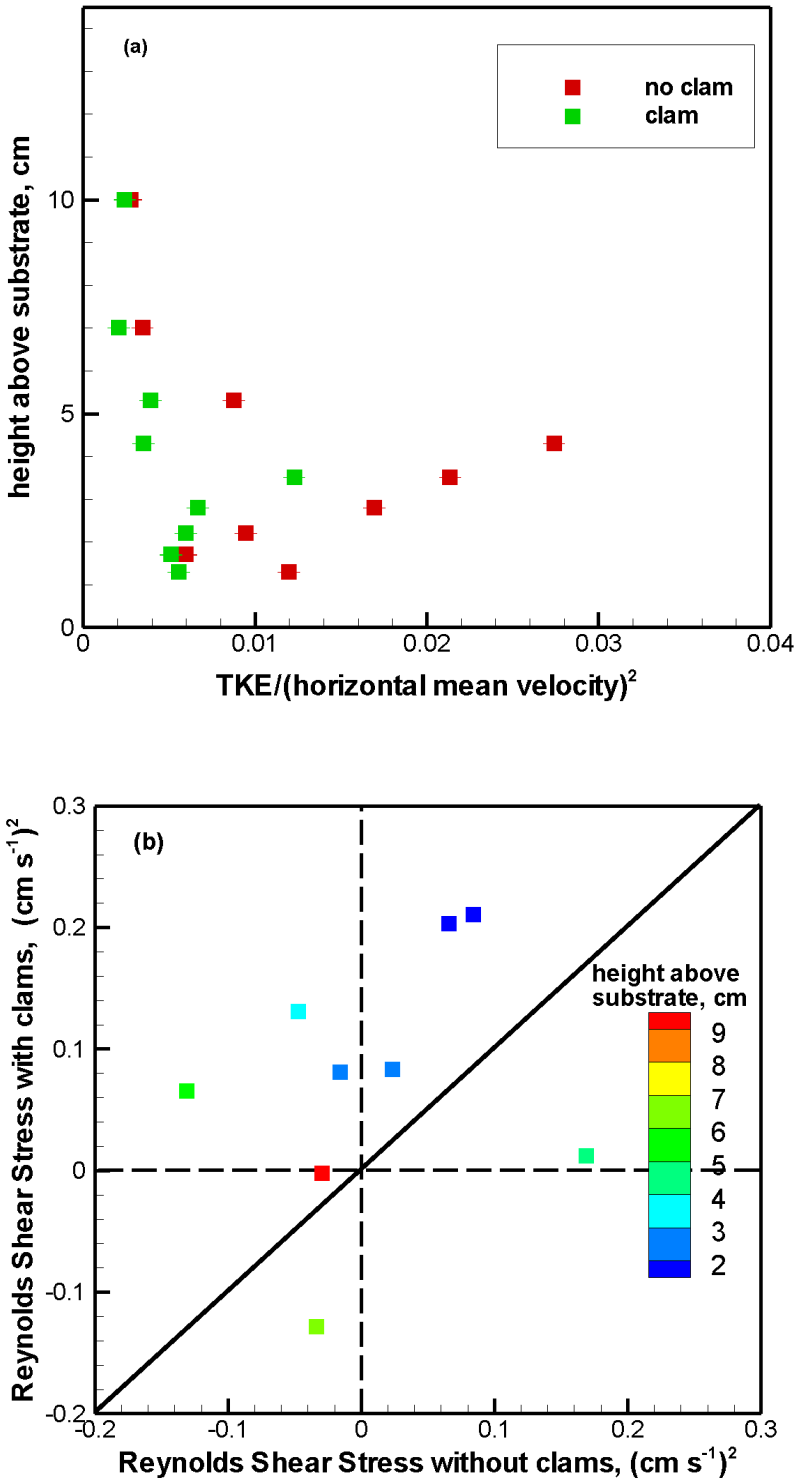

Figure 4.9: For the sand site, (a) vertical measurement sequence of Turbulent Kinetic Energy (TKE), and (b) comparison of Reynolds shear stress ($\overline{u'w'}$) values. Samples were collected simultaneously at matching elevations with and without clams buried in the sediment. Color in (b) indicates distance above the bed. Error bars represent measurement uncertainty.

measurement devices here are placed directly downstream of an oyster bed according to the flow direction of the incoming tide (Figure 3.3).

Figure 4.10(a) compares the average velocity components without clams verses the average velocity components with clams for the measurement volumes downstream of an oyster bed. Unlike both the mud and sand sites, there does not seem to be a pattern in the effect of clams on the velocity measurement sequence. In fact, clams may even reduce the vertical momentum of the system in this treatment case (Figure 4.10(d)). Since the ambient horizontal crossflow velocity is similar in magnitude to that of the second mud measurement sequence, the lack of influence of the clams on the average velocity values can be attributed to the presence of oysters in the upstream flow.

Figure 4.10(b) shows that clams do not appear to influence the TKE values either close to the sediment or higher in the water column.

For the Reynolds shear stress values downstream of the oyster bed, the clams do not have an influence near the sediment, Figure 4.10(c). However, with larger heights, the case with clams has minimally larger values in the Reynolds shear stress, often changing the sign from negative to positive. This indicates a change in the shape of the boundary layer profile, similar to the results at the sand site.

4.4 Results for the Downstream of Sea Grass Bed Sites

Clams regularly bury themselves within and directly outside of sea grass beds. We were able to collect three velocity measurement sequences at two sea grass bed sites. With these measurement sequences we are able to compare two measurement sequences from within a site and measurement sequences from similar types of sites. These sites are located at Priest Landing and have mud as the predominant sediment type (Figure 3.4).

The velocity values shown in Figure 4.11(a) indicate that the ambient horizontal

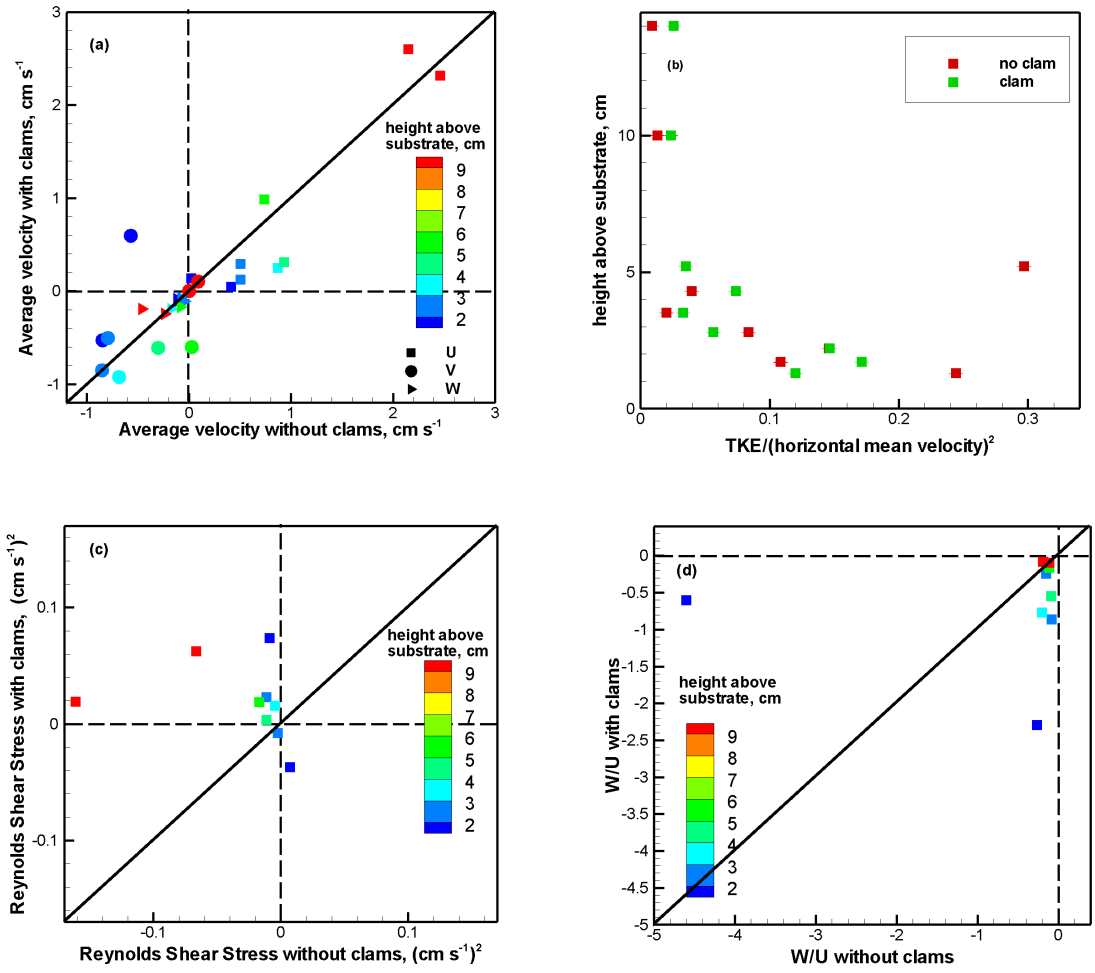

Figure 4.10: For the oyster bed site, (a) comparison of the average velocity components, (b) vertical measurement sequence of Turbulent Kinetic Energy (TKE) values, (c) comparison of Reynolds shear stress ($\overline{u'w'}$) values, and (d) comparison of $\frac{W}{U}$ values. Samples with and without clams buried in the sediment were collected simultaneously at matching elevations. For (a), (c), and (d), color indicates distance above the bed. Error bars represent measurement uncertainty.

crossflow velocity value is smaller than those collected for the mud, sand, and oyster bed sites. This reduced velocity is to be expected since sea grass beds (and vegetation in general) have been shown to reduce the velocity of the flow, Lightbody and Nepf (2006) and Bouma et al. (2007). From the measurement sequences, clams seem to generally increase the horizontal velocity values. This may be a result of the reduced velocity of the ambient flow through the sea grass beds and therefore a proportionally larger influence of clams on the boundary layer momentum when compared to the oyster bed measurements. For this seagrass bed case, clams do not appear to influence the vertical momentum of the system (Figure 4.11(d)).

The TKE values of sea grass site #1 seem to follow one another quite closely for both cases, with and without clams, Figure 4.11(b) or may be slightly decreased with clams in the sediment.

Figure 4.11(c) shows that the Reynolds shear stress values for the cases without clams are generally larger in value than those with clams downstream of this sea grass bed. Therefore, the presence and behavior of clams reduces the value of the Reynolds shear stress, often changing the sign from positive to negative. This type of influence on the Reynolds shear stress has not been observed in the results above and could be a result of the presence of the sea grass or the small horizontal crossflow velocity in this case. The sign change in the Reynolds shear stress indicates that the clams are changing the shape of the velocity measurement sequence to appear more like a typical boundary layer profile. This change is opposite of what the jets-in-crossflow literature suggests, [7].

The sea grass site #2 is downstream of sea grass site #1 according to the flow direction of the incoming tide (Figure 3.3). The results are expected to be similar to those of sea grass site #1, and yet, highlight the variance in the effects of biological structures in the flow. The first measurement sequence collected has mean velocity values similar to those of the sea grass site #1, and the second measurement sequence

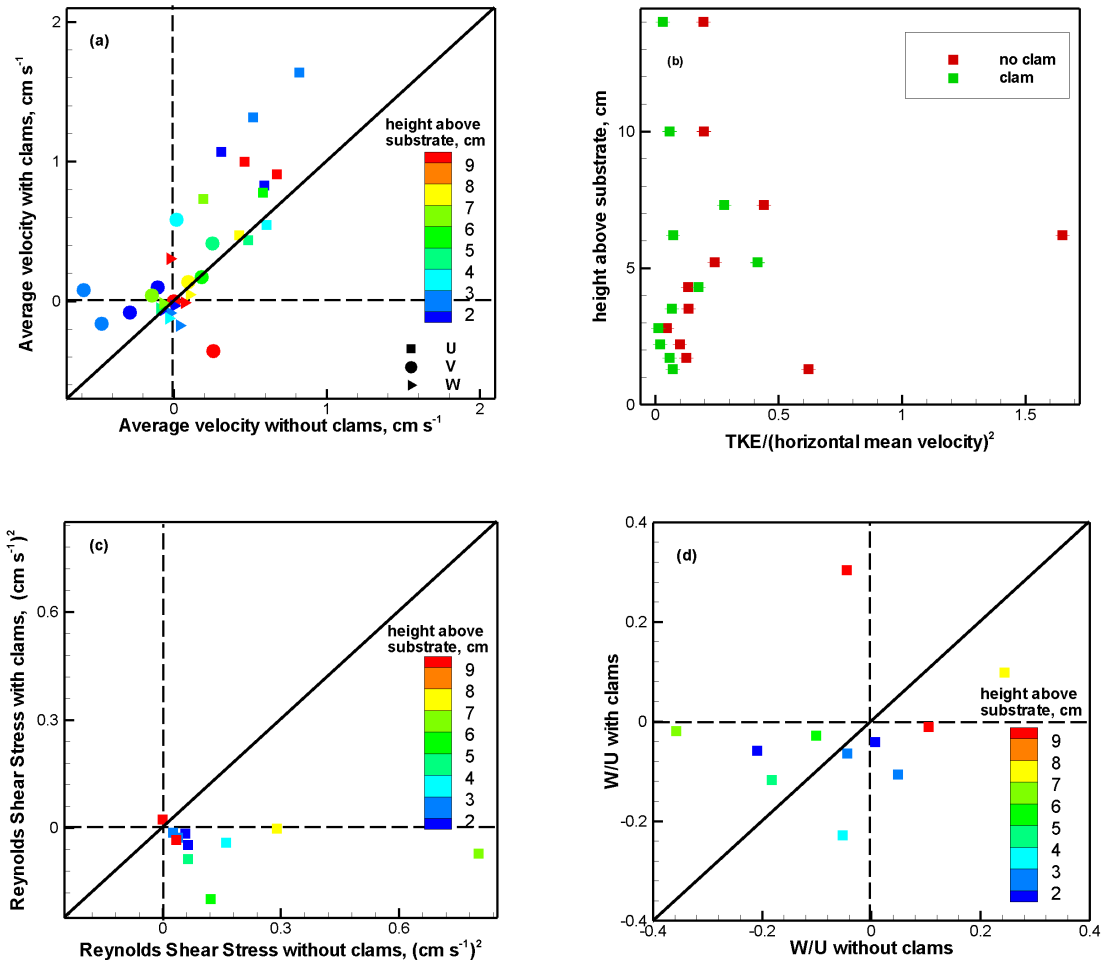

Figure 4.11: For sea grass site #1, (a) comparison of the average velocity components, (b) vertical measurement sequence of Turbulent Kinetic Energy (TKE) values, (c) comparison of Reynolds shear stress ($\overline{u'w'}$) values, and (d) comparison of $\frac{W}{U}$ values. Samples with and without clams buried in the sediment were collected simultaneously at matching elevations. For (a),(c), and (d), color indicates distance above the bed. Error bars represent measurement uncertainty.

has larger mean velocity values that are comparable to those of the mud site measurement sequence #2 and the oyster bed measurement sequence. From the average velocity measurement sequences and the comparison of Figure 4.12(a), there does not seem to be a pattern in the influence of clams on the velocity measurement sequence in sea grass site #2 for either S1 or S2. Although, clams do appear to be adding vertical momentum to the crossflow (Figure 4.13), particularly near the sediment.

Not shown on the average velocity plot is the mean ambient crossflow velocity at the high point in the water column for the sea grass site #2 measurement sequences. The differences in the clam influence between the two sequences for the second seagrass site should highlight the variability in the influence of different sea grass beds on how the presence and behavior of clams alters the crossflow momentum distribution. The sea grass site #2 second measurement sequence, S2, has a crossflow velocity of approximately $U = 1.8\ cms^{-1}$, which can be grouped with the mid-range of the collected velocities collected here (the oyster bed site and the second measurement sequence of the mud site). This measurement sequence should highlight the influence of the sea grass bed when compared to the oyster bed site and the mud site.

With similar ambient crossflow velocities, the results for sea grass site #1 and the first measurement sequence of sea grass site #2 ($U = 0.8\ cms^{-1}$) indicate that the influence of clams downstream of sea grass is not universal. For sea grass site #1 there is a slight increase in the horizontal velocity values, there is no trend in the TKE plots, and the clams reduce the value of the Reynolds shear stress (Figure 4.11). The opposite trend is observed for the first measurement sequence of sea grass site #2 (Figure 4.12(a,b,d)). For this sequence, there is no trend in the influence of clams on the average velocities, clams increase the values of the TKE particularly near the sediment, and clams increase the peak value of the Reynolds shear stress. Therefore, the influence of clams downstream of sea grass beds is specific to the two sea grass beds used in this study.

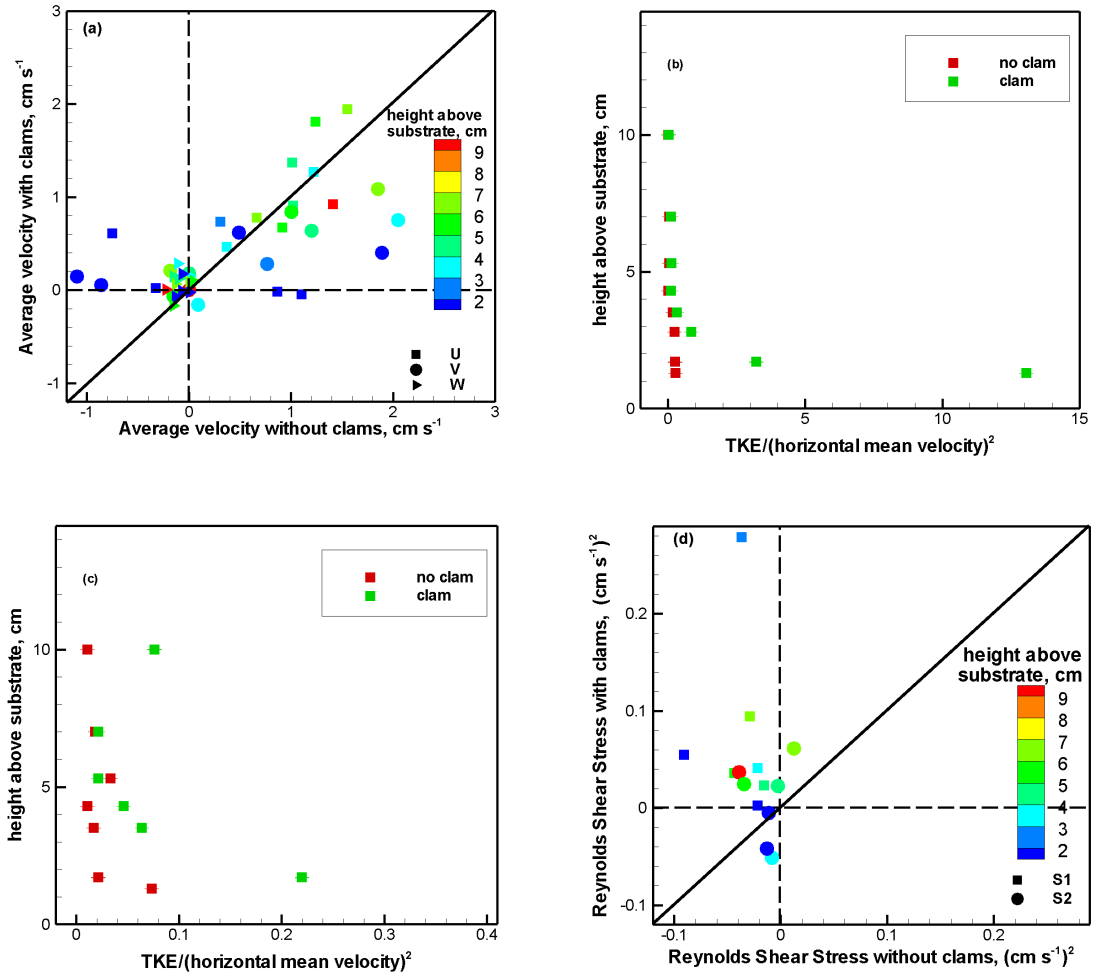

Figure 4.12: For sea grass site #2, (a) comparison of the average velocity components for two measurement sequences, (b) vertical measurement sequence #1 of Turbulent Kinetic Energy (TKE) values, (c) vertical measurement sequence #2 of Turbulent Kinetic Energy (TKE) values, and (d) comparison of Reynolds shear stress ($\overline{u'w'}$) values. Samples with and without clams buried in the sediment were collected simultaneously at matching elevations. For (a) and (d), color indicates distance above the bed. "S1" indicates measurement sequence #1, and "S2" indicates measurement sequence #2. Error bars represent measurement uncertainty.

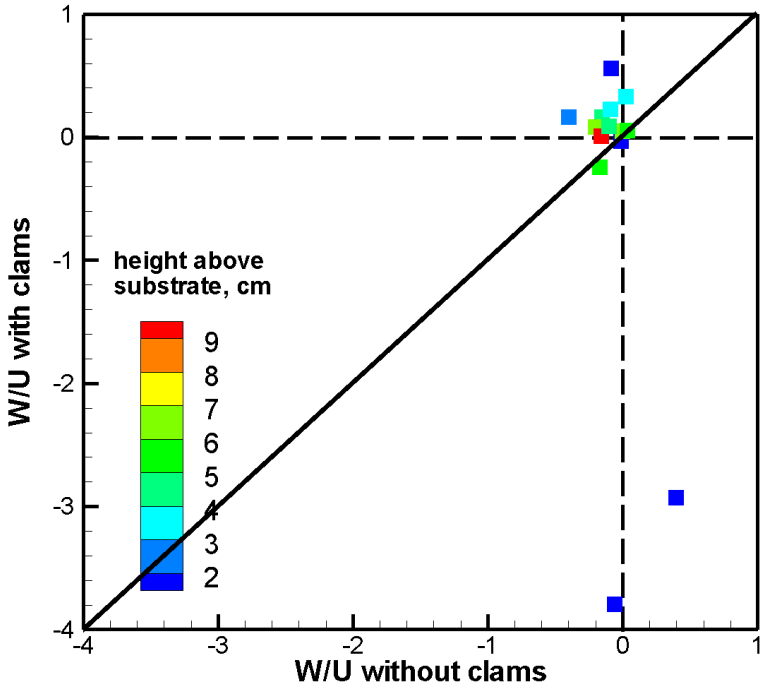

Figure 4.13: For sea grass site #2 comparison of $\frac{W}{U}$ values. Samples with and without clams buried in the sediment were collected simultaneously at matching elevations. Color indicates distance above the bed.

The second measurement sequence for seaqrass site #2 can be compared to the second mud site sequence (S2) and the oyster bed sequence since they have similar ambient crossflow velocities. When there are obstacles upstream of the clam plots, there does not seem to be a trend in the influence of clams on the average velocity values, Figures 4.10(a) and 4.12(a). However, for the second mud site sequence (S2), without obstacles in the flow, clams slow the ambient velocity values, Figures 4.1(b), and 4.2.

For the second sequence of the sea grass site #2 clams are increasing the peak TKE value (Figure 4.12(c)). In this case, the presence of sea grass may be homogenizing the TKE values and the presence of clams increases the TKE peak value by the addition of vertical momentum from the clam jets.

The influence of clams on the Reynolds shear stress for the second sequence of sea grass site #2 is similar to that of the oyster bed. Clams increase the Reynolds shear stress values and often change the signs from negative to positive (Figures 4.10(c) and 4.12(d)). For the second measurement sequence at the mud site, clams are increasing the magnitude of the peak and raising the peak location in the water column (Figure 4.6(b,c)), which could be accounted for by the lack of obstacles in the flow for this treatment.

Both the mud site and sea grass site #2 have multiple measurement sequences captured. These multiple measurement sequences highlight the influence of the ambient horizontal crossflow velocity at the same treatment site on how the presence and behavior of clams alters the crossflow momentum distribution. For sea grass site #2, clams have a similar influence on the values of the Reynolds shear stress and the average velocity values, with opposite influences on the TKE (Figure 4.12). Whereas for the mud site, clams have similar influences on the TKE values (Figure 4.5) and the average values (Figures 4.1 and 4.2) with an opposite effect on the Reynolds shear stress (Figure 4.6). Therefore, the influence of clams on turbulence characteristics

appears both dependent on the ambient crossflow velocity and the type of treatment site.

4.5 Discussion

4.5.1 Summary of Field Experiment

Table 4.1 provides a qualitative summary of the influence of the presence and behavior of clams on the crossflow momentum distribution in natural field conditions. With mud substrates, the presence and behavior of clams decreases the average velocity values for the horizontal direction and increases the vertical momentum, particularly near the bed. On the other hand, over sand substrates the clams increase the magnitude of average velocity values (although, the reverse flow and the tidal flow dominance from the two rivers could influence the behavior of the clams, in this case). When there are obstacles upstream in the flow, the clams minimally influence the shape of the mean velocity vertical distribution (Table 4.1). The only exception is the sea grass site #1, the clams slightly increase the values of the mean velocities (Table 4.1).

The horizontal homogeneity assumption of Trowbridge (1998) does not apply to absolute velocity values; however, several field studies in the past have made the assumption that the velocity values separated by this distance are comparable, [53], [174], [166], and [84]. This assumption is particularly suspect in shallow estuaries, [161], and the results presented here for mean velocity values must be interpreted with this caveat in mind. The horizontal homogeneity assumption does, however, apply to the Reynolds shear stress and Turbulent Kinetic Energy comparisons.

In general, the presence and behavior of clams increases the value of the peak TKE of the measurement sequences, particularly close to the sediment, and there is evidence that their influence may be dependent on the ambient velocity, see Table 4.1. Results from sea grass sites suggest that the influence of clams on the TKE may

Table 4.1: Summary of field results: The effect of clams on the flow and turbulence characteristics. "Near bed" is defined as below 4.3 cm, and "above bed" is defined as above 4.3 cm.

Measurement Sequence	Characteristic horizontal velocity cms^{-1}	Mean Velocity		$\frac{W}{U}$	TKE		Reynolds shear stress $(\overline{u'w'})$	
		near bed	above bed		near bed	above bed	near bed	above bed
Mud Site S1	7	decrease	slight decrease	increase	increase lower peak	decrease	decrease	slight increase magnitude
Mud Site S2	2.5	decrease	slight decrease	increase	increase	no trend	increase raise peak	increase magnitude
Sand Site	9	increase	slight increase	increase	decrease peak	decrease	increase, change sign	
Oyster Bed Site	2.5	no trend		decrease	no trend		no trend	slight increase change sign
Sea grass Site #1	0.7	slight increase		no trend	slight decrease		decrease, change sign	
Sea grass Site #2, S1	0.8	no trend		increase	increase peak	no trend	create peak, increase change sign	
Sea grass Site #2, S2	1.8	no trend		increase	increase peak	no trend	increase, change sign	

be a dependent the horizontal crossflow velocity.

The influence of clams on the Reynolds shear stress sequences appears to be treatment site and ambient horizontal velocity specific (Table 4.1). Most often, clams generally increase the Reynolds shear stress values over the entire sequence or increase the peak Reynolds shear stress value. Often this increase includes changing the values from negative to positive values. This indicates a change in the mean velocity gradients by the presence of clams. The two exceptions to this trend is the influence of clams on the Reynolds shear stresses of the sea grass site #1 and the first sequence of the mud site (S1).

4.5.2 Influence on Horizontal Momentum Distribution

Clams in the mud site appeared to decrease the average velocity values with increasing influence close to the sediment surface (Table 4.1). This type of influence also was recorded by Crimaldi et al. (2007) for clam mimics in the laboratory over smooth plates for velocity profiles, which cannot be directly compared to the measurement sequences of this study due to the tidal movements during the collection. Since the influence of the clams on the velocity measurement sequences was sediment type specific in this study (Table 4.1), we can assume that the mud site is most closely related to smooth plate laboratory measurements. For rougher substrates, in laboratory settings without clams, the ambient velocities are increased and moved closer to the sediment, [142], although fine sand was used as the smooth bed laboratory case. For the sand case of the current study, clams minimally increase the magnitude of the velocity measurement sequences (Table 4.1); however, the tidal flow is coming from several directions in this site. The results of this study indicate that the TKE peak is increased or the TKE values are increased for nearly all treatment cases, Table 4.1. Crimaldi et al. (2007) found that in the laboratory clam mimics decreased the peak of Turbulence Intensity (similar measure to TKE) and alter the height of the peak in

the water column, particularly for low ambient velocities. Therefore, clam mimics of the type used by Crimaldi et al. (2007) capture the types of influence clams have on TKE only for the sand site and the first seagrass site in our field settings. A similar laboratory experiment was completed over mussel beds, Van Duren et al. (2006) and a field experiment with pinnid bivalves, Nikora et al. (2002). Van Duren et al. (2006) found that inactive mussels increased the TKE value by being present in the flow and their impact was even more pronounced when mussels were actively pumping.

The effect of clams on the Reynolds shear stress does not seem to have a general trend in the results of this study, Table 4.1. Clams both increase and decrease the values, change the magnitude of the Reynolds shear stress peak, and alter the heights at which those peaks occur. This lack of a pattern is consistent with Nikora et al. (1997) who found that periphyton mats influenced turbulence characteristics of the flow selectively and the current study also found selective influence of clams in several types of treatment sites. Clam mimics were found to increase the Reynolds shear stress magnitude by Crimaldi et al. (2007). Although, when two profiles are collected at the same site, at the mud site and sea grass site #2, the differences in the influence of clams on the Reynolds shear stress could be attributed to the differences in the ambient velocities in these cases (Table 4.1). Hence, clams may have crossflow velocity specific influences on the Reynolds shear stress values.

In the cases presented here, the clam pumping behavior contributed to the modification of the boundary layer measurement sequence (Table 4.1). The differences in the boundary layer measurement sequences between the two measurement devices are consistent with the way in which clam mimics and jets-in-crossflow affect the boundary layer momentum (Table 4.1). For example, Andreopoulis and Rodi (1984) record velocity profiles of turbulent jets in turbulent crossflow with similar shapes as those of this study in the mud (slowing the velocity values, particularly near the boundary), although, they cannot be directly compared since our measurement series

are not actual profiles. Also, Monismith et al. (1995) and O'Riordan (1993) show clam mimics and clams in the laboratory slow the mean velocity values and alter the shape of the velocity profile. Therefore, clams in the field control the crossflow momentum in similar ways to the jets-in-crossflow literature, clam mimic studies, and clams in the laboratory.

4.5.3 Upstream Structures in the Flow

Flow downstream of sea grass beds has the lowest average velocity values collected in this study, which is expected due to the impact of the structure of the vegetation on the velocity of the flow [16] (Table 4.1). Jumars and Nowell (1984) concluded that biological impacts on flow momentum and sediment transport characteristics occur during times of low Reynolds number flow, as for sea grass site #1 and the first sequence of sea grass site #2 (Table 4.1).

The velocity measurement sequences of the current study downstream of the sea grass beds compare favorably with velocity profiles collected in the laboratory downstream of sea grass mimics [16] (although, not directly comparable, since the current study does not collect boundary layer profiles, see Figures 4.11(a) and 4.12(a)). Irlandi and Peterson (1991) noticed that clams in and around sea grass beds grew faster than over sand flats despite reduced velocity and, therefore, reduced resource abundance. They attributed this phenomenon to reduced predation pressure and larger rates of feeding, particularly downstream of the sea grass beds according to the direction of the flood tide [80]. Another explanation of the lowered growth rates over mud flats is that there is evidence that as the ambient velocity increases, the clam filtering rate decreases, [192].

Clams appear to minimally alter the shape of the vertical distribution of mean velocity when upstream biological structures are located within the flow (Table 4.1). From these results, it is evident that both oyster beds and sea grass beds reduce the

impact of clams on the flow when compared to the clam impact over mud sediments. In this study, the upstream structures are altering the turbulence characteristics of the flow, by either increasing roughness size (oysters) or decreasing Re through reducing average velocity (seagrass). Jumars and Nowell (1984) predicted that biological impacts would be comparable in magnitude to other types of flow impacts at low Reynolds number flows; they did not consider other turbulence characteristics beyond Reynolds number. In this study, downstream of oyster beds, with a relatively larger Reynolds number, clams do not influence the mean velocity values of the measurement sequence which supports the predictions of Jumars and Nowell (1984).

4.5.4 Ecological Impacts

TKE was generally increased by the presence of clams within the sediment over most of the treatment sites, particularly the mud and second seagrass treatment sites,(Table 4.1). Increased TKE corresponds to increased dilution of the chemical signal based on the lab results of Rahman and Webster (2005). This suggests that clam filaments of chemical metabolites remain at higher concentrations as they move downstream with the flow over sand treatments. Clams have higher predation rates in sandy areas rather than within sea grass beds where their growth rates are substantially larger, [80]. This phenomenon may be related to the way they affect the boundary layer momentum and turbulence characteristics that dilute their chemical metabolites, since this study suggests that over the sand sites the TKE is decreased (Table 4.1), resulting in higher chemical concentrations in the downstream plume. There are higher abundances of clams found in regions of higher flow and areas with larger roughness elements [188]. The higher predation rates over sand flats, the lowered turbulence values, and the higher abundances over regions with high turbulence collectively suggest that an increase in turbulence intensity could create a hydrodynamic refuge from predation and that clams are not necessarily active participants in the creation of those

refuges. The clams of the current study did not substantially influence the velocity measurement sequence downstream of the oyster beds, Table 4.1. This may indicate that in areas of high turbulence, such as flows with large roughness elements, the ambient turbulence may be sufficiently mixing the chemical metabolites of the clams to reduce predation and that the reduction of TKE by clams in the oyster bed case (Table 4.1) may not negatively impact clam survivorship.

The results of this study suggest that clams alter the crossflow mean momentum distribution, and it is hypothesized that this affects the predator-prey relationship. Through turbulence characteristics control, clams can reduce predation by predators that have variable tracking ability with specific turbulence regimes. Hart et al. (1996) concluded that whelks may have a hard time locating prey within sea grass beds due to the structure of the sea grass impeding whelk locomotion. Therefore, clams would have more incentive to reduce the turbulence in sand/mud flats where they are more exposed to those types of predators.

In sea grass site #2, clams increase the value of the TKE peak (Table 4.1). There may be a hydrodynamic advantage to avoidance of blue crab predation in this case. Blue crab predators have reduced rates of tracking success in higher turbulence flows, [187] and [82]. Therefore, with the mid-range velocity values observed at this site, avoidance of blue crab predation (increasing TKE) may be advantageous over strategies used for whelk predation avoidance (reducing TKE).

Other theories as to why clams could benefit if they contribute to the crossflow momentum characteristics include avoidance of concentration boundary layers and larval recruitment. By controlling the crossflow momentum as this study shows, clams may extend the patch stability through periods of non-typical hydrodynamic conditions signalling to larval clams the suitability of the location. Clam larvae settlement is based on hydrodynamic cues from the environment, [70], which may have developed in response to predation rates of clams within these flows or their ability to

influence the turbulence. Coco et al. (2006) found that patch size, patch density, and patch recruitment depend on the dominant hydrodynamic conditions and that there are multiple stable patch states for those conditions, [26]. Turbulence conditions may contribute to patch characteristics through potential predation pressures due to those turbulence conditions.

4.5.5 Limitations of this Study

The field experiments of this study suggest that bivalve clams have an influence on the field crossflow similar to that of laboratory experiments, [131] and [33]. Biological impacts, at least in the conditions for shallow estuaries at the tidal flows collected here, could be an important contributor to fluid characteristics in the field. This study quantifies the bulk influence of the presence and behavior of clams on the crossflow, but does not determine the differences in the effect of the behaviors verses the presence and what factors control those behaviors. To understand specific influences of the presence of clams separate from the possible behavioral influences further experiments must be completed. Since clams are organisms with a complex array of behaviors, a better understanding of what external cues trigger certain clam behavioral changes would enable greater understanding as to the effect of clams on the fluid characteristics.

CHAPTER V

LABORATORY EXPERIMENTS ON UNSTEADINESS OF CLAM EXCURRENT FLOW

Three sets of laboratory experiments are presented to quantify the clam excurrent velocity unsteadiness/randomness according to external environmental factors. First, several control data sets are presented for flows over non-feeding animals and clam mimics with several jet flow rates. Second, the first clam treatment set compares clam behavior according to the size of the clam, the nearest neighbor distance of conspecifics, and the velocity of the ambient cross-flow. These factors may contribute to differences in clam excurrent velocity randomness, as controlled by the organism. Third, the second set of clam treatments attempts to quantify whether jet velocity randomness is influenced by the presence or absence of predator cues in the upstream flow and how those cues alter behavior depending on the external flow characteristics.

The PIV system measured a two-dimensional array of velocity vectors in a plane that bisects the clam excurrent siphon. An example of a clam vector plot is shown in Figure 5.1 where the arrows represent the velocity vector at that point in the flow field and the color contours represent positive (upward) vertical velocity. This example clam will be used throughout the following subsection for demonstration purposes and it is typical of the results for the entire data set. The color contours highlight the location of the clam excurrent jet. Figure 5.2 is a cartoon of the vector plot of Figure 5.1 with the location of the buried clam shown for clarity. In this case, the clam was not completely buried beneath the sediment and the siphons were extended in the upstream direction with the incurrent siphon located upstream of the excurrent siphon.

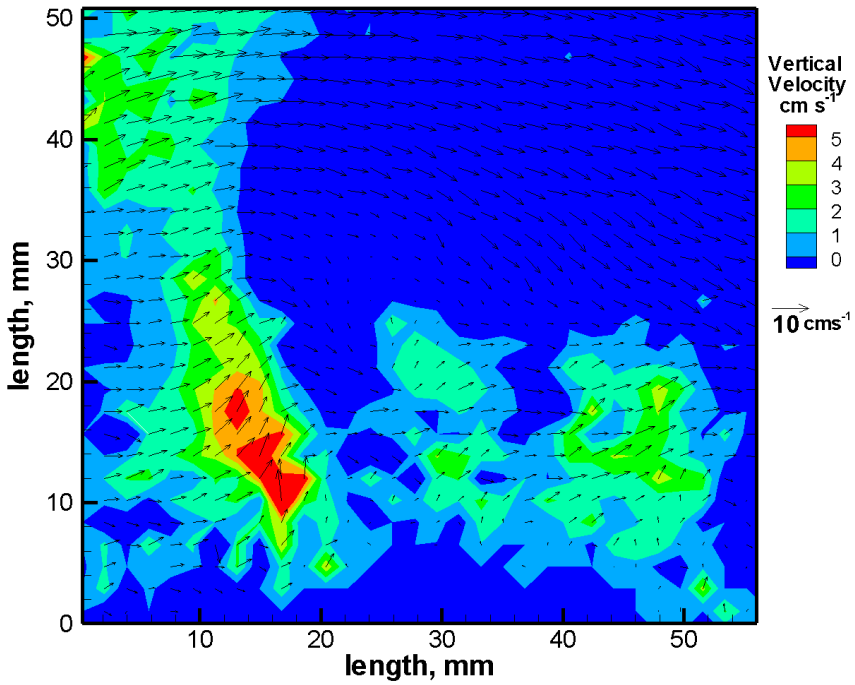

Figure 5.1: Two-dimensional PIV velocity vector plot for a 5 cm square plane bisecting a clam excurrent jet for the case with $U = 0.55\ cms^{-1}$, clam length = 4.92 cm, and a nearest neighbor distance of 9 cm (Clam #5 listed in Table 5.7). The vertical excurrent jet is revealed by the red contours on the left side of the image.

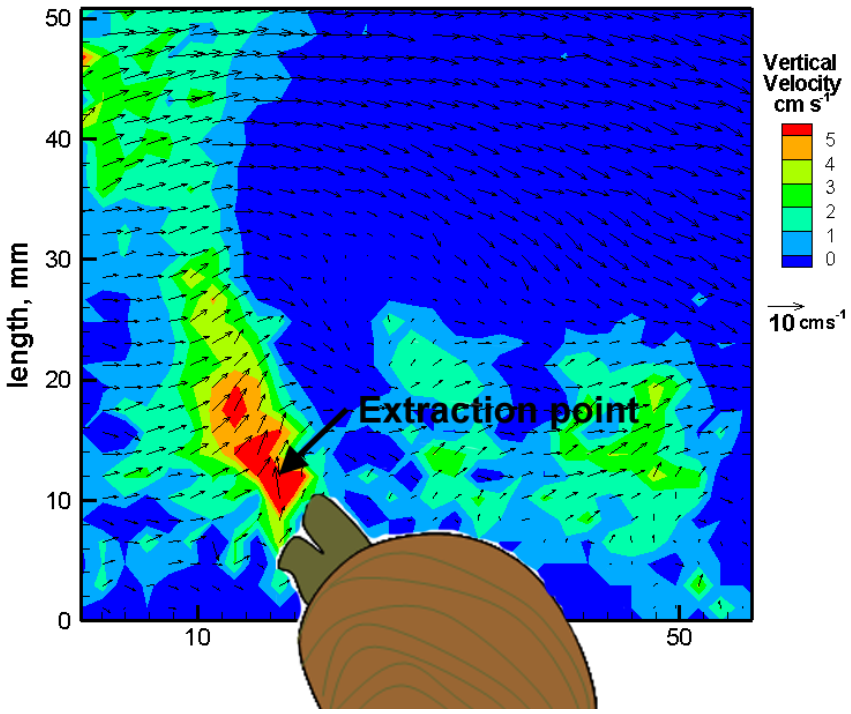

Figure 5.2: Cartoon of Figure 5.1 showing the approximate clam location and the extraction point for the time record of vertical velocity.

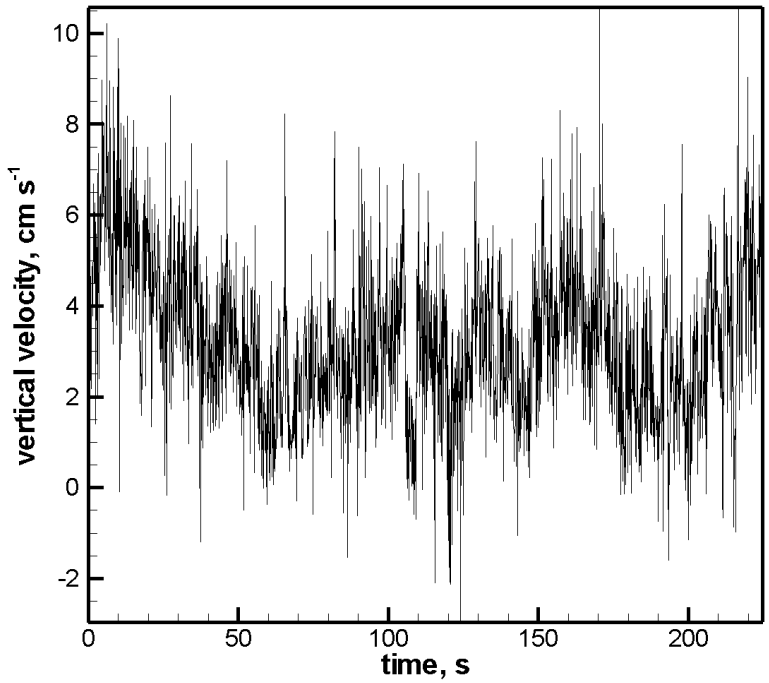

Figure 5.3: Example time record of jet vertical velocity. This example is 225 s in duration and corresponds to the extraction point depicted in Figure 5.2 for the clam of Figure 5.1.

Approximately 2250 consecutive velocity fields were collected via the PIV system and analysis. The extraction point was chosen manually for each data set for the period that the point was within the vertical jet and the clam is actively pumping. Figure 5.2 shows the extraction point for the example velocity field. In this case, vertical velocity time record of 225s is extracted and displayed in Figure 5.3. The time record of clam excurrent vertical velocity is highly unsteady with a mean of $\overline{u}$ = 3.26 cms^{-1} and variance of σ^2 = 3.07 cm^2s^{-2}. A few negative values of vertical velocity appear in the time record, which can be attributed to brief intrusions of the crossflow fluid to the centerline of the jet.

5.1 Time Series Analyses

The power spectral density (PSD) is calculated for the time record to quantify periodic unsteadiness in the excurrent jet velocity patterns. Figure 5.4 shows the PSD for the example time record on a log scale. When the frequency range of a power spectral density plot reaches that of the inertial range of the energy cascade, the slope of the data on a log plot is $-\frac{5}{3}$. However, in the current study we are not necessarily interested in the energy cascade but focus on identifying any dominant frequencies in the low frequency range. Therefore, Figure 5.5 plots the PSD on regular axes, and a dominant frequency cannot be identified. The example presented here is typical. All velocity-time records for the three sets of experiments were analysed via spectral analysis to determine possible frequency dominance in the time record. The spectral analysis did not reveal any dominant frequencies and will not be discussed further, other than to conclude that the time records of clam excurrent vertical velocity lack a dominant periodic variation.

A fractal analysis quantifies the randomness of the velocity values in the time record. For example, Figure 5.6 represents an artificially-generated time record of fractional Brownian motion or random walk, in which the jumps in time record values are scaled as Gaussian white noise. A fractal analysis of a time record yields a single fractal dimension value in the range $1 < d_{fl} < 2$. The time record in Figure 5.6 has a fractal dimension of 1.488, which is close to the theoretical fractal dimension of 1.5 for pure Brownian motion. Fractal dimension values between $1 < d_{fl} < 1.5$ are correlated, (example shown in Figure 5.7) and values between $1.5 < d_{fl} < 2$ are anti-correlated (example shown in Figure 5.8). Therefore, as the fractal dimension approaches 1.5, the time record values become more random. The three artificially generated time records, with the same mean and variance as the clam jet velocity time record, have distinct differences in texture and unsteadiness. Hence, the fractal analysis quantifies the unsteadiness of the time record beyond the typical statistical

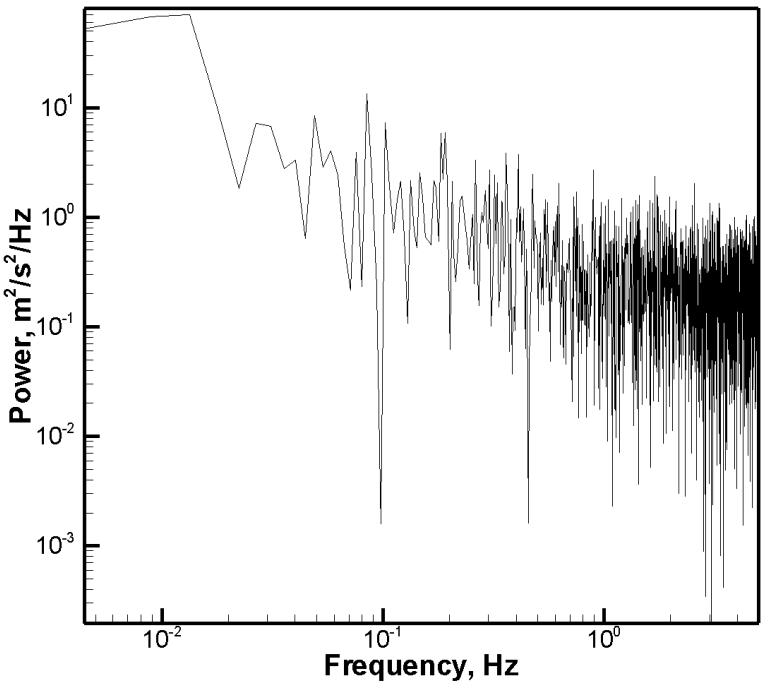

Figure 5.4: Power spectral density (log axes) for the vertical clam jet velocity time record of Figure 5.3.

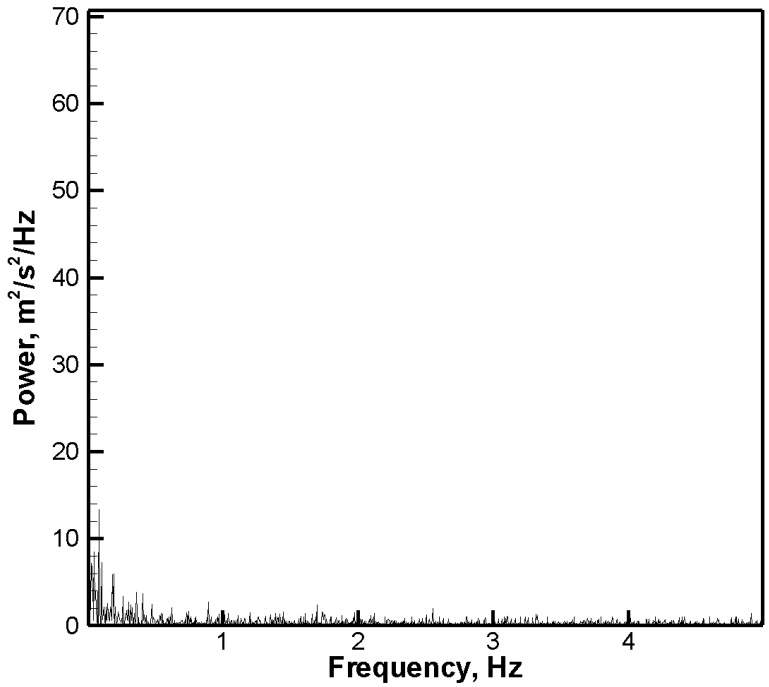

Figure 5.5: Power spectral density (linear axes) for the vertical clam jet velocity time record of Figure 5.3.

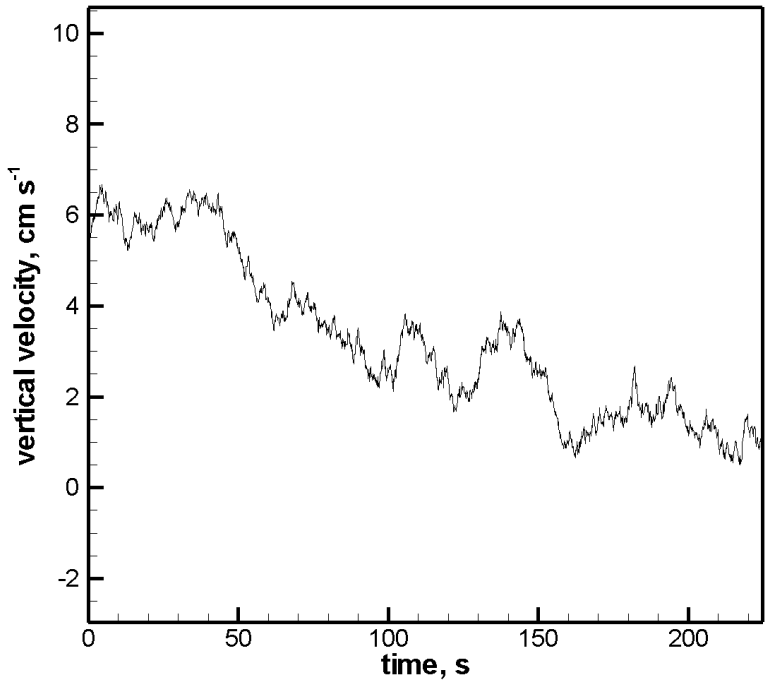

Figure 5.6: Artificially-generated time record of fractional Brownian motion (fractal dimension = 1.488). For comparison, the mean and variance of this artificially-generated time record match that of the vertical clam jet velocity time record of Figure 5.3.

quantities of mean and variance.

The clam jet excurrent velocity time record most qualitatively matches that of the anti-correlated time record of Figure 5.8. As expected, when the fractal analysis, i.e., Hurst's rescaled range analysis, is applied to the example time record of clam excurrent vertical velocity (Figure 5.3), the resulting fractal dimension is $d_{fl} = 1.7704$. This value indicates that the clam jet time record is more anti-correlated than random (i.e. a large value is likely to be followed by a small value of velocity).

In addition, a lacunarity analysis is used to quantify the "texture" or the distribution of velocity unsteadiness. Lacunarity analysis is used to further quantify data sets with similar fractal dimensions [107]. The analysis yields a plot of lacunarity versus box size, which for a time record corresponds to a time period. Figure 5.9 shows the

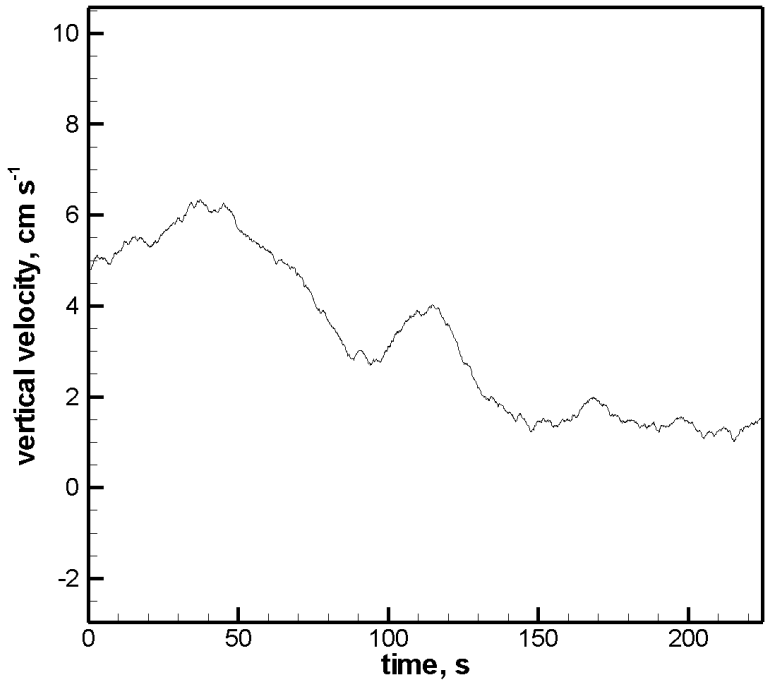

Figure 5.7: Artificially-generated persistent (correlated) time record (fractal dimension = 1.3408). For comparison, the mean and variance of this artificially-generated time record match that of the vertical clam jet velocity time record of Figure 5.3.

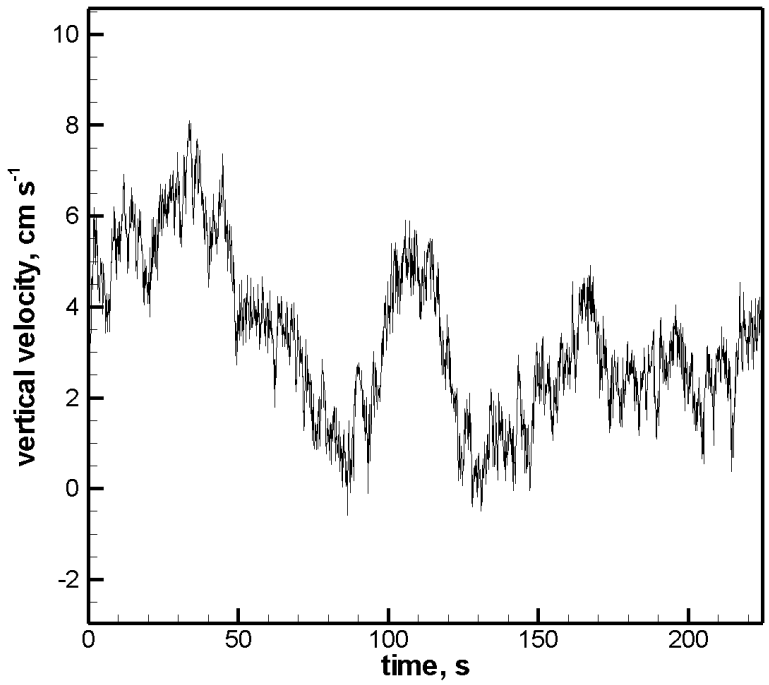

Figure 5.8: Artificially-generated anti-persistent (anti-correlated) time record (fractal dimension = 1.6427). For comparison, the mean and variance of this artificially-generated time record match that of the vertical clam jet velocity time record of Figure 5.3.

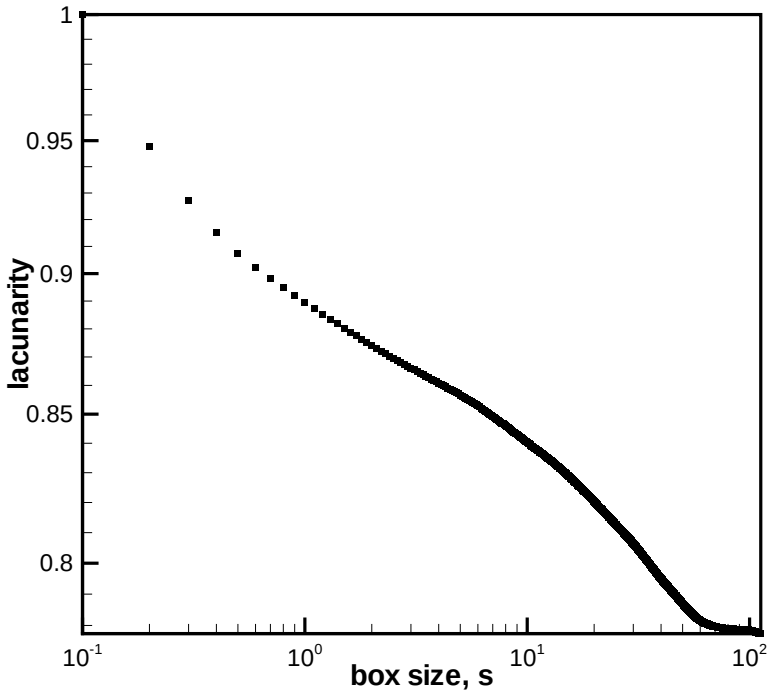

Figure 5.9: Lacunarity as a function of box size (i.e., time period) for the time record of vertical jet velocity shown Figure 5.3 (log axes).

lacunarity plot for the example time record shown in Figure 5.3. The lacunarity plots shown here are normalized by the lacunarity value at the smallest box size for comparison purposes. Hence, the largest value of normalized lacunarity is always equal to one.

The shape of the lacunarity plot reveals the deviation of a fractal (in this case the time record) from established geometric patterns [137]. Further, the shape of the lacunarity curve indicates features of the velocity time record. For example, high lacunarity values indicate "clumping" or closely clustered values of velocity. At a box size value that corresponds to the size of the clumped or clustered values, the lacunarity value decreases and curve "drops off" as can be seen in Figure 5.13.

A lacunarity analysis of white noise is shown in Figure 5.10 and has a concave up shape. Time records that have velocity values or gap sizes close to random values

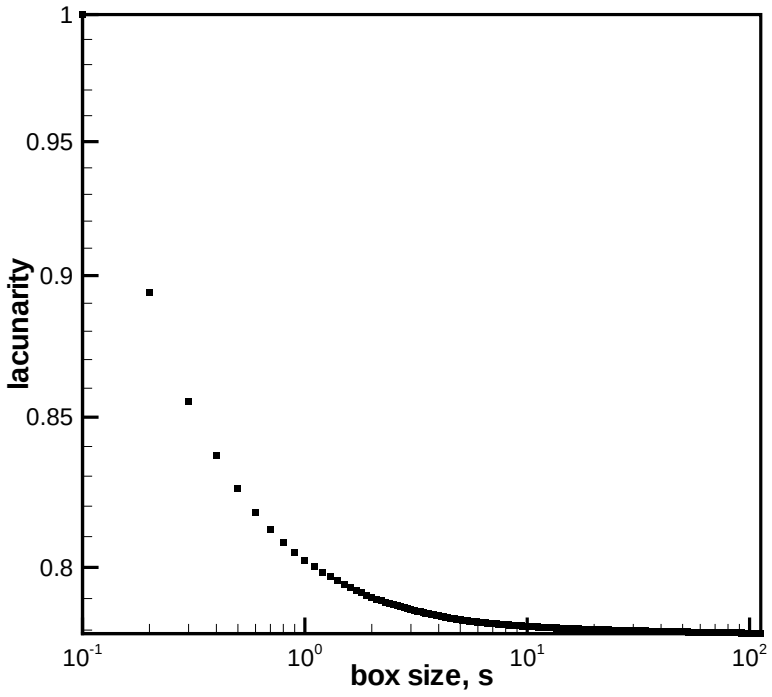

Figure 5.10: Lacunarity as a function of box size (i.e., time segment) for Gaussian white noise (log axes).

will also have a lacunarity curve with a concave-upward shape. For example, Figure 5.11 for a large clam with large nearest neighbor distance, and the largest crossflow velocity matches this description.

Fractals, by definition, have a power law relationship between geometric ratios and the box size and which suggests that on a log-log scale a lacunarity curve would be a straight line for a pure fractal. Lacunarity curves that are more linear in shape represent the geometric scale independence of true fractals [137]. An example of a clam jet velocity time record with a "linear" lacunarity curve is shown in Figure 5.12.

When there is a distinct gap-size scale within the clam jet velocity time record, the lacunarity curve will have a break in slope at that box size. An example of this type of lacunarity curve is shown in Figure 5.13 for a large clam with close neighbors and the largest crossflow velocity. There is a distinct break in the slope of the lacunarity

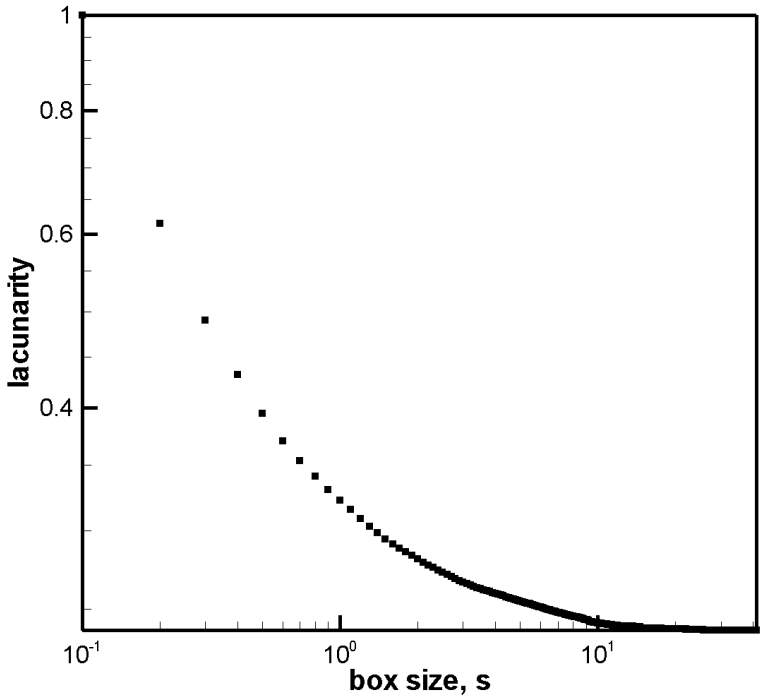

Figure 5.11: Lacunarity as a function of box size (i.e., time segment) for the time record of vertical jet velocity for Clam #8 of Table 5.7, $U = 2.86\ cms^{-1}$, clam length = 6.91 cm, and nearest neighbor distance of 9 cm. (log axes)

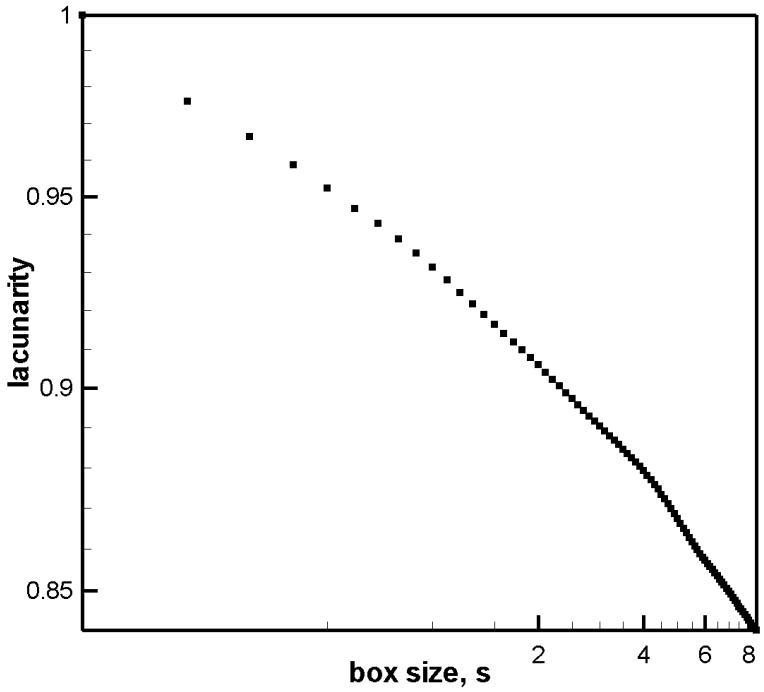

Figure 5.12: Lacunarity as a function of box size (i.e., time segment) for the time record of vertical jet velocity for Clam #4 of Table 5.7, $U = 2.86\ cms^{-1}$, clam length = 4.6 cm, and nearest neighbor distance of 3 cm (log axes).

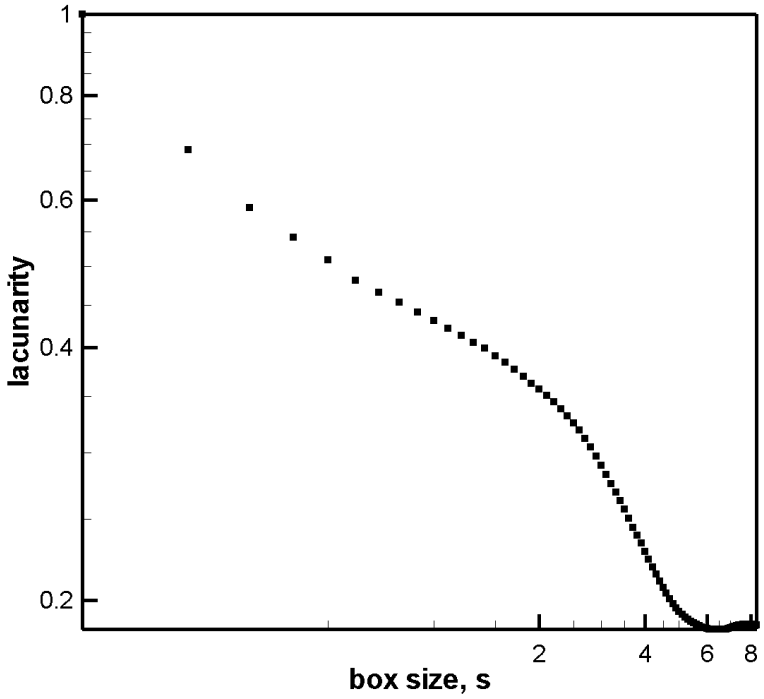

Figure 5.13: Lacunarity as a function of box size (i.e., time segment) for the time record of vertical jet velocity for Clam #6 of Table 5.7, $U = 2.86\ cms^{-1}$, clam length = 7.30 cm, and nearest neighbor distance of 3 cm (log axes).

curve at a box size of approximately 3 s. This indicates that the velocity values of the time record of vertical velocity clump in time scales smaller than 3 s, and that there is a distinct lack of clumping in scales greater than 3 s.

Clam behavioral changes during the measurement period often interrupts the time record collection since the jet velocity extraction point can move locations or the clam may stop pumping momentarily or altogether. Therefore, for several of the treatment types there are multiple shorter jet velocity time records rather than one long time record. In these cases, the fractal dimension values are averaged over the ensemble of time records. In contrast, the lacunarity plot values are not averaged. The lacunarity plots for each time record are plotted and the dominant lacunarity shape type is noted for that case. An example case is shown in Figure 5.14 with four time records

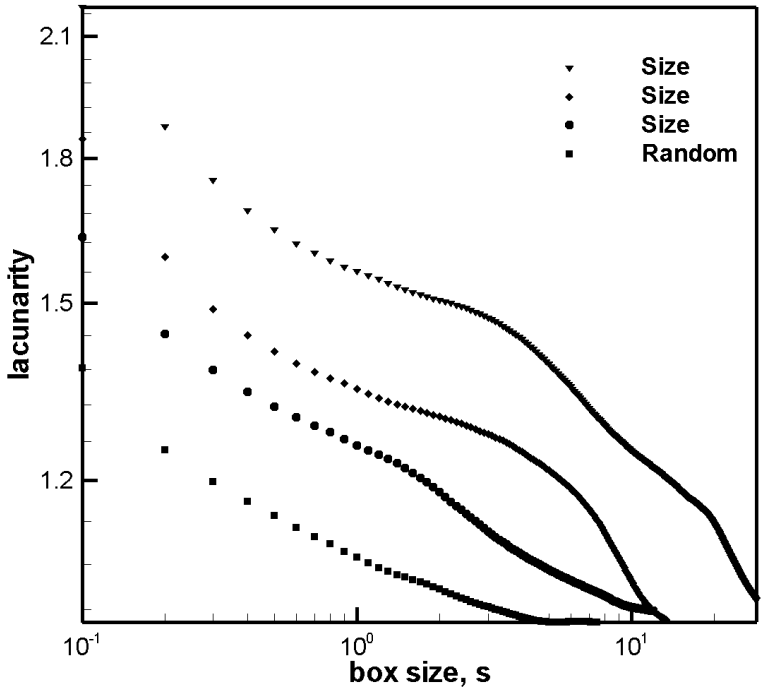

Figure 5.14: Non-normalized lacunarity plots for four time record segments collected for a clam of length = 4.68 cm, U =1.98 cms^{-1}, and nearest neighbor distance of 3 cm (log axis). Triangles represent a time record of 57.1 s, Diamonds represent a time record of 26.8 s, circles represent a time record of 24.1 s, and squares represent a time record of 15.1 s. The legend indicates the curve type for each record.

for a small clam with small nearest neighbor distance and a crossflow velocity of 1.98 cms^{-1}. In this case there are four time record segments. The lacunarity curves have not been normalized, and hence they do not have the same y-axis intercept value. Also, the length of the time records are not the same, and therefore the lacunarity curves do not have the same range of box size. The key information from these plots is the general shape of the curve. For this case there are three time records with a distinct break in slope and one that appears as a random shape (i.e., concave up). Hence, the conclusion is that this data set is dominated by lacunarity plots with a size distinction.

With the analysis tools described above, the current study calculates the fractal

dimension values and categorizes the shape of the lacunarity curves for clams exposed to several treatment types. The lacunarity plots are given a nominal category upon visual inspection of the plot of either "Random" for a shape similar to that of Figure 5.11, "Fractal" for a shape similar to that of Figure 5.12, and "Size" for a plot with a distinct break in slope similar to that of Figure 5.13.

5.2 Results for Control Cases

Several time records of vertical velocity were collected for control cases of clam mimics, clam shells only, and no clams present in the flow for comparison with the active clam jet data. These control cases include time records from a man-made vertical jet (clam mimic) with flow rates of 0.467 cm^3s^{-1} and 0.0 cm^3s^{-1} (see Table 5.1). A 0.95 cm inner diameter plastic tube was used to deliver a constant flow rate to the vertically-oriented tube (mimic clam). The clam mimic tube inner diameter is larger than that of typical clam excurrent siphons; however, this disparity was necessary to maintain the jet mimic flow within the range of typical clam jet Reynolds numbers. The mimic clam tube extends 0.75 cm into the water column, which is a similar height to many of the clam siphons in the current study. The zero flow rate case will indicate the effect of the physical presence of the clam mimic siphon on the vertical velocity. In addition, time records of vertical velocity were extracted for the case of a non-pumping clam to determine the effects of the presence of the body of the clam in the flow. Finally, a time record was extracted for a case without clams or a mimic present to quantify the effect of the disturbance of the sediment by the clams without the animal present. repeated-measures ANOVA reveals a significant difference ($p < 0.001$) in the mean jet/vertical velocities depending on the control case type (i.e. clam shell only, clam mimic, etc.).

Table 5.1 summarizes the control cases and reports the mean jet velocity values

Table 5.1: Mean jet velocities in cms^{-1} and standard deviations of the jet velocity/vertical velocity time record collected for the laboratory control cases. Four control cases were employed, as described in the first three columns, in order to compare to the trends observed in the clam excurrent jet data.

	Jet flow rate (cm^3s^{-1})	diameter (cm)	Crossflow velocity (cms^{-1})			
			0.55	1.2	1.98	2.86
No clam, no jet			-0.08±0.50	-0.084±0.67	-0.08±0.78	0.00±2.15
Clam shell only (6.99 cm)			0.33±0.78	0.82±1.02	1.42±1.61	2.23±3.81
Clam mimic	0.467	0.9525	13.59±1.25	12.74±0.61	11.00±1.51	4.83±5.65
Clam mimic	0	0.9525	-3.44±0.98	-3.50±1.43	-3.87±2.02	-4.61±4.34

Table 5.2: Jet/vertical to crossflow velocity ratio for the laboratory control cases. Four control cases were employed, as described in the first three columns, in order to compare to the trends observed in the clam excurrent jet data.

	Jet flow rate (cm^3s^{-1})	diameter (cm)	Crossflow velocity (cms^{-1})			
			0.55	1.2	1.98	2.86
No clam, no jet			-0.15	-0.07	-0.04	0
Clam shell only (6.99 cm)			0.6	0.68	0.72	0.78
Clam mimic	0.467	0.9525	24.71	10.62	5.56	1.69
Clam mimic	0	0.9525	-6.25	-2.92	-1.95	-1.61

or the mean vertical velocity values (in cases without jets) and the standard deviations for each clam jet velocity time record. A repeated-measures ANOVA reveals a significant difference ($p < 0.001$) in the mean jet/vertical velocities depending on the control case type (i.e. clam shell only, clam mimic, etc.). Since the jets-in-crossflow literature deems the jet-to-crossflow velocity ratio as a significant determinate of the type of jet structures present in the flow, Table 5.2 reports the jet-to-crossflow velocity ratios for the control cases (in cases without actual jets, the vertical velocity was used in calculation of the ratio). A repeated measures ANOVA finds a significant difference ($p < 0.03$)in the jet-to-crossflow velocity ratio (vertical velocity to crossflow velocity ratio) according to the control case type.

The fractal dimension calculated for each case are presented in Table 5.3. A two-way, repeated measures ANOVA (analysis of variance) did not find significant differences in the fractal dimension values among the control cases for any of the factors (crossflow velocity, nearest neighbor distances, and clam size). An ANOVA is an extension of the Student's two-sample t-test to compare means of several groups, simultaneously, to reduce error due to possible interaction between groups. The ANOVA determines any differences in means in the groups and whether there is a dependence on one factor in the means of another factor.

The lacunarity curve types for the control cases are presented in Table 5.4, and the majority of cases are described as "Random" particularly for the clam mimic cases.

Table 5.3: Fractal dimension of the time record of vertical velocity collected for the laboratory control cases. Four control cases were employed, as described in the first three columns, in order to compare to the trends observed in the clam excurrent jet data.

	Jet flow rate (cm^3s^{-1})	diameter (cm)	Crossflow velocity (cms^{-1})			
			0.55	1.2	1.98	2.86
No clam, no jet			1.8028	1.8166	1.8323	1.8697
Clam shell only (6.99 cm)			1.7973	1.8077	1.7596	1.7936
Clam mimic	0.467	0.9525	1.518	1.7643	1.5716	1.9197
Clam mimic	0	0.9525	1.7315	1.8288	1.8642	1.9049

A two-way, repeated measures NANOVA (nominal analysis of variance) found a significant difference in lacunarity plot type for the control cases according to velocity ($p < 0.001$), [181]. NANOVA differs from ANOVA in the respect that ANOVA is a comparison of quantitative means whereas NANOVA is a comparison of the distribution of nominal values. The advantage for this analysis is that it allows for comparison of treatments that do not necessarily have quantitative measures associated with them. It is often used in drug treatment trials, for example, to compare drug side effects from patient questionnaires. The disadvantage of this statistical comparison test is that, without quantitative values, the test can only determine if the nominal values are qualitatively different, but not necessarily how they are different quantitatively. The NANOVA in the current study tells us whether or not the randomness is different in the trials but does not give us a trend or the ability to say one treatment gives more or less randomness than another. For these control cases, a majority of the lacunarity curves have random type lacunarity curves, there are two cases in which there is a size selection, Table 5.4.

5.3 Results for Laboratory Clam Jets with Varying Environmental Conditions

The data presented in this section address the effect of external environmental factors on clam feeding behavior. Clam size, the density of clams, and the hydrodynamic characteristics of the crossflow may contribute to alterations in clam jet velocity behavior. Table 5.5 summarizes the time record collection for the controlled external factors and the mean and standard deviations for the jet velocity time records calculated for each case for four horizontal crossflow velocity values (0.55, 1.2, 1.98, 2.86 cms^{-1}), two nearest neighbor distances (3 and 9 cm), and two clam sizes (4.86$\pm$0.22 cm and 7.32$\pm$0.32 cm). Non-dimensionalizing the nearest neighbor distance by the mean clam size in each case give you non-dimensional nearest neighbor distances of 0.62 and 1.85 for the smaller size clam and 0.41 and 1.23 for the larger size clam.

Table 5.4: Lacunarity curve type for time records of vertical velocity for the laboratory control cases.

	Jet flow rate (cm^3s^{-1})	diameter (cm)	Crossflow velocity (cms^{-1})			
			0.55	1.2	1.98	2.86
No clam, no jet			Size	Random	Random	Random
Clam shell only (6.99 cm)	0		Random	Random	Random	Random
Clam mimic	0.467	0.9525	Random	Random	Size	Random
Clam mimic	0	0.9525	Random	Random	Random	Random

A multi-way repeated measures ANOVA reveals a significant interaction ($p < 0.034$) for the mean jet velocities according to the length of the clam and the crossflow velocity. In other words, the clam mean jet velocity values are influenced by the crossflow velocity but those values are dependent on the size of the clam. This suggests that blue crabs may dominate the predator-prey system if this modification is related to predation interactions.

The jet-to-crossflow velocity ratios are reported in Table 5.6 and the fractal dimensions calculated for each case are shown in Table 5.7. A multi-way repeated measures ANOVA finds that there is a significant difference in the jet-to-crossflow velocity ratios according to the size of the clam ($p < 0.044$) and according to the crossflow velocity ($p < 0.001$). The jet-to-crossflow velocity ratio at a crossflow velocity of 0.55 cms^{-1} is significantly larger than the jet-to-crossflow velocity ratio of the three other crossflow velocity values ($p < 0.05$). This suggests that as the crossflow velocity increases from a value of 0.55 cms^{-1}, the clams either do not maintain the jet-to-crossflow velocity ratio by increasing the jet velocity proportionally or that they are incapable of doing so. Also, the jet-to-crossflow velocity ratio for the smaller size clams ($\frac{v}{U} = 3.58 \pm 0.10$) is significantly larger than the jet-to-crossflow velocity ratio for the larger size clams ($\frac{v}{U} = 2.48 \pm 0.06$). This could indicate that there may be an advantage for smaller clams to have larger velocity ratios than larger clams. This also may indicate that Blue crabs dominate the predator-prey system, since the clams are changing their behavior according to their size range (given that the alteration in the clam jet behavior is controlled by predation pressure).

Table 5.7 shows the fractal dimension values calculated with the Hurst's Rescaled Range Analysis for this laboratory experiment. A multi-way, repeated measures ANOVA found no significant differences in the fractal dimension values of the time records according to crossflow velocity, clam nearest neighbor distance, or clam size. The lacunarity plots were categorized with nominal types according to the shape of

Table 5.5: Mean jet velocities and standard deviations for the clam excurrent jet vertical velocities. The table reports data for varying nearest neighbor distance (NND), crossflow velocity, and clam size class.

		NND = 3 cm, non-dim NND = 0.62				NND = 9 cm, non-dim NND = 1.85			
focal	length	Crossflow velocity (cms^{-1})				Crossflow velocity (cms^{-1})			
clam	(cm)	0.55	1.2	1.98	2.86	0.55	1.2	1.98	2.86
1	4.68	3.19±3.49	4.50±8.27	5.65±3.67	2.15±3.65	3.11±2.33	3.57±3.95	8.20±8.45	2.83±2.03
2	5.16	4.15±3.78	0.89±0.93	0.79±1.33	1.68±5.46	10.46±5.48	4.48±7.01	4.62±2.69	3.30±7.53
3	4.92	1.99±2.15	4.39±2.81	1.79±1.35	1.62±2.09	5.23±5.36	1.62±2.64	0.64±4.75	1.31±2.55
4	4.6	4.88±2.73	6.97±2.94	2.56±1.92	2.55±2.22	3.65±4.44	8.05±11.35	4.11±6.55	0.36±1.81
5	4.92	7.65±3.78	2.45±4.19	2.04±2.74	0.52±1.84	3.26±1.75	3.08±4.41	2.98±2.12	2.63±2.09
		NND = 3 cm, non-dim NND = 0.41				NND = 9 cm, non-dim NND = 1.23			
focal	length	Crossflow velocity (cms^{-1})				Crossflow velocity (cms^{-1})			
clam	(cm)	0.55	1.2	1.98	2.86	0.55	1.2	1.98	2.86
6	7.3	2.33±1.22	0.80±1.16	1.47±2.08	0.90±2.01	1.58±1.67	1.66±2.13	2.12±3.39	4.70±6.19
7	7.54	3.83±3.69	3.33±2.36	4.20±7.43	3.17±10.64	2.61±3.54	2.34±3.15	0.99±2.20	2.06±3.66
8	6.91	3.26±2.81	4.95±11.63	5.83±2.14	6.19±7.13	1.83±9.69	2.61±2.52	1.90±10.85	5.40±5.60
9	8.57	1.94±2.25	2.09±1.84	3.17±1.51	5.17±5.27	5.20±2.46	3.24±4.23	1.65±3.08	1.12±4.16

the plot (Table 5.8). A multi-way, repeated measures NANOVA found a significant difference in the lacunarity curves according to the horizontal crossflow velocity ($p < 0.001$) and a significant interaction between the nearest neighbor distance and the clam size ($p < 0.001$). Therefore, although the amount of randomness in the velocity time records may be statistically similar (as measured by fractal dimension), the distribution of the randomness or the texture of the randomness is crossflow velocity specific. Hence, the data indicate that clams have behavioral differences in their jet velocity unsteadiness according to the crossflow velocity value.

Also, the ANOVA reveals a significant interaction between the nearest neighbor distance and the size of the organism. This implies that the reaction of clams to the density of the clam patch is dependent on the size of that particular animal.

5.4 Results for Laboratory Clam Jets with Predator Effects

In these data, predators (blue crabs recently fed with frozen shrimp) were caged upstream of the clam plots to determine whether predator cues induce feeding behavior modifications in clams. Velocity time records were collected with and without predator cues in the upstream flow and the crossflow velocity was altered. The data in this section were collected exclusively for the smaller clam size and nearest neighbor distance of 3 cm.

Treatment details and are shown in Table 5.9 along with mean jet velocity values and standard deviations of the jet velocity values. There is no significant difference in the mean jet velocity values for the second laboratory experiment according to a two-way repeated measures ANOVA. Table 5.10 contains the jet-to-crossflow velocity values for the second laboratory experiment. There is a significant difference in the jet-to-crossflow velocity values according to the crossflow velocity, revealing the same patterns as the first laboratory experiment (jet-to-crossflow ratio is significantly larger in the 0.55 cms^{-1} crossflow velocity case, $p < 0.015$). Table 5.11 contains the fractal

Table 5.6: Jet to crossflow velocity ratios. The table reports data for varying nearest neighbor distance (NND), crossflow velocity, and clam size class.

		NND = 3 cm,non-dim NND = 0.62				NND = 9 cm, non-dim NND = 1.85			
focal	length	Crossflow velocity (cms^{-1})				Crossflow velocity (cms^{-1})			
clam	(cm)	0.55	1.2	1.98	2.86	0.55	1.2	1.98	2.86
1	4.68	5.80	3.75	2.85	0.75	5.65	2.98	4.14	0.99
2	5.16	7.55	0.74	0.40	0.59	19.02	3.73	2.33	1.15
3	4.92	3.62	3.66	0.90	0.57	9.51	1.35	0.32	0.46
4	4.6	8.87	5.81	1.29	0.89	6.34	6.71	2.08	0.13
5	4.92	13.91	2.04	1.03	0.18	5.93	2.57	1.51	0.92
		NND = 3 cm, non-dim NND = 0.41				NND = 9 cm, non-dim NND = 1.23			
focal	length	Crossflow velocity (cms^{-1})				Crossflow velocity (cms^{-1})			
clam	(cm)	0.55	1.2	1.98	2.86	0.55	1.2	1.98	2.86
6	7.3	4.24	0.67	0.74	0.31	2.87	1.38	1.07	1.64
7	7.54	6.96	2.78	2.12	1.11	4.75	1.95	0.5	0.72
8	6.91	5.93	4.13	2.94	2.16	3.33	2.18	0.96	1.89
9	8.57	3.53	1.74	1.60	1.81	9.45	2.70	0.83	0.39

Table 5.7: Fractal dimension for the time records of clam excurrent vertical velocity. The table reports data for varying nearest neighbor distance (NND), crossflow velocity, and clam size class.

		NND = 3 cm, non-dim NND = 0.62				NND = 9 cm, non-dim NND = 1.85			
focal	length	Crossflow velocity (cms^{-1})				Crossflow velocity (cms^{-1})			
clam	(cm)	0.55	1.2	1.98	2.86	0.55	1.2	1.98	2.86
1	4.68	1.8015	1.8627	1.829	1.7941	1.7353	1.6404	1.7287	1.7509
2	5.16	1.6607	1.7563	1.7885	1.7017	1.7172	1.7634	1.6668	1.7434
3	4.92	1.7412	1.7943	1.7219	1.7058	1.6873	1.6705	1.8098	1.6871
4	4.6	1.7539	1.7349	1.7027	1.6658	1.8206	1.8087	1.7164	1.5706
5	4.92	1.6141	1.7767	1.6995	1.8001	1.7704	1.7834	1.7985	1.6609
		NND = 3 cm, non-dim NND = 0.41				NND = 9 cm, non-dim NND = 1.23			
focal	length	Crossflow velocity (cms^{-1})				Crossflow velocity (cms^{-1})			
clam	(cm)	0.55	1.2	1.98	2.86	0.55	1.2	1.98	2.86
6	7.3	1.7491	1.7605	1.7311	1.6694	1.8196	1.8093	1.7558	1.8634
7	7.54	1.763	1.7841	1.7827	1.7987	1.7371	1.81	1.8381	1.7425
8	6.91	1.7237	1.7506	1.5799	1.7267	1.832	1.7853	1.5122	1.838
9	8.57	1.7974	1.7679	1.6277	1.7895	1.7014	1.7887	1.7328	1.6849

Table 5.8: Lacunarity curve type for time records of clam excurrent vertical velocity. The table reports data for varying nearest neighbor distance (NND), crossflow velocity, and clam size class.

		NND = 3 cm, non-dim NND = 0.62				NND = 9 cm, non-dim NND = 1.85			
focal	length	Crossflow velocity (cms^{-1})				Crossflow velocity (cms^{-1})			
clam	(cm)	0.55	1.2	1.98	2.86	0.55	1.2	1.98	2.86
1	4.68	Random	Random	Random	Random	Size	Size	Random	Random
2	5.16	Size	Size	Random	Random	Random	Random	Size	Size
3	4.92	Random	Size	Size	Fractal	Size	Size	Random	Size
4	4.6	Size	Size	Random	Fractal	Random	Random	Size	Size
5	4.92	Size	Size	Size	Random	Size	Random	Random	Fractal
		NND = 3 cm, non-dim NND = 0.41				NND = 9 cm, non-dim NND = 1.23			
focal	length	Crossflow velocity (cms^{-1})				Crossflow velocity (cms^{-1})			
clam	(cm)	0.55	1.2	1.98	2.86	0.55	1.2	1.98	2.86
6	7.3	Random	Size	Size	Size	Random	Size	Fractal	Random
7	7.54	Size	Random	Random	Random	Random	Random	Random	Random
8	6.91	Fractal	Random	Fractal	Random	Random	Random	Random	Random
9	8.57	Random	Size	Size	Random	Fractal	Random	Random	Random

Table 5.9: Mean jet velocities and standard deviations for the time records of clam excurrent vertical velocity. The table reports data for varying horizontal crossflow velocity with and without a predator in the upstream flow.

focal clam	length (cm)	predator	Crossflow velocity (cms^{-1}) 0.55	1.2	1.98	2.86
1	4.76	no	0.92±1.26	1.38±1.77	3.25±2.75	1.09±3.98
2	4.76	no	1.66±2.03	2.67±2.08	2.93±4.28	4.13±6.63
3	4.60	no	2.79±2.31	0.77±0.77	1.28±1.17	1.77±1.52
4	4.45	yes	3.22±4.23	0.77±2.54	1.06±2.07	0.71±2.58
5	4.45	yes	1.29±1.45	0.70±2.02	0.80±3.19	4.42±5.33
6	4.76	yes	0.58±1.20	1.11±1.24	1.27±2.25	0.71±2.88

Table 5.10: Jet to crossflow velocity ratios. The table reports data for varying horizontal crossflow velocity with and without a predator in the upstream flow.

focal clam	length (cm)	predator	Crossflow velocity (cms^{-1}) 0.55	1.2	1.98	2.86
1	4.76	no	1.67	1.15	1.64	0.38
2	4.76	no	3.02	2.23	1.48	1.44
3	4.60	no	5.07	0.64	0.65	0.62
4	4.45	yes	5.85	0.64	0.54	0.25
5	4.45	yes	2.35	0.58	0.40	1.55
6	4.76	yes	1.05	0.925	0.64	0.25

dimension values for each jet velocity time record. A two-way, repeated measures ANOVA reveals that there is a significant difference in the fractal dimension value depending on whether or not predators are present in the upstream flow ($p < 0.015$). A plot of the mean fractal values according to the presence of predators is shown in Figure 5.15. The fractal dimension values are closer to 1.5 when predators are present, which signifies that the clam jet velocity values are more random when the predator is present upstream. A two-way, repeated measures NANOVA finds that there is no significant difference in the shape of the lacunarity curves in this data set (Table 5.12).

Table 5.11: Fractal dimension for the time records of clam excurrent vertical velocity. The table reports data for varying horizontal crossflow velocity with and without a predator in the upstream flow.

focal clam	length (cm)	predator	Crossflow velocity (cms^{-1}) 0.55	1.2	1.98	2.86
1	4.76	no	1.8245	1.814	1.7873	1.8468
2	4.76	no	1.8701	1.8836	1.8714	1.8721
3	4.60	no	1.839	1.7896	1.8126	1.7566
4	4.45	yes	1.8413	1.744	1.7953	1.8177
5	4.45	yes	1.7697	1.7428	1.8098	1.6304
6	4.76	yes	1.6871	1.7256	1.8226	1.7374

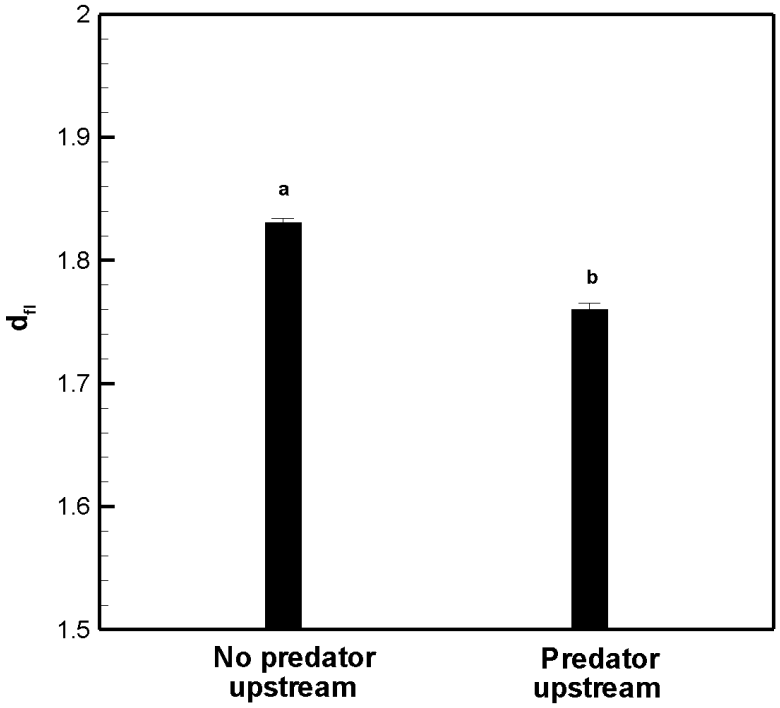

Figure 5.15: Mean fractal dimension value for time records of vertical velocity for the cases reported in Table 5.11 according to the presence or absence of predators. Error bars represent standard error values. The letters indicate significant difference with a two-way, repeated measures ANOVA ($p = 0.015$).

Table 5.12: Lacunarity curve type for time records of clam excurrent vertical velocity. The table reports data for varying horizontal crossflow velocity with and without a predator in the upstream flow.

focal clam	length (cm)	predator	Crossflow velocity (cms^{-1}) 0.55	1.2	1.98	2.86
1	4.76	no	Random	Random	Random	Random
2	4.76	no	Random	Random	Random	Random
3	4.60	no	Size	Random	Random	Fractal
4	4.45	yes	Random	Random	Random	Random
5	4.45	yes	Size	Fractal	Random	Fractal
6	4.76	yes	Size	Fractal	Random	Random

5.5 Discussion

5.5.1 Clam Pumping Behavior

Our qualitative observations of the clam excurrent jet suggests behavior that is similar to previously reported observations. For instance, clam filtering "resting periods" rates are comparable to those of de Bruin and Davids (1970), (personal observation, not recorded). As a result, many of the clam measurement events in the current data collection consisted of several discrete time records that began and ended due to "resting periods".

Troost et al. (2009) used a PIV system to measure the incurrent velocities and modelled the excurrent jet velocities of three bivalves: a mussel, oyster, and cockle. They were unable to use the PIV system to determine excurrent jet characteristics due to the filter feeding nature of the organisms removing the suspended synthetic white particles of 25-50 μm diameter. They predicted excurrent jet velocity values an order of magnitude larger than those collected for clams in the current study, which suggests that the model may have significant limitations. Frank et al. (2008) found PIV systems to accurately characterize the excurrent jet flow of *Mercenaria mercenaria* along with an ascidian, a mussel, an oyster, and a scallop. Titanium dioxide (TiO_2, 2 μm diameter) provided a seeding particle that was sufficient for the PIV system requirements and passed through the bivalve filter. They found similar

mean jet velocity values as those collected in the current study without disturbing either the fluid or the animal in quiescent flow conditions. They were interested in bulk jet velocity values to determine a direct method of finding clearance rates rather than the quantitative characteristics of the excurrent jet flow.

Based on these observations, the clams used in this study are pumping in a manner that appears consistent with observations of previous studies. The measurements of Frank et al. (2008) and the extensive testing of seeding particles indicates that titanium dioxide particles pass through *Mercenaria mercenaria* with sufficient density to facilitate PIV measurements and do not visibly alter the pumping behavior.

The control cases in the current study document a background characteristic of randomness or unsteadiness in vertical velocity values for steady jets, clam shell only, mimic siphon only, and sediment pockets due to clam burying. The patterns in the lacunarity curves seen for the clam jets (Table 5.8) are not present in any of the control cases (Table 5.4). Most notable is the lack of coherence in the comparison between the lacunarity plot patterns for the biological clam jets and the steady clam mimic jets. Steady jet clam mimics or chemical sources do not mimic the source characteristics for actual clam chemical metabolite plumes. Therefore, the information available to predators in the downstream plume of a steady source does not necessarily represent the information available to predators in actual clam chemical plumes. Also, steady jet clam mimic results may underestimate the mixing of the excurrent jet chemicals. Other observations from the control cases include that there are no contributions to the patterns seen in the lacunarity plot shapes due to the pockets created by the burying action of clams, the presence of the clam shell or non-pumping clams, or the presence of the clam mimic siphon. Finally, since the clam source characteristics are highly unsteady and have lacunarity shapes that are not seen in steady source clam mimics, studies that use clam mimics may be underestimating the mixing/dilution of the clam jet. This could impact calculations of concentration boundary layers or

clam refiltration rates. The novel information provided by the current measurements is the quantification of the unsteadiness of clam excurrent jet flow, and the impacts of the results are discussed in the following subsection.

5.5.2 Dominant Predator-Prey Interaction

The predator-prey system of interest here is the relationship between bivalve clams (*Mercenaria mercenaria*) and their predators, whelks (*Busycon carica*) and blue crabs (*Calinectes sapidus*). While both predators use olfactory tracking to locate their clam prey, they have specific consumption methods and are successful in flows possessing different hydrodynamic characteristics. For example, blue crabs prefer to consume smaller, more easily crushed clams, depending on the availability and level of starvation [114]. In contrast, whelks consume clams of all sizes and have higher predation success in high turbulence regimes [54]. The reaction of the clams to the density of the patch is dependent on the size of the clam (Table 5.8) which suggests that if the clam behavioral modifications are related to predation, blue crabs dominate the predator-prey system. Since clams of all sizes are susceptible to whelk predation, whelks are not likely controlling the predator-prey relationship here because there is a dependence of clam size their reaction to clam patch density. It may be advantageous for clams to develop feeding strategies that avoid predation by blue crabs when members of clam patches are of certain sizes and densities. A large chemical plume, resulting from the interaction of many clam excurrent jets, may attract blue crabs to the area, in which case the smallest clams are the most susceptible to predation. On the other hand, since crabs have been shown to react to more discreet filaments of chemical cues [82], it may be advantageous for small clams, when individuals, to employ feeding behavior that avoids predation by controlling the distribution of their jet velocity values. The dependence of clam reaction to patch density on the clam size, in the current data (Table 5.8), suggests that blue crabs dominate the predator-prey

relationship.

Blue crabs tend to be more successful at locating prey in lower turbulence regimes (unless the flow rate decreases to quiescent) and their success decreases with increasing ambient turbulence [187]. If blue crab predation pressure is dominating the predator-prey relationship, as the density/size results suggest, then clam behavioral changes according to the ambient turbulence, or in this case, crossflow velocity may also increase survivorship. The textural distribution of the clam jet velocity values changes according to the ambient horizontal crossflow velocity (Table 5.8), a pattern which is not observed in any of the control cases (Table 5.4). As the ambient turbulence regime changes, clams are altering the chemical plume source characteristics. Clam behavior, in response to hydrodynamic conditions, may be a result of predation pressure during those conditions. Clam feeding behavior could contribute to creation of a hydrodynamic refuge or avoidance of a hydrodynamic predation hotspot. They may also be controlling the mixing of the chemical cues in dominant ambient hydrodynamic conditions.

Blue crab tracking success is also decreased when the chemical source plume has a pulsed release rather than a continuous release [92]. Pulsed release plumes are a simple mimic to test the crab's ability with unsteady chemical source releases. The clam jet velocity time records of the current study have highly unsteady velocity values (e.g., Figure 5.3) and the lacunarity curves suggest that there are often documented gaps between values of velocity (Table 5.8). Therefore, with unsteady clam excurrent jets, as observed here, crabs may have less predation success. Weissburg and Zimmer-Faust (1993) suggest that there may be certain hydrodynamic conditions that provide a refuge from predation pressure by certain predators. A key component for study of the predator-prey system here is how the prey item may disguise their presence within the spatial and temporal environment [183], and our results suggest that clams are altering the randomness of the jet velocities according to predators and ambient

turbulence which may contribute to this "disguise". However, without evidence of how the behavioral changes actually alters the downstream chemical plumes, the above statement is speculative, at best.

5.5.3 Predator Avoidance Behavior

Clams have been shown to have reduced growth rates when predator chemical cues are present, even without direct predation pressure [126]. Nakaoka (2000) suggests that the growth rate reduction is mediated by clam predator avoidance behavior. Smee and Weissburg (2006) found that predator-induced predation avoidance behavior does increase the survivorship of clams in the field and the results presented in the current study may be a quantification of that predator avoidance behavior. Smee and Weissburg (2006) also found that clam reduction in feeding was specific to the type of predator and the ambient flow characteristics.

In the current study, clams enhance the randomness of their excurrent jet velocity values when predator cues are present in the upstream flow (Figure 5.15), which is consistent with the findings of both Nakaoka (2000) and Smee and Weissburg (2006). The presence or absence of predators in the upstream flow of the current study alters the way in which clams are choosing to pump. The clam chemical source velocity values are more random when predators are present in the upstream flow. The randomness of the velocity values may reduce or change the amount of information in the downstream chemical plume. The clams of the current study are sensing the presence of predators in the upstream flow and altering manner in which they feed. This behavioral difference could account for the reduced growth rates through energy reallocation or reduced filtration rates. Smee and Weissburg (2006) found that clams that are in the presence of (caged) predators experience lowered predation rates which could be a direct result of the feeding behavioral changes seen here. There may be a trade-off between the reduced growth rates and increased survival rates that is worth

the effort of altering the jet velocity randomness in the presence of predators.

Irlandi and Peterson (1991) suggested that predation avoidance behavior is responsible for reduced clam growth rates on sand flats when compared to those on the fringes of sea grass beds and when compared to clams within the sea grass beds. Predation pressure is higher on sand flats than within the sea grass beds due to the sea grass structure hindering predator locomotion. Clams located in sand flats would have higher rates of predation avoidance behavior due to the higher rates of direct and indirect predation pressure. Reduced growth rates could be due to reduced amounts of food particles reaching the interior of the clam by avoiding feeding during times of high predation pressure. Also, predator avoidance behavior could reduce growth rates by reallocating energy from growth to controlling the excurrent jet velocity randomness. The clams of the current study are altering their feeding behavior according to environmental conditions such as the size and density of clams, the horizontal crossflow velocity, and the presence or absence of predators. Jet velocity randomness strategies may have energy costs associated with them and these behaviors may reduce the energy available for clam growth in regions of high predation pressure or specific ambient flow rates. In fact, Wells (1957) found more clams in locations with faster currents and regions with sediments of shell hash rather than sand, which suggests that predation pressure is low in regions that have increased amounts of ambient turbulence. As the ambient turbulence increases, clam survivorship also increases and in the current study clam excurrent velocity time records have varying characteristics of unsteadiness depending on the horizontal crossflow velocity (Table 5.8). Although, Judge et al. (1992) found no relationship between the crossflow velocity and clam growth, which suggests that growth may be more dependent on predator effects.

5.5.4 Patch Dynamics

It may be advantageous to be part of a densely packed clam patch when of a certain size range and to be an individual at other size ranges. The difference in clam jet velocity randomness, as found in the current study, is dependent on the density of clams in the patch and the size of the organism (Table 5.8). The current study examined at excurrent jet behavior for clams separated by a small distances, such that in many cases the clam shells were touching one another. Clams of the patch densities used in the current study have been shown to have behavioral differences in their movement from the placement location [193]. The closely packed clams tend to move away from one another significantly more than those of the sparsely spaced patch. While clams are most often buried beneath the sediment, they do create pockets in the sediment through their burying action. Also as sediment transport occurs, they become more or less buried depending on the conditions, which could result in exposure of the clam shell. Therefore, the presence of clams adds roughness features to sand and mud flats. Green et al. (1998) found a critical mussel density where skimming flow began and the crossflow does not reattach to the sediment surface after moving past the roughness features. Skimming flow reduces the drag coefficient on the organisms and could provide a refuge for larval settlement or mutual bivalve sheltering. There may be a critical clam plot density according to the onset of skimming flow or even the onset of chemical plume interaction depending on the dominant size range within the plot. There may be a critical clam density in which the advantageous behavior changes from unsteady flow to steady flow when the clam chemical plumes begin to interact with one another. Coco et al. (2006) took a step further and theorized that bivalve patch dynamics were not necessarily the sum of the behaviors of individual animals. The current study found that clam response to the density of the patch is dependent on the size of the clam (Table 5.8). This suggests that individual clams have clam patch specific behaviors that when scaled-up to the

size of the patch have different characteristics than a sum of clam behaviors from individual clams.

Coco et al. (2006) modelled the patch dynamics and found that there may be multiple stable states and that the first factor that is controlled by the flow field, food concentration, and patch density is recruitment of larval clams. Therefore, the behavior of clams according to the clam density and clam size found herein (Table 5.8) may not necessarily be directly related to predation, but indirectly through larval recruitment. Hart et al. (1996) found that larval settlement is highly dependent on hydrodynamic cues. Adult clam feeding behavior may be contributing to those hydrodynamic conditions as a means of communication to larvae as to whether or not the patch is recruiting or deterring new patch members. In fact, Ertman and Jumars (1988) found that the presence of bivalve siphons may enhance the settlement of larvae. The results here indicate that clams of different sizes alter their feeding behavior depending on the density within the patch. If patch recruitment is more dominant than predation pressure, as Coco et al. (2006) suggests, the differences in feeding behavior may not be fostering a refuge from predation but signalling clam larvae or promoting the hydrodynamic conditions that induces or deters larvae from settling. Through this hydrodynamic signalling method, clams of certain sizes may control the clam patch density.

5.5.5 Influence of Siphon Flow on the Plume

Clam excurrent jets are biological examples of a jet-in-crossflow. Much of the jet-in-crossflow literature cites the jet to crossflow velocity ratio as a dominant controlling feature of the system. Andreopoulos and Rodi (1984) found that as the jet to crossflow ratio decreases, the jet tends to bend over and the crossflow is deflected over the jet fluid. Also, as the jet to crossflow velocity ratio increases, the jet bending is much more gradual and the crossflow is deflected around the jet fluid. Entrainment of ambient

fluid into the jet flow increases as jet fluid height increases. This entrainment would result in lowered concentrations of the clam chemical metabolites in the downstream chemical plume.

The mean clam jet velocities collected in the current study have jet to crossflow velocity ratios of roughly between 1 and 2, which is in the mid-high range of ratios tested by Andreopolous and Rodi (1984) (although, their velocity magnitudes and Reynolds numbers were much higher). With mid-high velocity ratios, the clam jets of the current study should be reaching relatively large heights in the water column. Clam mimics jets, which were supplied with steady jet flow, were shown to increase in height with a decrease in jet to crossflow velocity ratio [116]. O'Riordan et al. (1993) found that in a dense clam patch (with steady clam mimic jets), more mixing occurs with higher siphon heights and smaller jet velocities. Also, a dominant factor in chemical metabolite concentrations is the clam patch density, with the siphon height being a secondary factor, [133], with larger clams having larger excurrent siphon lengths. However, Thorin et al. (1998) found that another clam species (*Mya arenaria*) tended to avoid extending their siphons above the sediment surface. Although the siphon heights were not quantified in the current study, they were often above the sediment surface. This suggests that the siphon height is an important factor for mixing of metabolites when clam excurrents are interacting with other clams. This could account for the size depended response to patch density (Table 5.8), in that, large clams could compensate more easily for patches of high density when promoting the mixing of their chemical plume. In contrast, small clams, with short siphons, would have higher energy costs when promoting the mixing of their downstream chemical plume. In this context, clams of different size ranges would be likely to have different jet velocity unsteady characteristics depending on the density of clams in the patch, as was found in the current study (Table 5.8).

The clam jet velocity time records presented here are highly unsteady (Figure

5.3) and the character of the unsteadiness changes with horizontal crossflow velocity , size and density of clams, and the presence of predators (Table 5.8 and Figure 5.15). While the velocity time records of the clams do not necessarily have specific pulsing frequencies associated with them, we can compare the time records to literature quantifying the effects of pulsed jets and pulsed jets-in-crossflow due to the unsteady nature of pulsed jet flow. Bera et al. (2001) found that unsteady (pulsed) jets had higher rates of entrainment of the receiving fluid into the jet fluid. The larger rates of entrainment result in lower concentration of the jet fluid in the plume. For clams, this may result in the dilution of chemical metabolites, and it may be advantageous to encourage the mixing of the chemical plume depending on the ambient turbulence level or when predators are detected in the flow. Laminar pulsed jets have a more spread plume than continuous jets and laminar vortex rings are more persistent due to the unsteadiness [20]. As vortex rings are more persistent, they are present longer and travel higher in the water column before they are dissipated, resulting in more entrainment of the ambient fluid. When predators are present in the upstream flow, clams increase the randomness of their excurrent (Figure 5.15). Unsteadiness is associated with higher rates of entrainment and therefore, lowered jet fluid concentrations in the downstream plume. It may be advantageous to encourage the dilution of the chemical metabolites with predators cues in the flow. Hermanson et al (1998) found that as the injection time of the pulsed flow decreased, the shedding vortex rings were more persistent. The lacunarity curves found in the current study could inform as to the injection time by equating injection time with the clumped nature of the velocity values in the jet velocity time records. A break in the slope of the lacunarity plot could indicate a dominant clam injection time scale. A smaller dominant box size corresponds to more persistent vortex rings, according to the results of Hermanson et al. (1998).

Low frequency pulsing has been found to lead to more entrainment because it

fosters large vortex ring formation and persistence [22]. The PSD curves of the current study, while not revealing a dominant frequency, had more power with the lowest frequencies (Figure 5.5). Also, Johari et al. (1999) found that there are optimal combinations of frequency of pulsing and the duration of the pulse for enhancement of the penetration of the vortex rings into the water column. They found that as the vortex rings were separated in time/space the entrainment of the ambient fluid into the jet plume increased. Wegner et al. (2004) found that jet flow unsteadiness and mixing increased according to the jet angle with respect to the crossflow dominant direction. With a jet angled upstream to the crossflow, more mixing of the jet fluid should occur. The example clam presented had the siphon pointing in the upstream direction (Figure 5.2), as did many of the clam jets collected. Clams have the ability to, and often do, change the angle, location, and size of their excurrent siphons. This behavior was not necessarily quantified here, however it was observed quite frequently. By angling the jet siphon in the upstream direction, the downstream chemical plume may be wider and more dilute than with other siphon positions.

Clams are altering their feeding behavior according to external environmental conditions such as the ambient horizontal crossflow velocity (Table 5.8) and the presence or absence of predators in the upstream flow (Figure 5.15). Also, the reaction of clams to the density of the clam patch is dependent on the size of the animal (Table 5.8). Therefore, clams have dynamic feeding behaviors that are influenced by many external conditions and they react by controlling the unsteady character and distribution of randomness in the velocity of the excurrent jet.

CHAPTER VI

SUMMARY AND CONCLUSIONS

This study has three distinct experimental sections that looked at aspects of the reciprocal relationship between bivalve clams and their predators: field measurements of vertical distribution of velocity, laboratory experiments quantifying the effect of environmental cues on clam pumping behavior, and laboratory experiments quantifying the effect of predator influence on clam feeding. This chapter summarizes the findings of each set of experiments, integrates the experiments, and makes conclusions about the predator-prey system as a whole. The chapter also summarizes the unique contributions of this study and gives suggestions for future work in this area.

6.1 Summary

The relationship between the predators (blue crabs and whelks) and prey (hard clams) is mediated by the generation, transmission, and acquisition of clam chemical metabolites. Generally, this study attempts to quantify the control that clams have on the generation and transmission of the chemical signal.

Clams are filter feeders that uptake ambient fluid through their incurrent siphon, filter food particles out of the fluid, and release waste products with the filtered sea water through their excurrent siphon in a jet-like flow structure. Clams are able to control the height, diameter, and velocity of the excurrent jet.

6.1.1 Field Experiments Addressing Crossflow

The clam excurrent jet flow adds vertical momentum to the ambient boundary layer, and the field experiments of the current study quantify the clam effect on the crossflow. The current study quantifies the effects of actual clam jets in field conditions to

determine the relative magnitude of the influence of clams when compared to other field influences.

ADV measurements were collected of the u, v, and w components of velocity simultaneously above patches of clams and above sediment with no clams for several sites that are typical of clam habitats. Treatment sites included tidal flats with mud substrates and flats with sand substrates. Also, velocity measurements were collected for clam patches downstream of oyster beds and downstream of sea grass beds with mud as the dominant substrate type.

The effect of clams on the crossflow and turbulence characteristics such as Turbulent Kinetic Energy (TKE) and Reynolds shear stress ($\overline{u'w'}$) were determined for the field treatment sites. The horizontal homogeneity assumption allows direct comparison of the turbulence characteristics for the simultaneous measurements with and without clams. The assumption of flow uniformity over the probe separation distance of 1 m is consistent with many previous studies, [53], [174], [166], and [84].

For the mud and sand sites, clams alter the horizontal velocity, particularly close to the sediment. However, they appear to decrease the velocity values over the mud substrates and increase the velocity values over the sand substrates. A primary difference between the mud and sand sites is that the mud site consists of unidirectional flow, whereas the sand site has reverse flow near the bed, which indicates that the boundary layer is separated.

The effect of clams on the TKE appears to be dependent on the magnitude of the horizontal flow and the site treatment type. In general though, clams tended to increase the peak values of the TKE for most of the treatment sites of this study. In a few cases, clams altered the height in which the peak TKE value occurred.

The Reynolds shear stress measurements did not reveal a clear pattern in the type of clam influence, which suggests that there may be a factor(s) that controls clam influence that this study does not take into account. Although, there is evidence

that the horizontal crossflow velocity is one of the controlling factors. There may be some other confounding factor that influences the way in which clams are altering the shear stress of the boundary layer flow. Often, clams changed the sign of the shear stress values, which indicates a shape change in the velocity gradients of the flow. It is worth noting that, of course, experiments of this type in the field are much more difficult to interpret compared to laboratory experiments in which the researcher has much greater control of the flow environment and conditions.

6.1.2 Laboratory Experiments Addressing Environmental Cues

To quantify the clam excurrent jet behavior and decouple the influence of behavior and presence of clams, PIV images were collected for a plane that bisects clam excurrent jets in a laboratory flume. This laboratory experiment quantifies the clam jet velocity unsteadiness according to environmental cues such as the horizontal crossflow velocity, clam patch density, and organism size/age. Since the influence of clams on TKE and shear stress in the field experiment, above, was ambient velocity specific, an understanding of clam behavioral changes according to the horizontal ambient velocity would inform as to the cause of the alterations to the turbulence characteristics. Clams may be controlling their feeding behavior according to the crossflow velocity to promote hydrodynamic conditions that alter the transmission of their chemical metabolites and ultimately the chemosensory information available to predators in the downstream chemical plume.

The PIV images allowed for an extraction of a clam jet velocity time record and a lacunarity analysis quantified the "texture" of the unsteadiness of the clam jet velocity. Clams are altering the unsteadiness of their jet velocity depending on the horizontal crossflow velocity.

As clams grow they become less susceptible to predation by blue crabs, since crabs use their claws to crush their prey items. Also, clam patches may have a

different downstream chemical signature due to the interaction of clam jets than the downstream chemical signature of an individual clam. Therefore, this study collected clam jet velocity time records in the laboratory flume for clams of two different size ranges and two nearest neighbor distances. The lacunarity analysis of the excurrent jet velocity time records found that clam reaction to patch density is dependent on the size of the organism. This result suggests that it may be advantageous for clams of certain size ranges to be associated with patches of certain densities. It also suggests that blue crab predation dominates the system.

6.1.3 Laboratory Experiments Addressing Predator Cues

The field experiment described above does not control the presence or absence of predators and how that influences the way in which clams alter the crossflow. To understand the influence predators have on the way in which clams alter their feeding behavior, a laboratory PIV experiment was conducted to quantify the randomness of clam excurrent jet velocities depending on the presence or absence of predators.

Clam jet velocity time records were extracted from the PIV images in the same manner as the first laboratory experiment. A fractal analysis of the jet velocity time records found that clams jet velocity values are more random when predator cues are present in the upstream flow than when there are no predator cues.

When clams detect predator cues in the upstream flow their feeding behavior alters to increase the randomness of the velocity values. This alteration increases the unsteadiness of the jet velocity values. According to the jets-in-crossflow literature unsteady jets result in higher rates of mixing than steady jets. With unsteady jets, more ambient fluid is entrained into the downstream jet flow diluting the jet fluid concentration. When clams detect the presence of predators, their feeding behavior modifications result in more dilute downstream chemical plumes. This apparent predator avoidance behavior may contribute to clam survival rates.

6.2 Conclusions

This study sought to quantify the reciprocal relationship between the bivalve clam, *Mercenaria mercenaria*, and the hydrodynamics of the fluid flow in which they live. The jet-like flow from the excurrent siphon of the clam, due to filter feeding, alters the crossflow of estuarine tidal flow. The results suggest that despite the fact that there are many confounding factors that could both contribute to the boundary layer characteristics and overwhelm the biological contributions, the clams of this study altered the boundary layer velocity profiles, the Turbulent Kinetic Energy, and the Reynolds shear stress in the field. The alterations by clams were dependent on several factors such as the type of sediment, the type of obstacles present in the flow, and the ambient horizontal crossflow velocity.

The TKE and Reynolds shear stress are influenced by the presence and behavior of clams depending on the ambient crossflow velocity. This interaction may be controlled by the relative influence of the ambient turbulence overwhelming the influence of the biology for the large flow rate situations. Alternatively, the differences in clam influence according to the crossflow velocity may, in fact, be due to clam behavioral changes according to the ambient flow conditions. Therefore, quantification of the types of clam behaviors and the factors that control those behaviors will further quantify the effects of clams on the flow. The field experiments indicate that clams alter the crossflow in ecologically relevant flow cases, which then alters the information in the downstream chemical metabolite plume.

Knowing that clams are altering the crossflow in the field, the laboratory experiments were designed to decouple the effects of the presence and behavior of clams. Since the influence on the crossflow is dependent on the ambient crossflow velocity, the laboratory experiments quantified the clam jet velocity behavior according to the crossflow velocity. Clams alter the excurrent velocity unsteadiness according to the crossflow velocity. These changes were not seen in control cases. Thus, the differences

in the boundary layer turbulence characteristics that were found in the field experiments are due to the behavioral changes in clam feeding according to the ambient crossflow velocity.

The laboratory experiments also found that clam reactions to the density of the clam patch is dependent on the size of the organism. There are differences according to clam size and patch density, which suggests that blue crabs are the dominant predator of the system, since blue crabs have diminishing predation success as clam size increases [114]. Hence, clams altering their behavior in response to ambient flow turbulence may have a greater influence on predation rates in relation to avoiding blue crabs. The second set of laboratory experiments determined that, in fact, clams were increasing the jet velocity randomness depending on the presence of blue crab cues in the upstream flow. Further, the field results suggest that those behavioral changes alter the ambient flow characteristics. An increase in the randomness of the jet velocity (as is seen here) presumably increases the mixing of the jet fluid and decreases the concentration of the clam chemical metabolites in the downstream flow. Blue crabs have been shown to use instantaneous concentration filaments to track the chemical plume, [121], [187], and [185]. Therefore, by increasing the randomness of the excurrent jet velocity and increasing the TKE values (as shown in the field experiments) clams may decrease the success rate of blue crabs.

In conclusion, the results suggest that clam behavior influences both the chemical plume source characteristics and the transmission of the chemical metabolites within the downstream chemical plume.

6.3 Unique Contributions

The unique contributions to the fields of experimental fluid mechanics and ecology are divided into contributions to methods, flow dynamics, and ecology:

6.3.1 Contributions to Methods

- Evidence that the Bricker and Monismith (2007) method for wave energy removal could be confounded by the addition of noise, particularly in the calculation of off diagonal Reynolds stress values.

- Successful design and implementation of a direct method of collecting clam excurrent jet flow dynamics without disturbing either the fluid or the animal.

- Identification of Titanium Dioxide as an effective seeding particle for PIV analysis of *Mercenaria mercenaria* siphon flow.

- Successful application of the Hurst's rescaled range fractal analysis to biologically-generated time records to quantify randomness.

- Successful application of a lacunarity analysis to both biological time records with equal and unequal fractal dimensions as a measure of the "texture" of the randomness.

6.3.2 Contributions to Flow Dynamics

- Evidence of measurable biological influence on field boundary layer dynamics.

- Evidence that clam excurrent jets appear as jets-in-crossflow and behave similar to the cases of jets-in-crossflow in the engineering literature.

- Observation that clams do not have dominant periodic unsteadiness in the jet excurrent velocity.

- Control time record analysis confirms that clam body presence or clam influence on the sediment does not alter the vertical velocity unsteadiness.

- Observation that clam chemical source characteristics cannot be mimicked with steady jet flow.

- Observation that clam mimic siphons, themselves, do not contribute to the differences in the crossflow.

6.3.3 Contributions to Ecology

- Quantification of clam feeding behavioral alterations in the presence of predator cues.
- Quantification of clams feeding behavioral alterations according to hydrodynamic conditions.
- Observation that clams of different size ranges alter their feeding behavior according to the patch dynamics.
- Observation that clams alter behavior according to size, indicating dominance of Blue Crab predation on the predator-prey system.
- Quantifiable explanation as to differences in clam survival rates depending on field environment, i.e. mud, seagrass, oyster beds.

6.4 Future Directions

The horizontal homogeneity assumption put forth by Trowbridge (1998) does not extend beyond Reynolds stress values and has previously been unknowingly applied to mean velocity values over small distances in field settings, [53], [174], [166], and [84]. Quantification of the applicability of the assumption of comparable mean velocity values over short distances, specifically in shallow tidal estuaries would confirm the conclusions made in this and other field studies. A simple application of the simultaneous ADV measurements made in this study over the distances used here (without clams in the sediment) could give an indication of the relative differences in the velocity values for the system. With an accurate quantification of the range of differences in velocity values over the horizontal distances of this study, the effect of

the influence of clams on the velocity boundary layer profiles could be solidified. The current study can only theorize that differences in the simultaneous measurements for the field clam patches are due to the presence and behavior of clams rather than the horizontal distance between the measurement volumes.

The boundary layer characteristics captured for the field sites of mud, sand, downstream of oyster beds, and downstream of sea grass beds are for, at most, two vertical measurement sequences at each site. The results and conclusions made in this study cannot necessarily be projected to clam influence over all mud flats or sand flats, etc. Replication of the field experiments over the sites of the current study, over other sites in the Wassaw Sound region, and over sites in other shallow estuaries would strengthen the results of this study. Also, these replications should use an ADCP rather than the ADV's of the current study. Two field Acoustic Doppler Current Profiler's (ADCP's) used from above with the measurements taken in the downward (negative z) direction would be useful to remove the need for presence of the field operator and lengthen the time available for data collection. ADCP's could be deployed over multiple tides and would provided velocity data at each height in the water column simultaneously. This would also remove the need for a time offset between the data collection instruments.

There is evidence that clams within the sea grass beds grow faster than those adjacent to sea grass beds and than those on mud flats. An extension of the field methods here to clam plots within the sea grass beds would discern the relative relationship between clams within and without sea grass beds.

ADV's can collect velocity measurements to within approximately one centimeter of the sediment surface. This region is an important region for clams and their predators and an accurate assessment of the flow characteristics in this region could give insight into the types of information available to predators that have chemosensors located there. PIV or LDV measurements could capture velocity values closer to

the sediment, but would be difficult to implement in field settings where suspended sediments impair visual access. Also, the measurement volume for the ADV's of this study were larger compared to the clam jet diameters. PIV and LDV measurement volumes are much smaller than those of ADV's and would be able to capture velocity measurements on a resolution of the order of the clam jets. In that case, clam jet velocity measurements, similar to those captured in the laboratory experiments of this study, could be completed in field settings. However, a different field site would be necessary due to the clarity of the estuary waters in Wassaw Sound. In such a study, clam behaviors could be coupled with both the ambient horizontal crossflow velocity and the effect of clams behavior on the crossflow.

Both the fractal analysis and the lacunarity analysis used in this study have proven to be easily adapted for use in quantifying clam feeding behavioral modifications. These analyses can be extended to quantify types of behaviors according to other environmental factors such as the presence of food particles, the presence of injured conspecifics, or other. Past studies have used the presence or absence of the clam siphon as an indication of unsafe feeding conditions. The results here suggest that clams that perceive a threat (predator) do not necessarily stop pumping or retract their siphons, but alter the way in which they are filter feeding. There may also be a hierarchy of threat conditions that illicit steps of threat avoidance behavior. When a threat becomes more apparent, there may be further stages of predator avoidance behavior. The time record analysis used in this study could be useful in quantifying the hierarchy of environmental threats.

Other extensions of the fractal and lacunarity analysis could be an extension of the findings that the size of the clam influences the reaction to clam density. Clam patches of the densities used in this study have been shown to relocate more frequently in the high density distribution compared to the low density distribution [193]. Since this study looked at clam behavior of only two patch densities and of only two size

ranges, an array of both these factors would inform as to critical values for each. There may be a critical value of clam density when they change from behaving as a clam patch and begin behaving as an individual clam. Also, there may be a size range that has an advantage to being in a clam patch rather than as an individual, etc. A coupling of critical clam patch densities, clam size ranges, typical patch ranges in the field, and predation rates according to those patch ranges would be useful.

Also, an understanding of the downstream chemical plume characteristics according to the jet unsteadiness found here would be useful in understanding both the information available in the downstream chemical plume and the behavioral responses of predators to that information. The clam mimics used in past studies have used steady, mean velocity values reported by literature using indirect methods of capturing clam excurrent flow rates. Laboratory flume experiments could be conducted using clam mimics designed to have the types of unsteady flows documented here. A Laser Induced Fluorescence (LIF) system, coupled with the randomness quantities for clam behavior captured in this study, could determine the concentrations of chemical metabolites in the downstream clam chemical plumes. This concentration data could be coupled with predation experiments and field or lab clam behavioral experiments to determine if altering the clam jet velocity randomness is responsible for increased clam survival rates when predator cue are present or when clams are located in and around sea grass beds.

APPENDIX A

EXAMPLE LACUNARITY PLOTS FOR LABORATORY EXPERIMENTS

The following plots show the calculated lacunarity plots for the first clam in Table 5.8 as an example set of lacunarity curves for a clam data collection set. Table 5.8 outlines the lacunarity plot shape distinction for each data collection set for the first laboratory experiment.

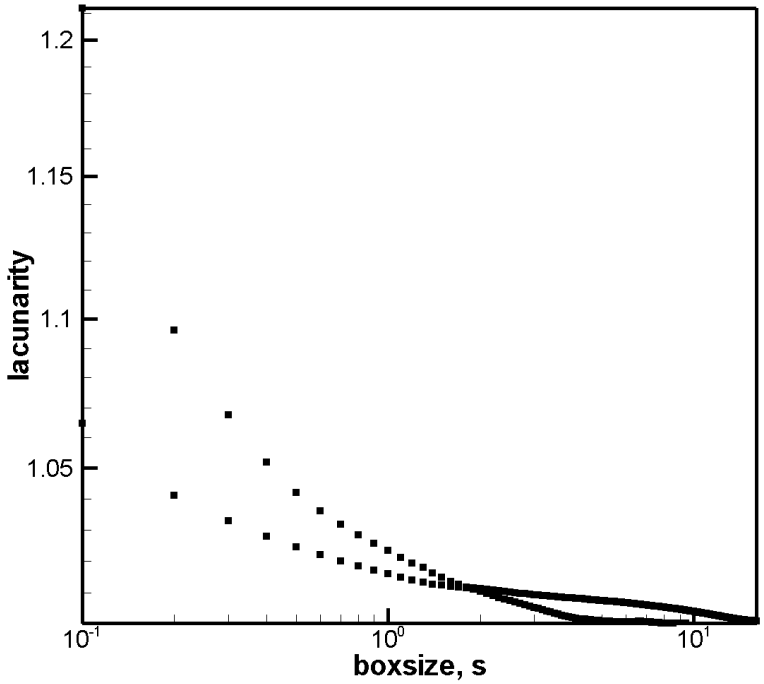

Figure A.1: Lacunarity as a function of box size (i.e., time segment) for the time record of vertical jet velocity for Clam #1 of Table 5.7, $U = 0.55\ cms^{-1}$, clam length = 4.68 cm, and nearest neighbor distance of 3 cm (log axes).

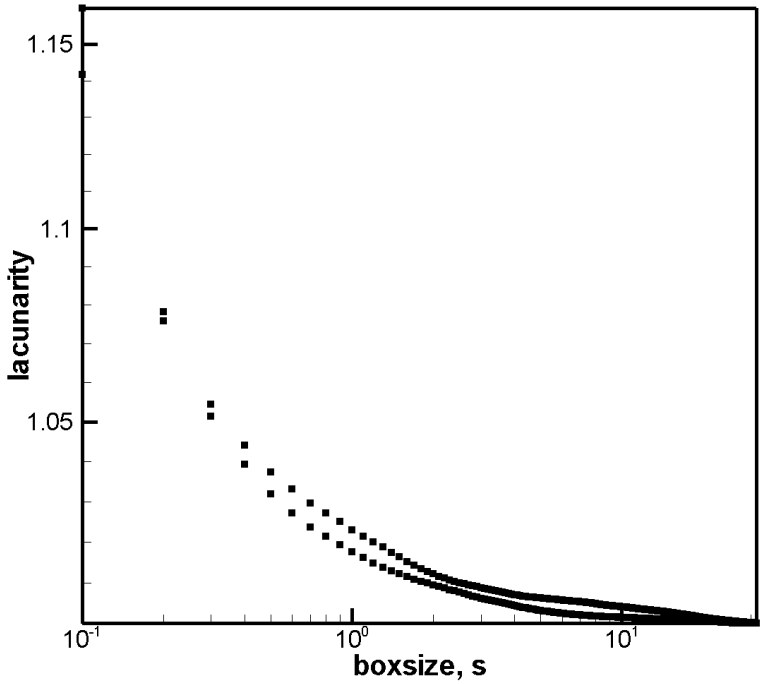

Figure A.2: Lacunarity as a function of box size (i.e., time segment) for the time record of vertical jet velocity for Clam #1 of Table 5.7, $U = 1.2\ cms^{-1}$, clam length = 4.68 cm, and nearest neighbor distance of 3 cm (log axes).

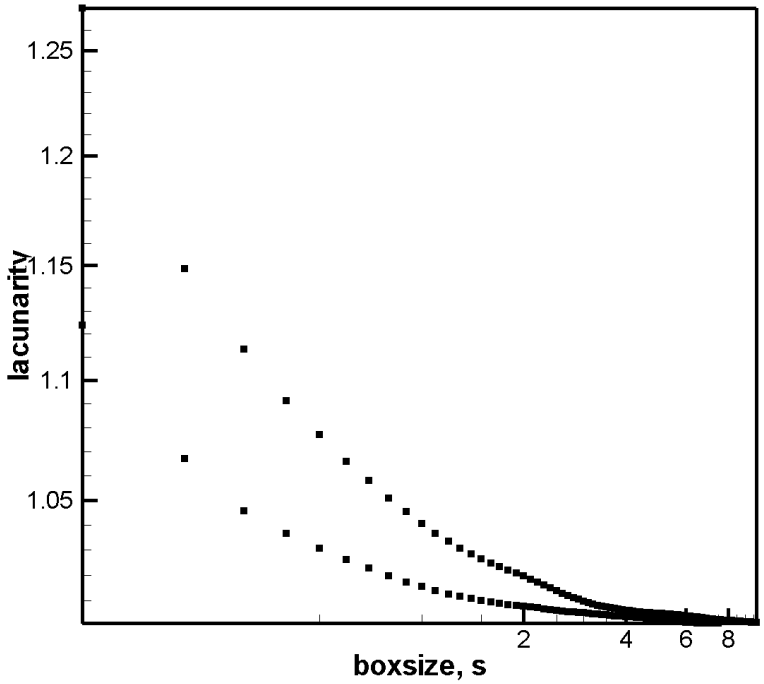

Figure A.3: Lacunarity as a function of box size (i.e., time segment) for the time record of vertical jet velocity for Clam #1 of Table 5.7, $U = 1.98\ cms^{-1}$, clam length = 4.68 cm, and nearest neighbor distance of 3 cm (log axes).

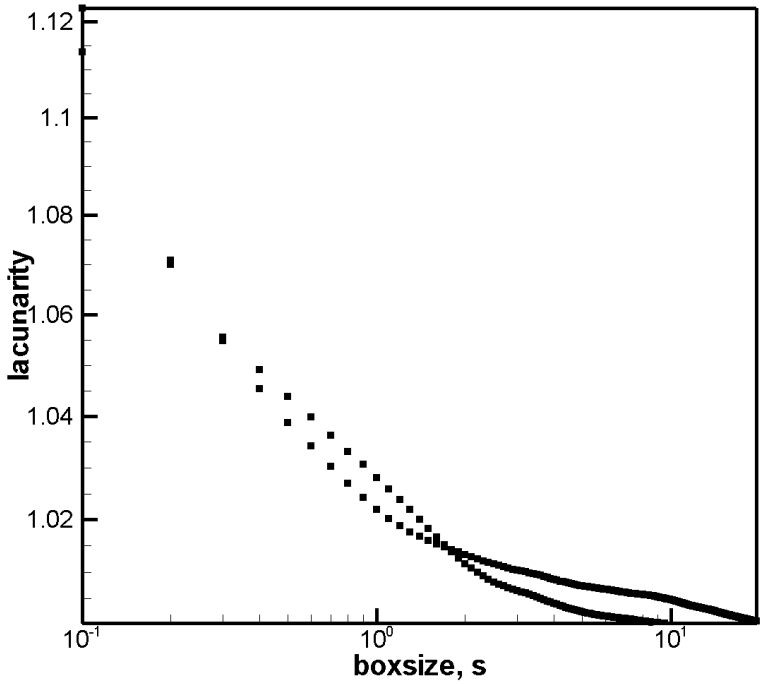

Figure A.4: Lacunarity as a function of box size (i.e., time segment) for the time record of vertical jet velocity for Clam #1 of Table 5.7, $U = 2.86\ cms^{-1}$, clam length $= 4.68\ cm$, and nearest neighbor distance of 3 cm (log axes).

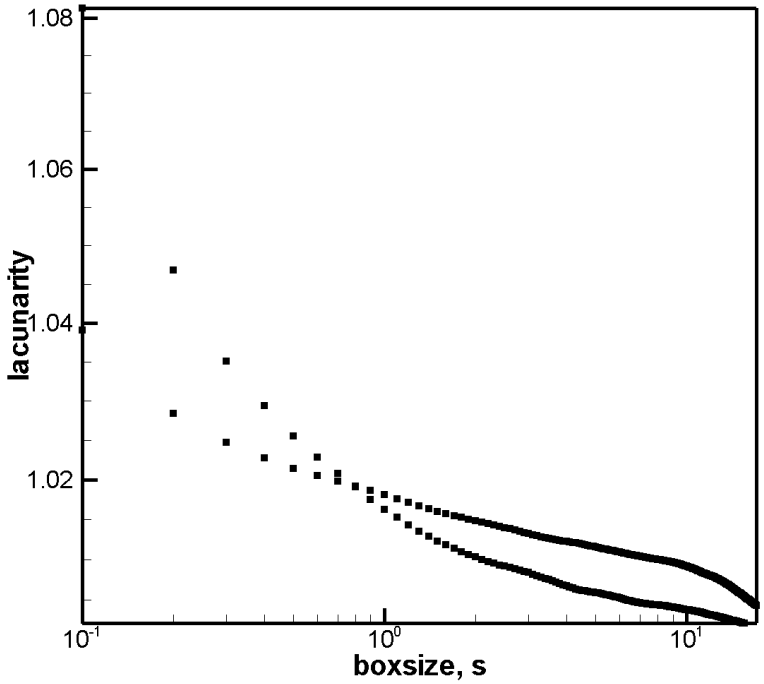

Figure A.5: Lacunarity as a function of box size (i.e., time segment) for the time record of vertical jet velocity for Clam #1 of Table 5.7, $U = 0.55\ cms^{-1}$, clam length = 4.68 cm, and nearest neighbor distance of 9 cm (log axes).

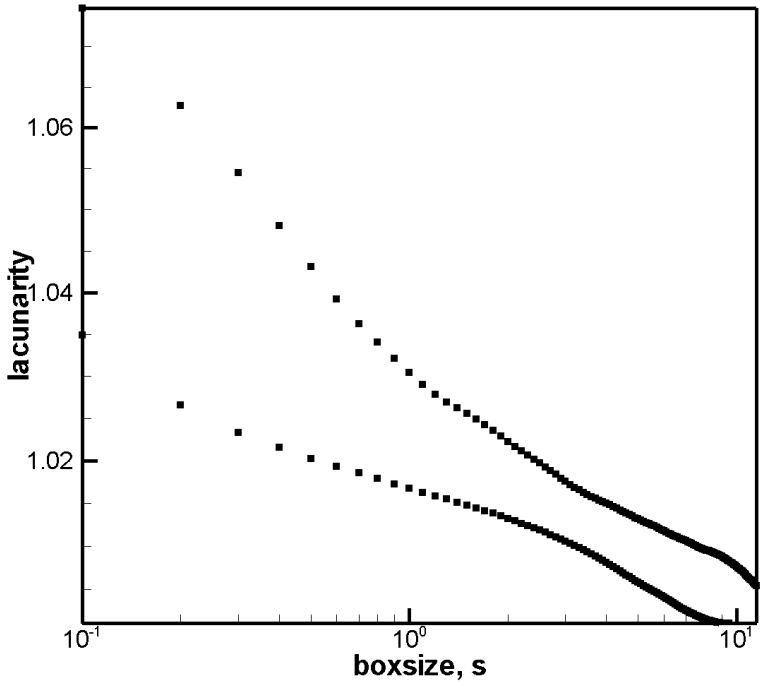

Figure A.6: Lacunarity as a function of box size (i.e., time segment) for the time record of vertical jet velocity for Clam #1 of Table 5.7, $U = 1.2\ cms^{-1}$, clam length = 4.68 cm, and nearest neighbor distance of 9 cm (log axes).

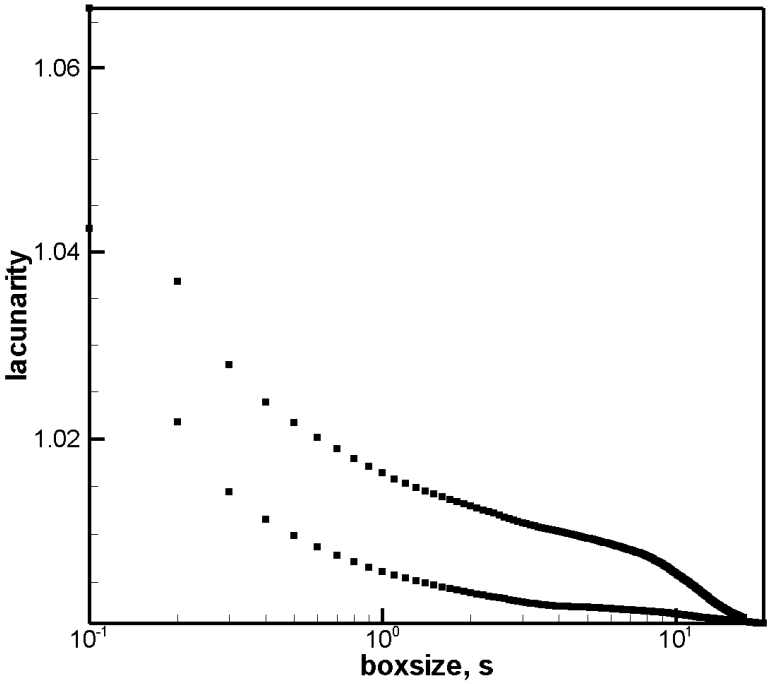

Figure A.7: Lacunarity as a function of box size (i.e., time segment) for the time record of vertical jet velocity for Clam #1 of Table 5.7, $U = 1.98\ cms^{-1}$, clam length = 4.68 cm, and nearest neighbor distance of 9 cm (log axes).

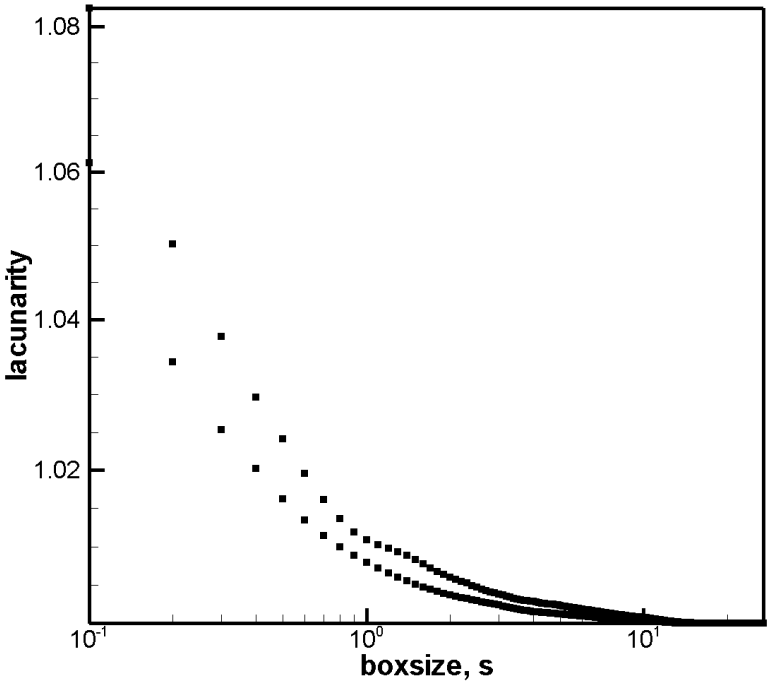

Figure A.8: Lacunarity as a function of box size (i.e., time segment) for the time record of vertical jet velocity for Clam #1 of Table 5.7, $U = 2.86\ cms^{-1}$, clam length = 4.68 cm, and nearest neighbor distance of 9 cm (log axes).

APPENDIX B

ERROR UNCERTAINTY CALCULATIONS FOR PIV AND ADV DATA COLLECTIONS

B.1 PIV Error Uncertainty

Velocity values are collected with the following equation:

$$u = \frac{\Delta x}{m\Delta t} \tag{B.1}$$

where m is the number of pixels per inch for the individual data collection, Δx is change in distance of the particle between images, and Δt is the change in time between images. The uncertainty in the u value

$$\delta u = \{(\frac{\partial u}{\partial \Delta x}\delta\Delta x)^2 + (\frac{\partial u}{\partial m}\delta m)^2 + (\frac{\partial u}{\partial \Delta t}\delta\Delta t)^2\}^{\frac{1}{2}} \tag{B.2}$$

$\Delta t = 10\ ms \pm 0.005\ ms$

$m = 364\ \frac{pix}{in} \pm 1\ \frac{pix}{in}$

$\delta\Delta t$ and δm are small compared to $\delta\Delta x$

Therefore,

$$\delta u \sim \frac{\delta\Delta x}{m\Delta t} \tag{B.3}$$

$\delta\Delta x \cong 0.01\ mm$ by Abbas study with a stagnant water tank image.

$\delta\Delta x \cong 0.01\ mm(364\frac{pix}{in})(\frac{1in}{25.4mm}) = 0.14\ pix$

$\delta u = \frac{0.14pix}{(14.33\frac{pix}{mm})(0.01s)} = 0.98\ mms^{-1}$

$\frac{\delta u}{U} = \frac{0.98mms^{-1}}{52.3mms^{-1}} = 1.9\% \sim 2.0\%$

The standard deviation for this case is 5.36 cms^{-1}, which is approximately 100% of the mean value.

B.2 ADV Error Uncertainty

Turbulent Kinetic energy values are calculated with the following equation:

$$TKE = \frac{1}{2}(u'u' + v'v' + w'w') \tag{B.4}$$

where u', v', and w' are the velocity fluctuation values collected from the ADV measurement data collection.

The uncertainty in the TKE value

$$\delta TKE = \{(\frac{\partial TKE}{\partial u'}\delta u')^2 + (\frac{\partial TKE}{\partial v'}\delta v')^2 + (\frac{\partial TKE}{\partial w'}\delta w')^2\}^{\frac{1}{2}} \tag{B.5}$$

From the Sontek ADV manual: $\delta u' = \delta v' = \delta w' = 1\%$ of the measured value. Therefore, $\frac{\delta TKE}{\delta u'} = 2u'$, etc.

$\delta TKE = [\{2u'(0.01u')\}^2 + \{2v'(0.01v')\}^2 + \{2w'(0.01w')\}^2]^{\frac{1}{2}}$

$\delta TKE = [0.0004(-0.4181 cms^{-1})^4 + 0.0004(-0.9701 cms^{-1})^4 + 0.0004(-0.9598 cms^{-1})^4]^{\frac{1}{2}} = 0.027(cms^{-1})^2$

$\frac{\delta TKE}{TKE} = \frac{0.027(cms^{-1})^2}{3.4939(cms^{-1})^2} = 0.008 \sim 1\%$

This calculation would include the wave energy that is also collected with the ADV's. After wave energy removal, we would assume that the error uncertainty in the TKE value would remain 1% of the mean TKE value.

REFERENCES

[1] Abelson, A., Miloh, T., and Loya, Y., "Flow patterns induced by substrata and body morphologies of benthic organisms, and theier roles in determining availability of food particles," *Limnology and Oceanography*, vol. 38, no. 6, pp. 1116–1124, 1993.

[2] Ackerman, J. D., Loewen, M. R., and Hamblin, P. F., "Benthic–pelagic coupling over a zebra mussel reef in western Lake Erie," *Limnology and Oceanography*, vol. 46, no. 4, pp. 892–904, 2001.

[3] Ackerman, J. D. and Nishizaki, M. T., "The effect of velocity on the suspension feeding and growth of the marine mussels *Mytilus trossulus* and *M. calufornianus*: implications for niche separation," *Journal of Marine Systems*, vol. 49, pp. 195–207, 2004.

[4] Adler, D. and Baron, A., "Predictions of a three-dimensional circular turbulent jet in crossflow," *AIAA Journal*, vol. 17, no. 2, pp. 168–174, 1979.

[5] Allain, C. and Cloitre, M., "Characterizing the lacunarity of random and deterministic fractal sets," *Physical Review*, vol. 44, no. 6, pp. 3552–3558, 1991.

[6] Andreopoulos, J., "On the structure of jets in a crossflow," *Journal of Fluid Mechanics*, vol. 157, pp. 163–197, 1985.

[7] Andreopoulos, J. and Rodi, W., "Experimental investigations of jets in a crossflow," *Journal of Fluid Mechanics*, vol. 138, pp. 93–127, 1984.

[8] Arianos, S. and Carbone, A., "De trending moving average algorithm: A closed-form approximation of the scaling law," *Physica A*, vol. 382, pp. 9–15, 2007.

[9] Atema, J., "Eddy chemotaxis and odor landscapes: exploration of nature with animal sensors," *Biological Bullitin*, vol. 191, no. 1, pp. 129–138, 1996.

[10] Baker, T. C., Hansson, B. S., Lofstedt, C., and Lofqvist, J., "Adaptation of antennal neurons in moths is associated with cessation of pheromone-mediated upwind flight," *Proceedings of the National Acadamy of Sciences of the United States of America*, vol. 85, pp. 9826–9830, 1988.

[11] Baker, T. C. and Kuenen, L. P. S., "Pheromone source location by flying moths: a supplementary non-anemotactic mechanism," *Science*, vol. 216, no. 4544, pp. 424–427, 1982.

[12] Belanger, J. H. and Arbas, E. A., "Behavioral strategies underlying pheromone-modulated flight in moths: lessons from simulation studies," *Journal of Comparative Physiology A*, vol. 183, pp. 345–360, 1998.

[13] Bera, J. C., Michard, M., Grosjean, N., and Comte-Bellot, G., "Flow analysis of two-dimensional pulsed jets by particle image velocimetry," *Experiments in Fluids*, vol. 31, pp. 519–532, 2001.

[14] Berry, W. A., "A Hydrodynamic characterization of tidal ecosystems with respect to predation," *Master's Thesis, Georgia Institute of Technology*, 2009.

[15] Boguslawski, L. and Popiel, C. O., "Flow structure of the free round turbulent jet in the initial region," *Journal of Fluid Mechanics*, vol. 90, no. FEB, pp. 531–539, 1979.

[16] Bouma, T. J., van Duren, L. A., Temmerman, S., Claverie, T., Blanco-Garcia, A., Ysebaert, T., and Herman, P. M. J., "Spatial flow and sedimentation patterns within patches of epibenthic structures: Combining field, flume and modelling experiments," *Continental Shelf Research*, vol. 27, no. 8, pp. 1020–1045, 2007.

[17] Bricker, J. D. and Monismith, S. G., "Spectral wave-turbulence decomposition," *Journal of Atmospheric and Oceanic Technology*, vol. 24, pp. 1479–1487, 2007.

[18] Butman, C. A., Freshette, M., Geyer, W. R., and Starczak, V. R., "Flume experiments on food-supply to the blue mussel *Mytilus edulis L* as a function of boundary layer flow," *Limnology and Oceanography*, vol. 39, no. 7, pp. 1755–1768, 1994.

[19] Cardinale, B., Gelmann, E., and Palmer, M., "Net spinning caddisflies as stream ecosystem engineers: the influence of Hydropsyche on benthic substrate stability," *Functional Ecology*, vol. 18, no. 3, pp. 381–387, 2004.

[20] Cater, J. E. and Soria, J., "The evolution of round zero-net-mass-flux jets," *Journal of Fluid Mechanics*, vol. 472, pp. 167–200, 2002.

[21] Catton, K. B., Webster, D. R., Brown, J., and Yen, J., "Quantitative analysis of tethered and free-swimming copepodid flow fields," *Journal of Experimental Biology*, vol. 210, pp. 299–310, 2007.

[22] Chang, Y. K. and Vakili, A. D., "Dynamics of vortex rings in crossflow," *Physics of Fluids*, vol. 7, no. 7, pp. 1583–1597, 1995.

[23] Chanson, H., Brown, R., Ferris, J., Ramsay, I., and Warburton, K., "Preliminary measurements of turbulence and environmental parameters in a sub-tropical estuary of eastern australia," *Environmental Fluid Mechanics*, vol. 5, pp. 553–575, 2006.

[24] Chanson, H., Trevethan, M., and ichi Aoki, S., "Acoustic doppler velocimetry (ADV) in small estuary: Field experience and signal post-processing," *Flow Measurement and Instrumentation*, vol. 19, pp. 307–313, 2008.

[25] Chhabra, S., Shipman, T. N., and Prasad, A. K., "The entrainment behavior of a turbulent axisymmetric jet in a viscous host fluid," *Experiments in Fluids*, vol. 38, pp. 70–79, 2005.

[26] Coco, G., Thrush, S. F., Green, M. O., and Hewitt, J. E., "Feedbacks between bivalve density, flow, and suspended sediment concentration on patch stable states," *Ecology*, vol. 87, pp. 2862–2870, 2006.

[27] Coelho, S. L. V. and Hunt, J. C. R., "The dynamics of the near field of strong jets in crossflows," *Journal of Fluid Mechanics*, vol. 200, pp. 95–120, 1989.

[28] Cole, B. E., Thompson, J. K., and Cloern, J. E., "Measurement of filtration rates by infaunal bivalves in a recirculating flume," *Marine Biology*, vol. 113, pp. 219–225, 1992.

[29] Collins, M. B., Ke, X., and Gao, S., "Tidally-induced flow structures over intertidal flats," *Estuarine, Coastal and Shelf Science*, vol. 46, pp. 233–250, 1998.

[30] Coughlan, J. and Ansell, A. D., "A direct method of determining the pumping rate of siphonate bivalves," *Journal Du Conseil*, vol. 29, no. 2, pp. 205–213, 1964.

[31] Cowen, E. and Monismith, S., "A hybrid digital particle tracking velocimetry technique," *Experiments in Fluids*, vol. 22, no. 3, pp. 199–211, 1997.

[32] Crimaldi, J. P., Koehl, M. A. R., and Kosseff, J. R., "Effects of the resolution and kinematics of olfactory appendages on the interception of chemical signals in a turbulent odor plume," *Environmental Fluid Mechanics*, vol. 2, pp. 35–63, 2002.

[33] Crimaldi, J. P., Koseff, J. R., and Monismith, S. G., "Structure of mass and momentum fields over a model aggregation of benthic filter feeders," *Biogeosciences*, vol. 4, pp. 269–282, 2007.

[34] Dahm, W. J. A. and Dimotakis, P. E., "Mixing at large Schmidt number in the self-similar far field of turbulent jets," *Journal of Fluid Mechanics*, vol. 217, pp. 299–330, 1990.

[35] Dasi, L. P., "The small-scale structure of passive scalar mixing in turbulent boundary layers," *PhD Thesis, Georgia Institute of Technology*, 2004.

[36] Davids, C., "The influence of suspensions of micro-organisms of different concentrations on the pumping and retention of food by the mussel (*Mytilus edulis L.*)," *Netherlands Journal of Sea Research*, vol. 2, pp. 233–249, 1964.

[37] de Bruin, J. P. C. and Davids, C., "Observations on the rate of water pumping of the freshwater mussel *Anodonta cycygnea zellensis* (gmelin)," *Netherlands Journal of Zoology*, vol. 20, no. 3, pp. 380–391, 1970.

[38] Defossez, J.-M., Daguzan, J., and Poulicek, M., "A new method for recording the *in situ* pumping activity of infaunal bivalves," *Journal of Molluscan Studies*, vol. 63, pp. 9–17, 1997.

[39] Demuren, A. O., "Multigrid acceleration and turbulence models for computations of 3d turbulent jets in crossflow," *International Journal of Heat and Mass Transfer*, vol. 35, no. 11, pp. 2783–2794, 1992.

[40] Demuren, A. O., "Characteristics of three-dimensional turbulent jets in crossflow," *International Journal of Engineering Science*, vol. 31, no. 6, pp. 899–913, 1993.

[41] Denis, L., Alliot, E., and Grzebyk, D., "Clearance rate responses of mediterranean mussels, *Mytilus galloprovincialis*, to variations in the flow, water temperature, food quality and quantity," *Aquatic Living Resources*, vol. 12, no. 4, pp. 279–288, 1999.

[42] Derby, C. D., "Learning from spiny lobsters about chemosensory coding of mixtures," *Physiology and Behavior*, vol. 69, pp. 203–209, 2000.

[43] Derby, C. D. and Steullet, P., "Why do animals have so many receptors? The role of multiple chemosensors in animal perception," *Biological Bullitin*, vol. 200, pp. 211–215, 2001.

[44] Drinnen, R. E., "An apparatus for recording the water-pumping behaviour of lamellibranchs," *Netherlands Journal of Sea Research*, vol. 2, pp. 223–232, 1964.

[45] Dusenbery, D. B., "Performance of basic strategies for following gradients in two dimensions," *Journal of theoretical Biology*, vol. 208, pp. 345–360, 2001.

[46] Englund, G., "Asymetric resource competition in a filter-feeding stream insect (*Hydropsyche siltalai*; trichoptera)," *Freshwater Biology*, vol. 26, pp. 425–432, 1991.

[47] Ertman, S. C. and Jumars, P. A., "Effects of bivalve siphonal currents on the settlement of inert particles and larvae," *Journal of Marine Research*, vol. 46, pp. 797–813, 1988.

[48] Falcone, A. and Cataldo, J., "Entrainment velocity in an axisymmetric turbulent jet," *Journal of Fluids Engineering-Transactions of the ASME*, vol. 125, no. 4, pp. 620–627, 2003.

[49] Fan, L. T., "Stochastic analysis of a three-phase fluidized bed: Fractal approach," *AIChE Journal*, vol. 36, no. 10, pp. 1529–1535, 1990.

[50] Farrell, J. A., Pang, S., and Li, W., "Plume mapping via hidden markov methods," *IEEE Transactions on Systems, Man, and Cybernetics–Part B: Cybernetics*, vol. 33, no. 6, pp. 850–862, 2003.

[51] Farrell, J. A., Pang, S., and Li, W., "Chemical plume tracing via an autonomous underwater vehicle," *IEEE Journal of Oceanic Engineering*, vol. 30, no. 2, pp. 428–442, 2005.

[52] Feddersen, F. and III, A. J. W., "Direct estimation of the Reynolds stress vertical structure in the nearshore," *Journal of Atmospheric and Oceanic Technology*, vol. 24, pp. 102–116, 2007.

[53] Ferner, M. C., Smee, D. L., and Weissburg, M. J., "Habitat complexity alters lethal and non-lethal olfactory interactions between predators and prey," *Marine Ecology Progress Series*, vol. 374, pp. 13–22, 2009.

[54] Ferner, M. C. and Weissburg, M. J., "Slow-moving predatory gastropods track prey odors in fast and turbulent flow," *Journal of Experimental Biology*, vol. 208, pp. 809–819, 2005.

[55] Finelli, C. M., "Velocity and concentration distributions in turbulent odor plumes in the presence of vegetation mimics: a flume study," *Marine Ecology Progress Series*, vol. 207, pp. 297–309, 2000.

[56] Finelli, C. M., Pentcheff, N. D., Zimmer, R. K., and Wethey, D. S., "Physical constraints on ecological processes: a field test of odor-mediated foraging," *Ecology*, vol. 81, no. 3, pp. 784–797, 2000.

[57] Finelli, C. M., Pentcheff, N. D., Zimmer-Faust, R. K., and Wethey, D. S., "Odor transport in turbulent flows: constraints on animal navigation," *Limnology and Oceanography*, vol. 44, no. 4, pp. 1056–1071, 1999.

[58] Frank, D. M., Ward, J. E., Shumway, S. E., Holohan, B. A., and Gray, C., "Application of particle image velocimetry to the study of suspension feeding in marine invertebrates," *Marine and Freshwater behaviour and physiology*, vol. 41, no. 1, 2008.

[59] Frederiksen, R. D., Dahm, W. J. A., and Dowling, D. R., "Experimental assessment of fractal scale similarity in turbulent flows. Part 2. Higher-dimensional intersections and non-fractal inclusions," *Journal of Fluid Mechanics*, vol. 338, pp. 89–126, 1997.

[60] Fric, T. F. and Roshko, A., "Vortical structure in the wake of a transverse jet," *Journal of Fluid Mechanics*, vol. 279, pp. 1–47, 1994.

[61] Goring, D. G. and Nikora, V. I., "Despiking acoustic doppler velocimeter data," *Journal of Hydraulic Engineering*, vol. 128, pp. 117–126, 2002.

[62] Grasso, F. W., "Invertebrate-inspired sensory-motor systems and autonomous, olfactory-guided exploration," *Biological Bullitin*, vol. 200, pp. 160–168, 2001.

[63] Grasso, F. W. and Basil, J. A., "How lobsters, crayfishes, and crabs locate sources of odor: current perspectives and future directions," *Neurobiology*, vol. 12, pp. 721–727, 2002.

[64] Grasson, F. W., Consi, T. R., Mountain, D. C., and Atema, J., "Biomimectic robot lobster performs chemo-orientation in turbulence using a pair of spatially separated sensors: progress and challanges," *Robotics and Autonomous Systems*, vol. 30, pp. 115–131, 2000.

[65] Green, M. O., Hewitt, J. E., and Thrush, S. F., "Seabed drag coefficient over natural beds of horse mussels (*Atrina zelandica*)," *Journal of Marine Research*, vol. 56, pp. 613–637, 1998.

[66] Grizzle, R. E., Langan, R., and Howell, W. H., "Growth responses of suspension-feeding bivalve molluscs to changed in water flow: differences between siphonate and nonsiphonate taxa," *Journal of Experimental Marine Biology and Ecology*, vol. 162, pp. 213–228, 1992.

[67] Gross, T. F. and Nowell, A. R. M., "Spectral scaling in a tidal boundary layer," *Journal of Physical Oceanography*, vol. 15, pp. 496–508, 1985.

[68] Growns, I. O. and Davis, J. A., "Longitudinal changes in near-bed flows and macroinvertibrate communities in a Western Australian stream," *Journal of the North American Benthological Society*, vol. 13, pp. 417–438, 1994.

[69] Gui, L. and Wereley, S. T., "A correlation-based continuous window-shift technique to reduce the peak-locking effect in digital piv image evaluation," *Experiments in Fluids*, vol. 32, pp. 506–517, 2002.

[70] Hart, D. D., Clark, B. D., and Jasentuliyana, A., "Fine-scale field measurement of benthic flow environments inhabited by stream invertebrates," *Limnology and Oceanography*, vol. 41, no. 2, pp. 297–308, 1996.

[71] Hart, D. D. and Finelli, C. M., "Physical-biological coupling in streams: the pervasive effects of flow on benthic organisms," *Annual Review of Ecological Systems*, vol. 30, pp. 363–395, 1999.

[72] Hermanson, J. C., Wahba, A., and Johari, H., "Duty-cycle effects on penetration of fully modulated, turbulent jets in crossflow," *AIAA Journal*, vol. 36, no. 10, pp. 1935–1937, 1998.

[73] Higuera, F. J. and Martinez, M., "An incompressible jet in a weak cross-flow," *Journal of Fluid Mechanics*, vol. 249, pp. 73–97, 1993.

[74] Hir, P. L., Roberts, W., Cazaillet, O., Christie, M., Bassoullet, P., and Bacher, C., "Characterization of intertidal flat hydrodynamics," *Continental Shelf Research*, vol. 20, pp. 1433–1459, 2000.

[75] Horner, A. J., Weissburg, M. J., and Derby, C. D., "Dual antennular chemosensory pathways can mediate orientation by caribbean spiny lobsters in naturalistic flow conditions,"

[76] Hurst, H. E., "Suggested statistical model of some time series which occur in nature," *Nature*, vol. 180, no. 4584, p. 494, 1957.

[77] Hurst, H. E., Back, R. P., and Simaika, Y. M., "A long-term plan for the nile basin," *Nature*, vol. 160, no. 4070, pp. 611–612, 1947.

[78] Hussein, H. J., Capp, S. P., and George, W. K., "Velocity-measurements in a high-Reynolds-number, momentum-conserving, axisymmetrical, turbulent jet," *Journal of Fluid Mechanics*, vol. 258, pp. 31–75, 1994.

[79] Inoue, T. and Nakamura, Y., "A new method for measuring flow structure in the benthic boundary layer using an acoustic doppler velocimeter," *Journal of Atmospheric and Oceanic Technology*, vol. 25, pp. 822–830, 2008.

[80] Irlandi, E. A. and Peterson, C. H., "Modification of animal habitat by large plants: mechanisms by which seagrasses influence clam growth," *Oecologia*, vol. 87, pp. 307–318, 1991.

[81] Jabbal, M. and Zhong, S., "The near wall effect of synthetic jets in a boundary layer," *International Journal of Heat and Fluid Flow*, vol. 29, pp. 119–130, 2008.

[82] Jackson, J. L., Webster, D. R., Rahman, S., and Weissburg, M. J., "Bed-roughness effects on boundary-layer turbulence and consequences for odor-tracking behavior of blue crabs (*callinectes sapidus*)," *Limnology and Oceanography*, vol. 52, no. 5, pp. 1883–1897, 2007.

[83] Johari, H., Pacheco-Tougas, M., and Hermanson, J. C., "Penetration and mixing of fully modulated turbulent jets in crossflow," *AIAA Journal*, vol. 37, no. 7, pp. 842–850, 1999.

[84] Jonsson, P., Petersen, J., Karlsson, O., Loo, L., and Nilsson, S., "Particle depletion above experimental bivalve beds: In situ measurements and numerical modeling of bivalve filtration in the boundary layer," *Limnology and Oceanography*, vol. 50, no. 6, pp. 1989–1998, 2005.

[85] Jørgensen, C. B., "Bivalve filter feeding revisited," *Marine Ecology Progress Series*, vol. 142, pp. 287–302, 1996.

[86] Judge, M. L., Coen, L. D., and Jr., K. L. H., "The effect of long-term alteration of in situ currents on the growth of *Mercenaria mercenaria* in the northern Gulf of Mexico," *Limnology and Oceanography*, vol. 37, no. 7, pp. 1550–1559, 1992.

[87] Jumars, P. A. and Nowell, A. R. M., "Effects of benthos on sediment transport - difficulties with functional grouping," *Continental Shelf Research*, vol. 3, no. 2, pp. 115–130, 1984.

[88] Jumars, P. A., Nowell, A. R. M., and Self, R. F. L., "A simple-model of flow-sediment-oranism interation," *Marine Geology*, vol. 42, no. 1-4, pp. 155–172, 1981.

[89] Kawanisi, K. and Yokosi, S., "Mean and Turbulence Characteristics in a Tidal River," *Estuarine, Coastal and Shelf Science*, vol. 38, pp. 447–469, 1994.

[90] Keller, T. A., Powell, I., and Weissburg, M. J., "Role of olfactory appendages in chemically mediated orientation of blue crabs," *Marine Ecology Progress Series*, vol. 261, pp. 217–231, 2003.

[91] Keller, T. A., Tomba, A. M., and Moore, P. A., "Orientation in complex chemical landscapes: spatial arrangement of chemical sources influences crayfish food-finding efficiency in artificial streams," *Limnology and Oceanography*, vol. 46, no. 2, pp. 238–247, 2001.

[92] Keller, T. A. and Weissburg, M. J., "Effects of odor flux and pulse rate on chemosensory tracking in turbulent odor plumes by the blue crab, *callinectes sapidus*," *Biological Bullitin*, vol. 207, pp. 44–55, 2004.

[93] Kim, S. C., Friedrichs, C. T., Maa, J. P. Y., and Wright, L. D., "Estimating bottom stress in tidal boundary layer from acoustic doppler velocimetry data," *Journal of Hydraulic Engineering*, vol. 126, no. 6, pp. 399–406, 2000.

[94] Kim, S. W. and Benson, T. J., "Calculation of a circular jet in crossflow with a multiple-time-scale turbulence model," *International Journal of Heat and Mass Transfer*, vol. 35, no. 10, pp. 2357–2365, 1992.

[95] Kindsvater, C. E. and Carter, R. W. C., "Discharge characteristics of rectangular thin-plate wiers," *Journal of the Hydraulics Division*, vol. 83, no. HY6, pp. 1453–1488, 1957.

[96] Kozlowski, C., Voigt, R., and Moore, P. A., "Changes in odour intermittency influence the success and search behaviour during orientation in the crayfish (*Orconectes rusticus*)," *Marine and Freshwater Behavioral Physiology*, vol. 36, no. 2, pp. 97–110, 2003.

[97] Kraus, N. C., Lohrmann, A., and Cabrera, R., "New Acoustic meter for measuring 3D Laboratory flows," *Journal of Hydraulic Engineering-ASCE*, vol. 120, no. 3, pp. 406–411, 1994.

[98] Krothapalli, A. and Lourenco, L., "Separated flow upstream of a jet in a crossflow," *AIAA Journal*, vol. 28, no. 3, pp. 414–420, 1989.

[99] LaBarbera, M., "Water flow patterns in and around three species of articulate brachiopods," *Journal of Experimental Marine Biology and Ecology*, vol. 55, pp. 185–206, 1981.

[100] Li, W., Farrell, J. A., Pang, S., and Arrieta, R. M., "Moth-inspired chemical plume tracking on an autonomous underwater vehicle," *IEEE Transactions on Robotics*, vol. 22, no. 2, pp. 292–307, 2006.

[101] Lightbody, A. F. and Nepf, H. M., "Prediction of velocity profiles and longitudinal dispersion in emergent salt marsh vegetation," *Limnology and Oceanography*, vol. 51, no. 1, pp. 218–228, 2006.

[102] Loosanoff, V. L. and Engle, J. B., "Feeding of oyster in relation to density of microorganisms," *Science*, vol. 105, no. 2723, pp. 160–261, 1947.

[103] Loosanoff, V. L. and Tommers, F. D., "Effect of suspended silt and other substances on rate of feeding of oyster," *Science*, vol. 107, no. 2768, pp. 69–70, 1948.

[104] Luckenback, M. W., Huggett, D. V., and Zobrist, E. C., "Sediment transport, biotic modifications and selection of grain-size in a surface deposit-feeder," *Estuaries*, vol. 11, no. 2, pp. 134–139, 1988.

[105] Mafra-Neto, A. and Carde, R. T., "Fine-scale structure of pheromone plumes modulates upwind orientation of flying moths," *Nature*, vol. 369, pp. 142–144, 1994.

[106] Mandelbrot, B. B. and Vanness, J. W., "Fractional brownian motions fractional noises and applications," *Siam Review*, vol. 10, no. 4, p. 422, 1968.

[107] Mandelbrot, B. B., *The Fractal Geometry of Nature*. W. H. Freeman and Company, 1977.

[108] Mead, K. S., "From odor molecules to plume tracking: an interdisciplinary, multilevel approach to olfaction in stomatapods," *Integrative and Comparative Biology*, vol. 42, pp. 258–264, 2002.

[109] Mead, K. S. and Koehl, M. A. R., "Stomatapod antennule design: the asymmetry, sampling efficiency and ontogeny of olfactory flicking," *The Journal of Experimental Biology*, vol. 203, pp. 3795–3808, 2000.

[110] Mead, K. S., Wiley, M. B., Koehl, M. A. R., and Koseff, J. R., "Fine-scale patterns of odor encounter by the antennules of mantis shrimp tracking turbulent plumes in wave-affected and unidirectional flow," *The Journal of Experimental Biology*, vol. 206, pp. 181–193, 2003.

[111] Meneveau, C. and Chhabra, A. B., "Two-point statistics of multifractal measures," *Physica A*, vol. 164, pp. 564–574, 1990.

[112] Meneveau, C. and Sreenivasan, K. R., "The multifractal nature of turbulent energy dissipation," *Journal of Fluid Mechanics*, vol. 224, pp. 429–484, 1991.

[113] Meyer, K. E. E., Pedersen, J. M., and Ozcan, O., "A turbulent jet in crossflow analysed with proper orthogonal decomposition," *Journal of Fluid Mechanics*, vol. 583, pp. 199–227, 2007.

[114] Micheli, F., "Behavioural plasticity in prey-size selectivity of the blue crab *Callinectes sapidus* feeding on bivalve prey," *Journal of Animal Ecology*, vol. 64, pp. 63–74, 1995.

[115] Mollendorf, J. C. and Gebhart, B., "Experimental and numerical study of viscous stability of a round laminar vertical jet with and without thermal buoyancy for symmetric and asymmetric distrubances," *Journal of fluid mechanics*, vol. 61, no. Nov 6, pp. 367–&, 1973.

[116] Monismith, S. G., Koseff, J. R., Thompson, J. K., O'Riordan, C. A., and Nepf, H., "A study of model bivalve siphonal currents," *Limnology and Oceanography*, vol. 35, no. 3, pp. 680–696, 1990.

[117] Moore, P. and Crimaldi, J., "Odor landscapes and animal behavior: tracking odor plumes in different physical worlds," *Journal of Marine Systems*, vol. 49, pp. 55–64, 2004.

[118] Moore, P. A. and Atema, J., "Spatial information in the three-dimensional fine structure of an aquatic odor plume," *Biological Bullitin*, vol. 181, pp. 408–418, 1991.

[119] Moore, P. A. and Grills, J. L., "Chemical orientation to food by the crayfish *Orconectes rusticus*: influence of hydrodynamics," *Animal Behaviour*, vol. 58, pp. 953–963, 1999.

[120] Moore, P. A., Scholz, N., and Atema, J., "Chemical orientation of lobsters, *Homarus americanus*, in turbulent odor plumes," *Journal of Chemical Ecology*, vol. 17, pp. 1293–1307, 1991.

[121] Moore, P. A., Weissburg, M. J., Parrish, J. M., Zimmer-Faust, R. K., and Gerhardt, G. A., "Spatial distribution of odors in simulated benthic boundary layer flows," *Journal of Chemical Ecology*, vol. 20, no. 2, pp. 225–279, 1994.

[122] Morton, B. R. and Ibbetson, A., "Jets deflected in a crossflow," *Experimental Thermal and Fluid Science*, vol. 12, pp. 112–133, 1996.

[123] Murlis, J., *The structure of Odour plumes*. Oxford: Clarendon, 1986.

[124] Murlis, J. and Jones, C. D., "Fine-scale structure of odour plumes in relation to insect orientation to distant pheromone and other attractant sources," *Physiological Entomology*, vol. 6, pp. 71–86, 1981.

[125] Murray, J., Meadows, A., and Meadows, P., "Biogeomorphological implications of microscale interactions between sediment geotechnics and marine benthos: a review," *Geomorphology*, vol. 47, no. 1, pp. 15–30, 2002.

[126] Nakaoka, M., "Nonlethal effects of predators on prey populations: predator-mediated change in bivalve growth," *Ecology*, vol. 81, no. 4, pp. 1031–1045, 2000.

[127] Needham, D. J., Riley, N., Lytton, C. C., and Smith, J. H. B., "A jet in crossflow. part 2," *Journal of Fluid Mechanics*, vol. 211, pp. 515–528, 1990.

[128] Needham, D. J., Riley, N., and Smith, J. H. B., "A jet in crossflow," *Journal of Fluid Mechanics*, vol. 188, pp. 159–184, 1988.

[129] Nikora, V., Goring, D., and Biggs, B., "On stream periphyton-turbulence interactions," *New Zealand Journal of Marine and Freshwater Research*, vol. 31, no. 4, pp. 435–448, 1997.

[130] Nikora, V., Green, M. O., Thrush, S. F., Hume, T. M., and Goring, D., "Structure of the internal boundary layer over a patch of pinnid bivalves (*Atrina zelandica*) in an estuary," *Journal of Marine Research*, vol. 60, pp. 121–150, 2002.

[131] O'Riordan, C. A., "The effects of near-bed hydrodynamics on benthic bivalve filtration rates," *PhD Thesis, Stanford University*, 1993.

[132] O'Riordan, C. A., Monismith, S. G., and Koseff, J. R., "A study of concentration boundary-layer formation over a bed of model bivalves," *Limnology and Oceanography*, vol. 38, no. 8, pp. 1712–1729, 1993.

[133] O'Riordan, C. A., Monismith, S. G., and Koseff, J. R., "The effect of bivalve excurrent jet dynamics on masss transfer in a benthic boundary layer," *Limnology and Oceanography*, vol. 40, no. 2, pp. 330–344, 1995.

[134] Pallikari, F. and Boller, E., "A rescaled range analysis of random events," *Journal of Scientific Exploration*, vol. 13, no. 1, pp. 25–40, 1999.

[135] Palmer, R. E., "Behavioral and rhythmic aspects of filtration in the bay scallop, *Argopecten irradians concentricus* (say), and the oyster, *Crassostrea verginica* (gmelin)," *Journal of Experimental Marine Biology and Ecology*, vol. 45, pp. 273–295, 1980.

[136] Peng, J., Dabiri, J. O., Madden, P. G., and Lauder, G. V., "Non-invasive measurement of instantaneous forces during aquatic locomotion: a case study of the bluegill sunfish pectoral fin," *Journal of Experimental Biology*, vol. 210, no. 4, pp. 685–698, 2007.

[137] Plotnick, R. E., Gardner, R. H., Hargrove, W. W., Prestegaard, K., and Perlmutter, M., "Lacunarity analysis: A general technique for the analysis of spatial patterns," *Physical Review*, vol. 53, no. 5, pp. 5461–5468, 1996.

[138] Powers, S. P. and Kittinger, J. N., "Hydrodynamic mediation of predatror-prey interactions: differential patterns of prey susceptibility and predator success explained by variation in water flow," *Journal of Experimental Marine Biology and Ecology*, vol. 273, pp. 171–187, 2002.

[139] Precht, E., Janssen, F., and Huettel, M., "Near-bottom performance of the acoustic doppler velocimeter (adv)-a comparative study," *Aquatic Ecology*, vol. 40, pp. 481–492, 2006.

[140] Press, W. H., Teukolsky, S. A., Vetterling, W. T., and Flannery, B. P., *Numerical Recipes in Fortran: The art of scientific computing*. Cambridge University Press, 1986.

[141] Price, R. E. and Schiebe, F. R., "Measurements of velocity from excurrent siphons of freshwater clams," *The Nautilus*, vol. 92, no. 2, pp. 67–69, 1978.

[142] Rahman, S. and Webster, D. R., "The effect of bed roughness on scalar fluctuations in turbulent boundary layers," *Experiments in Fluids*, vol. 38, no. 3, pp. 372–384, 2005.

[143] Rajaratnam, N. and Gangadharaiah, T., "Vortex structure of circular jets in crossflow," *Journal of Wind Engineering and Industrial Aerodynamics*, vol. 12, pp. 155–164, 1983.

[144] Reidenbach, M. A., Monismith, S. G., Koseff, J. R., Yahel, G., and Genin, A., "Boundary layer turbulence and flow structure over a fringing coral reef," *Limnology and Oceanography*, vol. 51, no. 5, pp. 1956–1968, 2006.

[145] Richards, J. R., Beris, A. N., and Lenhoff, A. M., "Steady laminar flow of liquid-liquid jets at high Reynolds numbers," *Physics of Fluids A*, vol. 5, no. 7, pp. 1703–1717, 1993.

[146] Robson, B. J., Chester, E. T., and Davis, J. A., "Maniplating the intensity of near-bed turbulence in rivers: effects on benthic invertebrates," *Freshwater Biology*, vol. 42, pp. 645–653, 1999.

[147] Sau, R. and Mahesh, K., "Dynamics and mixing of vortex rings in crossflow," *Journal of Fluid Mechanics*, vol. 604, pp. 389–409, 2008.

[148] Shaw, W. J. and Trowbridge, J. H., "The direct estimation of near-bottom turbulent fluxes in the presence of energetic wave motions," *Journal of Atmospheric and Oceanic Technology*, vol. 18, pp. 1540–1556, 2001.

[149] Shiono, K. and West, J. R., "Turbulent perturbations of velocity in the conway estuary," *Estuarine, Coastal and Shelf Science*, vol. 25, pp. 533–553, 1987.

[150] Smee, D. L. and Weissburg, M. J., "Clamming up: environmental forces diminish the preceptive ability of bivalve prey," *Ecology*, vol. 87, no. 6, pp. 1587–1598, 2006.

[151] Smee, D. L. and Weissburg, M. J., "Hard clams (*Mercenaria mercenaria*) evaluate predation risk using chemical signals from predators and injured conspecifics," *Journal of Chemical Ecology*, vol. 32, no. 3, pp. 605–619, 2006.

[152] Smith, W. A. M. N., Atsavapranee, P., Katz, J., and Osborn, T. R., "Piv measurements in the bottom boundary layer of the coastal ocean," *Experiments in Fluids*, vol. 33, pp. 962–971, 2002.

[153] Sreenivasan, K. R., "Fractals and multifractals in fluid turbulence," *Annual Review of Fluid Mechanics*, vol. 23, pp. 539–600, 1991.

[154] Statzner, B. and Arens, M.-F., "Silk-producing stream insects and gravel erosion: significant biological effects on critical shear stress," *Water Resources Research*, vol. 35, no. 11, pp. 3495–3506, 1999.

[155] Sykes, R. I., Lewellen, W. S., and Parker, S. F., "On the vorticity dynamics of a turbulent jet in a crossflow," *Journal of Fluid Mechanics*, vol. 168, pp. 393–413, 1986.

[156] Tammes, P. M. L. and Dral, A. D., "Observations on the straining of suspensions by mussels," *Archives Nerlandaises de Zoologie*, vol. 11, pp. 87–112, 1955.

[157] Thomsen, L. and Flach, E., "Mesocosm observations of fluxes of particulate matter within the benthic boundary layer," *Journal of Sea Research*, vol. 37, no. 1-2, pp. 67–79, 1997.

[158] Thorin, S., Bourdages, H., and Vincent, B., "Study of siphon activity in *Mya arenaria* (l.) in the intertidal zone by means of an underwater video camera," *Journal of Experimental Marine Biology and Ecology*, vol. 224, pp. 205–224, 1998.

[159] Tolle, C. R., McJunkin, T. R., and Gorsich, D. J., "An efficient implementation of the gliding box lacunarity algorithm," *Physica D-Nonlinear Phenomena*, vol. 237, pp. 306–315, 2008.

[160] Tolle, C. R., McJunkin, T. R., Rohrbaugh, D. T., and LaViolette, R. A., "Lacunarity definition for ramified data sets based on optimal cover," *Physica D-Nonlinear Phenomenon*, vol. 179, pp. 129–152, 2003.

[161] Trevethan, M. and Chanson, H., "Turbulent mixing in a small estuary: Detailed measurements," *Estuarine, Coastal, and Shelf Science*, vol. 81, pp. 191–200, 2009.

[162] Trevethan, M., Chanson, H., and Brown, R., "Turbulent measurements in a small subtropical estuary with simidiurnal tides," *Journal of Hydraulic Engineering*, vol. 134, no. 11, pp. 1665–1670, 2008.

[163] Troost, K., Stamhuis, E. J., van Duren, L. A., and Wolff, W. J., "Feeding current characteristics of three morphologically different bivalve suspension feeders, *C*," *Marine Biology*, vol. 156, pp. 355–372, 2009.

[164] Trowbridge, J. H., "On a technique for measurement of turbulent shear stress in the presence of surface waves," *Journal of Atmospheric and Oceanic Technology*, vol. 15, pp. 290–298, 1998.

[165] Trowbridge, J. H., Geyer, W. R., Bowen, M. M., and III, A. J. W., "Maniplating the intensity of near-bed turbulence in rivers: effects on benthic invertebrates," *Freshwater Biology*, vol. 42, pp. 645–653, 1999.

[166] van der Ham, R., Fontijn, H. L., Kranenburg, C., and Winterwerp, J. C., "Turbulent exchange of fine sediments in a tidal channel in the ems/dollard estuary. part i: Turbulence measurements," *Continental Shelf Research*, vol. 21, pp. 1605–1628, 2001.

[167] van Duren, L., Herman, P., Sandee, A., and Heip, C., "Effects of mussel filtering activity on boundary layer structure," *Journal of Sea Research*, vol. 55, no. 1, pp. 3–14, 2006.

[168] Vickers, N. J., "Mechanisms of animal navigation in odor plumes," *Biological Bullitin*, vol. 198, pp. 203–212, 2000.

[169] Vickers, N. J., "Winging it: moth flight behavior and responses of olfactory neurons are shaped by pheromone plume dynamics," *Chemical Senses*, vol. 31, pp. 155–166, 2006.

[170] Vigneau, O., Pignoux, S., Carreau, J.-L., and Roger, F., "Interaction of multiple gas jets horizontally injected into a vertical water stream," *Flow, Turbulence and Combustion*, vol. 66, pp. 183–208, 2001.

[171] Vincent, B., Desrosiers, G., and Gratton, Y., "Orientation of the infaunal bivalve *Mya arenaria* l. in relation to local current direction on a tidal flat," *Journal of Marine Biology and Ecology*, vol. 124, pp. 205–214, 1988.

[172] Virnstein, R. W., "The importance of predation by crabs and fishes on benthic infauna in Chesapeake Bay," *Ecology*, vol. 58, pp. 1199–1217, 1977.

[173] Voulgaris, G. and Trowbridge, J. H., "Evaluation of the Acoustic doppler velocimeter (ADV) for Turbulence measurements," *Journal of Atmospheric and oceanic technology*, vol. 15, pp. 272–289, 1997.

[174] Voulgaris, G. and Meyers, S. T., "Temporal variability of hydrodynamics, sediment concentration and sediment settling velocity in a tidal creek," *Continental Shelf Research*, vol. 24, pp. 1659–1683, 2004.

[175] Walne, P. R., "The influence of current speed, body size and water temperature on the filtration rate of five species of bivalves," *Journal of Marine Biological Association of the United Kingdom*, vol. 52, pp. 345–374, 1972.

[176] Webster, D. R., Rahman, S., and Dasi, L. P., "On the usefulness of bilateral comparison to tracking turbulent chemical odor plumes," *Limnology and Oceanography*, vol. 46, no. 5, pp. 1048–1053, 2001.

[177] Webster, D. R. and Weissburg, M. J., "Chemosensory guidance cues in a turbulent chemical odor plume," *Limnology and Oceanography*, vol. 46, no. 5, pp. 1034–1047, 2001.

[178] Webster, D. R. and Weissburg, M. J., "The hydrodynamics of chemical cues among aquatic organisms," *Annual Review of Fluid Mechanics*, vol. 41, no. In Press, 2009.

[179] Webster, D. R., Rahman, S., and Dasi, L. P., "Laser-induced flourescence measurements of a turbulent plume," *Journal of Engineering Mechanics*, vol. 129, pp. 1130–1137, 2003.

[180] Wegner, B., Huai, Y., and Sadiki, A., "Comparative study of turbulent mixing in jet in cross-flow configurations using les," *International Journal of Heat and Fluid Flow*, vol. 25, pp. 767–775, 2004.

[181] Weiss, D. J., "Nominal analysis of "variance"," *Behavior Research Methods*, vol. 41, no. 3, pp. 901–908, 2009.

[182] Weissburg, M. J., "The fluid dynamical context of chemosensory behavior," *Biological Bullitin*, vol. 198, no. 2, pp. 188–202, 2000.

[183] Weissburg, M. J. and Dusenbery, D. B., "Behavioral observations and computer simulations of blue crab movement to a chemical source in a controlled turbulent flow," *Journal of Experimental Biology*, vol. 205, pp. 3387–3308, 2002.

[184] Weissburg, M. J., Ferner, M. C., Pisut, D. P., and Smee, D. L., "Ecological consequences of chemically mediated prey perception," *Journal of Chemical Ecology*, vol. 28, pp. 1953–1970, 2002.

[185] Weissburg, M. J., James, C. P., Smee, D. L., and Webster, D. R., "Fluid mechanics produces conflicting constraints during olfactory navigation of blue crabs, *Callinectes sapidus*," *Journal of Experimental Biology*, vol. 206, pp. 171–180, 2003.

[186] Weissburg, M. J. and Zimmer-Faust, R. K., "Life and death in moving fluids: Hydrodynamic effects on chemosensory-mediated predation," *Ecology*, vol. 74, no. 5, pp. 1428–1443, 1993.

[187] Weissburg, M. J. and Zimmer-Faust, R. K., "Odor plumes and how blue crabs use them in finding prey," *Journal of Experimental Biology*, vol. 197, pp. 349–375, 1994.

[188] Wells, H. W., "Abundance of the hard clam *Mercenaria mercenaria* in relation to environmental factors," *Ecology*, vol. 38, no. 1, pp. 123–128, 1957.

[189] Wereley, S. T. and Meinhart, C. D., "Second-order accurate particle image velocimetry," *Experiments in Fluids*, vol. 31, pp. 258–268, 2001.

[190] Widdows, J. and Brinsley, M., "Impact of biotic and abiotic processes on sediment dynamics and the consequences to the structure and functioning of the intertidal zone," *Journal of Sea Research*, vol. 48, pp. 143–156, 2002.

[191] Wildish, D. J., Kristmanson, D. D., Hoar, R. L., DeCoste, A. M., McCormick, S. D., and White, A. W., "Giant scallop feeding and growth responses to flow," *Journal of Experimental Biological Ecology*, vol. 113, pp. 207–220, 1987.

[192] Wildish, D. J. and Miyares, M. P., "Filtration rate of blue mussels as a function of flow-velocity: preliminary experiments," *Journal of Experimental Marine Biology and Ecology*, vol. 142, pp. 213–219, 1990.

[193] Wilson, M. personal communication of unpublished data.

[194] Winter, J. E., "A review on the knowledge of suspension-feeding in lamellibranchiate bivalves, with special reference to artificial aquaculture systems," *Aquaculture*, vol. 13, pp. 1–33, 1978.

[195] Wright, L., Friedrichs, C., and Hepworth, D., "Effects of benthic biology on bottom boundary layer processes, Dry Tortugas Bank, Florida Keys," *Geo-Marine Letters*, vol. 17, no. 4, pp. 291–298, 1997.

[196] Wright, L., Schaffner, L., and Maa, J., "Biological mediation of bottom boundary layer processes and sediment suspension in the lower Chesapeake Bay," *Marine Geology*, vol. 141, no. 1-4, pp. 27–50, 1997.

[197] Wu, J., "Near-field trajectory of turbulent jets discharged at various inclinations into a uniform crossflow," *AIAA Journal*, vol. 11, no. 11, pp. 1579–1581, 1973.

[198] Wygnanski, I. and Fiedler, H., "Some measurments in the self-preserving jet," *Journal of Fluid Mechanics*, vol. 38, no. 3, pp. 577–612, 1969.

[199] Zar, J. H., *Biostatistical Analysis*. Prentice Hall, 4 ed., 1998.

[200] Zimmer, R. K. and Butman, C. A., "Chemical signaling processes in the marine environment," *Biological Bullitin*, vol. 198, pp. 168–187, 2000.

[201] Zimmer, R. K., Commins, J. E., and Browne, K. A., "Regulatory effects of environmental chemical signals on search behavior and foraging success," *Ecology*, vol. 80, no. 4, pp. 1432–1446, 1999.

[202] Zimmer-Faust, R. K., Finelli, C. M., Pentcheff, N. D., and Wethey, D. S., "Odor plumes and animal navigation in turbulent water flow: a field study," *Biological Bullitin*, vol. 188, pp. 111–116, 1995.